4-2019

Experimental investigations of bio-syngas Production using microwave pyrolysis of UAE's Palm date seeds

Mahmmoud Muhammed Syam

Recommended Citation

UAEU

جامعة الإمارات العربية المتحدة
United Arab Emirates University

United Arab Emirates University

College of Engineering

Department of Mechanical Engineering

EXPERIMENTAL INVESTIGATIONS OF BIO-SYNGAS PRODUCTION USING MICROWAVE PYROLYSIS OF UAE'S PALM DATE SEEDS

Mahmmoud Muhammed Syam

This thesis is submitted in partial fulfilment of the requirements for the degree of Master of Science in Mechanical Engineering
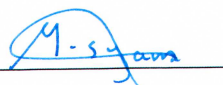
Under the Supervision of Dr. Emad Elnajjar

April 2019

Declaration of Original Work

I, Mahmmoud Muhammed Syam, the undersigned, a graduate student at the United Arab Emirates University (UAEU), and the author of this thesis entitled *"Experimental Investigations of Bio-Syngas Production Using Microwave Pyrolysis of Uae's Palm Date Seeds"*, hereby, solemnly declare that this thesis is my own original research work that has been done and prepared by me under the supervision of Dr. Emad Elnajjar, in the College of Engineering at UAEU. This work has not previously been presented or published, or formed the basis for the award of any academic degree, diploma or a similar title at this or any other university. Any materials borrowed from other sources (whether published or unpublished) and relied upon or included in my thesis have been properly cited and acknowledged in accordance with appropriate academic conventions. I further declare that there is no potential conflict of interest with respect to the research, data collection, authorship, presentation and/or publication of this thesis.

Student's Signature: _____   Date: 21 /05/ 2019
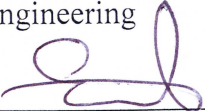
Approval of the Master Thesis

This Master Thesis is approved by the following Examining Committee Members:

1) Advisor (Committee Chair): Dr. Emad Elnajjar

   Title: Associate Professor

   Department of Mechanical Engineering

   College of Engineering

   Signature _____   Date April 23 2019

2) Member: Dr. Bobby Mathew

   Title: Assistant Professor

   Department of Mechanical Engineering

   College of Engineering

   Signature _____   Date 23/04/2019

3) Member: Dr. Tariq Darabseh

   Title: Associate Professor

   Department of Mechanical Engineering

   College of Engineering

   Signature _____   Date 23/4/2019

4) Member (External Examiner): Juan C. Ordonez   /Dr. Tariq Darabseh

   Title: Associate Professor

   Department of Mechanical Engineering

   Institution: Florida State University

   Signature _____   Date 23/4/2019

This Master Thesis is accepted by:

Dean of the College of Engineering: Professor Sabah Alkass

Signature _____ Date 12/5/2019

Acting Dean of the College of Graduate Studies: Professor Ali Al-Marzouqi

Signature _____ Date 21/5/2019

Copy 1 of 8

Abstract

From the start of the industrial revolution, the continued need for energy has been the most crucial issue in human history. An energy crisis started at the beginning of the 1970s when the number of machines, which became an essential part of our life, increased rapidly. Scientists made a huge effort to discover new sources of energy, with 'biomass' being one of the main focuses of researchers as a new renewable source of energy. In this thesis, a nonconventional method of heating, using microwave power in a pyrolysis process of biomass waste from palm trees (Allig's date seeds) for the production of bio-syngas to use in practical and industrial applications, is the main focus. Microwave heating has many advantages over conventional heating methods. In this method, the biomass heating occurs from the inside to the outside uniformly instead of heating the environment, as in the case of conventional heating. In designing the experimental work, a full factorial approach is utilized, using three parameter factors: particle sizes of (1790 μm, 783 μm, and 467 μm), microwave powers of (1,000 W, 700 W, and 300 W) and sample moisture contents of (0, 0.2, and 0.4). The yield of bio-syngas and temperature samples are monitored and measured throughout the tests using an "ETG MCA 100 Syn BIOGAS MULTIGAS ANALYZER" and an Omega Thermocouple respectively. In the last part of this work, a statistical analysis is conducted to nonlinearly model the gas yield average concentration percentages for CH_4 and CO, as a function of all dependent parameters. The outcome of this study produces promising results, especially for CH_4 and CO gas yields, which shows an average of 21% and 15% volume bases respectively. The yield of H_2 gases is the lowest amongst all gas yields. The highest percentages of bio-syngas yield occurred at the highest microwave power, the smallest size of particles, and the driest samples. Allig date seeds as a biomass source in the microwave pyrolysis process demonstrate to be a promising source of renewable energy to be used in commercial and practical applications.

Keywords: Allig date seeds, microwave pyrolysis, bio-Syngas, cold gas efficiency, hot gas efficiency.

Title and Abstract (in Arabic)

فحوصات تجريبية لإنتاج الغاز باستخدام تأثير الميكروويفات على بذور التمور في الإمارات العربية المتحدة

الملخص

منذ بداية الثورة الصناعية، كانت الحاجة المستمرة للطاقة هي القضية الأكثر أهمية في تاريخ البشرية. ظهرت أزمة الطاقة في بداية السبعينات من القرن الماضي، عندما زاد عدد الآلات بسرعة في حين أصبحت جزءا لا يتجزأ من حياتنا. بذل العلماء جهدًا كبيرًا لاكتشاف موارد جديدة للطاقة. تعتبر الكتلة الحيوية كمورد للطاقة المتجددة موضوعًا ساخنًا من قائمة طويلة من الموارد المتجددة. في هذه الأطروحة، نحن نستخدم تقنية مبسطة للتسخين وهو الانحلال الحراري الذي يتمتع بإمكانيات هائلة لإنتاج كميات كبيرة من الغاز الحيوي للتطبيقات العملية والتجارية كمحركات توليد الطاقة.

الدارج هو استخدام أساليب الانحلال الحرارية التقليدية التي تقوم على الاحتراق. في هذه الرسالة، نقترح استخدام التسخين بطاقة الميكروويف الذي له العديد من المزايا في تسخين الكتلة الحيوية من الداخل إلى الخارج بشكل موحد بدلاً من تسخين البيئة المحيطة بالجسم المراد تسخينه كما حدث في الانحلال الحراري التقليدي التي تنتج التركيبات الحيوية. في تصميم العمل التجريبي، تم استخدام نهج توضيحي كامل. و قد غطت الدراسة ثلاثة عوامل يتم اختبارها: حجم الجسيمات (1790 μm، 783 μm، 467 μm)، والطاقة (1000W، 700W، 300W) ومحتوى الرطوبة في العينة "MC" (0، 0.2، 0.4). يتم رصد غاز التخليق العائد ودرجة الحرارة طوال الاختبارات باستخدام " BIOGAS MULTIGAS Syn ETG MCA 100 ANALYZER" و Omega thermocouple. وتهدف نتائج هذه الدراسة إلى الحصول على نتائج واعدة، خاصة بالنسبة للغازات التي تنتج غاز الميثان وأول أكسيد الكربون والتي تُظهر متوسط إنتاج للغازات بحوالي 21% و 15%. و تعتبر نتائج غازات الهايدروجين هي الأدنى بين جميع الغازات المُنتجة. حدثت أعلى النسب المئوية من الغازات الحيوية في أعلى طاقة للميكروويف، في أصغر حجم من الجسميات وباستخدام عينات جافة. يُعتقد أن استخدام بذور التمر كمصدر للكتلة الحيوية في عملية الانحلال الحراري باستخدام طاقة موجات المايكروويف جزء من ثورة الموارد المتجددة الرئيسية في التطبيقات التجارية والعملية.

مفاهيم البحث الرئيسية: بذور تمر السلاج، الانحلال الحراري باستخدام طاقة أشعة المايكروويف، الغازات العضوية، كفاءة الغاز البارد، كفاءة الغاز الحار.

Acknowledgments

Special thanks go to my adviser Dr. Emad Elnajjar for his guidance, support, and assistance throughout my preparation of this thesis. I would like to thank Dr. Salah Al Omari my co-advisor, the chair and all members of the Mechanical Engineering Department at the United Arab Emirates University for assisting me over my studies and research. My special thanks are extended to the College of Graduate Studies for providing me with the necessary information needed to complete this work. The author would like to extend his sincerest appreciation to United Arab Emirates University for funding this research through Research Projects Fund #31N200 and Fund #31R072.

I am especially grateful to my parents, brothers, sisters in law and niece who helped me along the way and gave me the moral support whenever needed. Also, special thanks are extended to Syam family for their assistance and friendship.

Dedication

To my beloved parents and family

Table of Contents

List of Tables

List of Figures

List of Abbreviations

Avg- GCVP	Average gas concentration volume percentage
c	Intercept X vs. Y
D	The infiltration profundity
d	Droplet diameter
do	c/n
do and n	Fitting parameters
DSP	Date Seeds Powder
Ei	The voltage stretch or the internal electric field intensity (V·m^{-3})
f	The frequency of the applied field (Hz)
GCVP	Gas concentration volume percentage
HV$_{BM}$	The heating value of the biomass in,(MJ/kg)
IEEE	The Institute of Electrical and Electronic Engineers
MC	Moisture content
MW	Microwave
MW$_{BM}$	The biomass molecular weight ($kg/kmole$)
MW$_i$	The molecular weight of the species
m'$_i$	The mass rate of the species in gm/hr
m'$_{total}$	The total mass rate of all species in gm/hr
n	slope X vs. Y
n'$_i$	The mole rate of the species in mole/hr
n'$_{total}$	The total mole rate of all species in mole/hr
p	mole fraction of Nitrogen per 1 mole of Carbon

p	The power dissipation density
$Q_{BM\text{-}in}$	Biomass input energy
$Q_{Cold\text{-}out}$	Cold energy output (MJ)
$Q_{Hot\text{-}out}$	Hot energy output (MJ)
R	The cumulative% retained at a size d
TGA	Thermogravimetric analysis
V'_i	The volume rate of the species in liter/hr
V'_{sample}	The volume rate of the sample in liter/hr
x_i	The individual volume percentage
y	Mole fraction of hydrogen per 1 mole of Carbon
z	Mole fraction of oxygen per 1 mole of Carbon
α	The level of significant
β	The phase factor
γ	The attenuation factor
ε	The dielectric permittivity
ε'	The dielectric constant
ε''	The dielectric loss factor
ε_0	The free space permittivity ($\varepsilon_0 = 8.854 \times 10{-}12\ F \cdot m^{-1}$)
$\eta_{Cold\text{-}Avg}$	The average cold gas Efficiency
$\eta_{Hot\text{-}Avg}$	The average hot gas Efficiency
λ_0	The free-space wavelength

Chapter 1: Introduction

1.1 Overview

Fuel, as the fundamental source of energy, is crucial in all aspects of life. However, in the manner the world functions presently, we experience the drawbacks of a lack of energy. Currently, energy is the primary concern of everyone in society due to the suffering people experience from the deficiency of energy resources. Prices for resources have been energetically raised over the last five years, because of the rising demand and the high efficiency of energy resources. This energy crises occurred due to the low reliance on renewable energy and the high dependency on non-renewable energy resources [1]. The hydrocarbons coal gas and oil together constitute eighty-five percent of the world's aggregate energy supply [2]; meanwhile, the renewable resources of energy such as hydro-electric, solar, wind, nuclear, geothermal, biogas and wave represent fifteen percent of the worldwide offer of energy supply.

The rapid development that has been taking place in recent years majorly affects the use of energy. It was recognized that humanity depends mainly on coal, oil, and petroleum gas as primary sources. Many nations are currently focusing on arranging high deals of sustainable power resource such as Denmark 100%, Germany 50% and California 33%, in the following twenty years [2]. However, a myth that states that efforts in renewable energy will never achieve high levels, due to the low efficiency of the outcome energy compared to oil or coal as a source of energy. International investment in renewable energy sources today, have reached up to 250 billion dollars. This enormous investment is greater than the that of non-renewable energy sources and nuclear power combined [2]. Different statistics predict that the need for energy will dramatically increase from 75% to 90% through the coming 20

years [2]. This can be easily noticed in Figure 1; that compares the energy generation in Germany as an example from 2003 to 2013. The main point to be discussed is that the dependence on renewable energy has increased from 7.5% to 23.4%, almost a three times increase; reflecting the industrial countries' plans that significantly supports this approach.
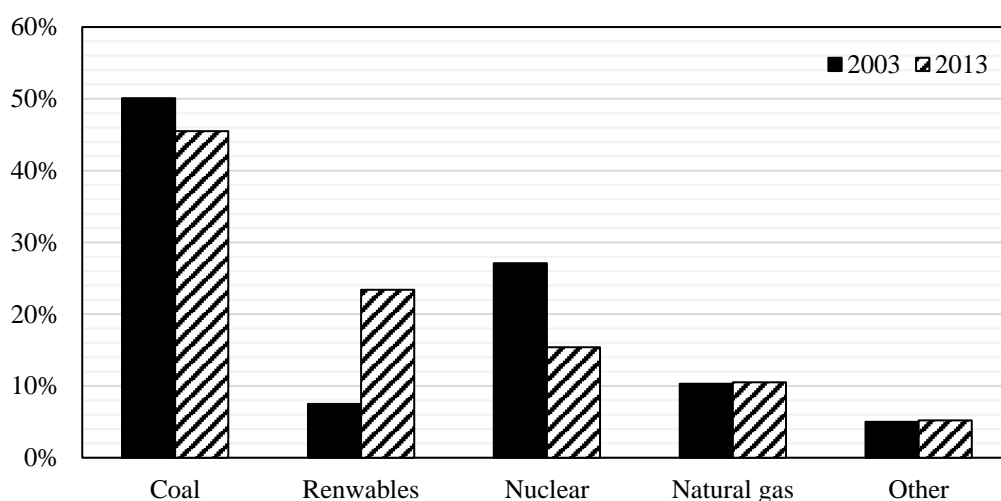
Figure 1: Generation of Electricity by Renewable Energy Source [2]

As per Arab Petroleum Investments Corporation (Apicorp), the Gulf Cooperation Council (GCC) showed 47% or 148 GW of the current Middle East and North Africa (MENA) power-generating limit. Factors, such as urbanization, enhancements in wage levels, industrialization, and low electricity costs, have prompted an ascent in the GCC's interest for energy.

The GCC region would require US$ 85 billion for the expansion of 69 GW of generating capacity and another US$ 52 billion for T&D throughout the following five years. The GCC power capacity needs to grow at an average yearly pace of 8% somewhere in the range of 2016 and 2020 as represented in Table 1. Saudi Arabia

(KSA) drives the efforts to make the necessary capacity augmentations by 2020 as the kingdom should contribute US$ 71 billion to increase the power to 114 GW [3].

Table 1: The required GCC investment in power from 2016 to 2020 [3]

REQUIRED GCC INVESTMENT (2016-2020)	GENERATION (US$ BN)	T&D (US$ BN)	TOTAL (US$ BN)
KSA	43	28	71
UAE	20	14	34
Kuwait	8	4	12
Qatar	6	3	9
Oman	6	2	8
Bahrain	2	1	3

New resources for energy have been the subject of interest for many researchers to satisfy the human needs from energy. They began to look for new untraditional natural resources by following the well-known hypothesis " any organic object with the main carbon structure has an amount of energy" [3]. As per human nature, which likes to exploit all resources for its interests, scientists used new resources to produce energy like feedstock, waste, and biomass [3]. The renewable power source is acquired from frequently renewing assets, for example, the sun, wind, rain, tides and geothermal warmth.

Bioenergy is the most prominent active supporter of worldwide energy demands, giving about 13% of the total energy supply. The current utilization of biomass in nations (for cooking and heating) represents an approximate of 8%. Current bioenergy provides around 4% of the needed heat in structures and 6% in industry. Not to mention, somewhere in the range of 2% in the worldwide generation of global electricity and 3% of transport energy needs.

Present day development in the utilization of bioenergy for heating has been generally moderate (underneath 2% every year) because of the fossil fuel prices. With generation from biomass expanding by 11% in 2017, the usage of biomass in the electric field has seen a more haste development. Table 2 shows the annual investment net capacity additions' production in 2017. China as the largest producer of bioelectricity during the year overwhelmed even the United States. Worldwide increases to the hydropower capacity in 2017 was an expected 19 GW, bringing the total capacity to roughly 1,114 GW. While noteworthy, this is the smallest yearly augmentation seen in the past five years. Representing about 40% of the new establishments of energy in 2017, china remains the enduring leader in authorizing new hydropower capacity, trailed by Brazil, India, Angola, and Turkey. Solar PV was one of the best new sources of power production in 2017, due to the significant extent of development in China. Worldwide capacity expanded by about 33%, to around 402 GW [4].

Renewable energy is directed in an upward direction in the UAE. Its power has been its primary consideration, driven by solar, waste-to-energy, and wind. Additionally, there are pilot extensions in thermal cooling and transport energies. In 2008-2009 the revelation for renewable power source initiated, when Abu Dhabi set an objective to obtain a 7% renewable power source (around 1500 MW) by 2020. Dubai at that point likewise reported an objective of 5% renewable power source (around 1000 MW) by 2030. Notwithstanding question territoriality and universally about the chances for a renewable power source in hydrocarbon-trading nations, the UAE's organization and advancement of renewable power source had a critical impact for it [5].

Table 2: Annual investment net capacity additions production in 2017 [4]

	1	2	3	4	5
Investment in renewable power and fuels(not including hydro over 50 MW)	China	USA	Japan	India	Germany
Investment in renewable power and fuels per unit GDP	Marshall Islands	Rwanda	Solomon Islands	Guinea-Bissau	Serbia
Geothermal power capacity	Indonesia	Turkey	Chile	Iceland	Honduras
Hydropower Capacity	China	Brazil	India	Angola	Turkey
Solar PV Capacity	China	USA	India	Japan	Turkey
Concentrating solar thermal power (CSP) Capacity	South Africa	-	-	-	-
Wind power Capacity	China	USA	Germany	UK	India
Solar water heating Capacity	China	Turkey	India	Brazil	USA
Biodiesel production	USA	Brazil	Germany	Argentina	Indonesia
Ethanol production	USA	Brazil	China	Canada	Thailand

1.2 Statement of the Problem

The energy crisis of the 1970s was a significant concern that threatened all nations all over the world. The world began to notice that oil, coal, and natural gas would be depleted shortly; therefore, the persistent need for a new energy source was a requirement to feed the vast and rapid improvements in technology, and to meet the needs of our ever increasing population [3]. To cope with this problem, a worldwide race looking for renewable resources commenced. Among all the promising solutions, was the use of biomass waste as a renewable source of energy. Consequently, each country looked at developing the use of the biomass waste which was frequently produced [6]. Biomass waste can occur through different processes; for example, in the thermochemical conversion process, Pyrolysis is one of the methods used to produce renewable resources.

Recently, the UAE has started using renewable energy, and It is essential to know that the UAE has millions of palm trees along the roads and in the farms [7]. These palm trees produce thousands of tons of dates, some of which are not being used as food sources, and some are damaged in the production process. A vast number of date seeds are thrown away in factories as waste. Thus, this waste can be used as a sustainable biomass source of energy for the UAE. The use of microwave heating on date palm waste (date seeds) in the pyrolysis process is an innovative approach to extract yield gases such as CH_4, CO, CO_2, and H_2.

1.3 Biomass

Biomass energy (bioenergy) can be delivered from an extensive variety of feedstock of natural origins, and can be utilized through various diverse procedures to deliver heat, power and transport fuels (biofuels). Numerous bioenergy conversion pathways are entrenched and fully commercial, while others are still at the exhibit and commercialization stages. As shown in Figure 2, Bioenergy contributed an expected 12.8% (46.4 exajoules (EJ) = (10^{18}) joules) in 2016. Nowadays bioenergy contributes 5% of the total energy consumption [8].
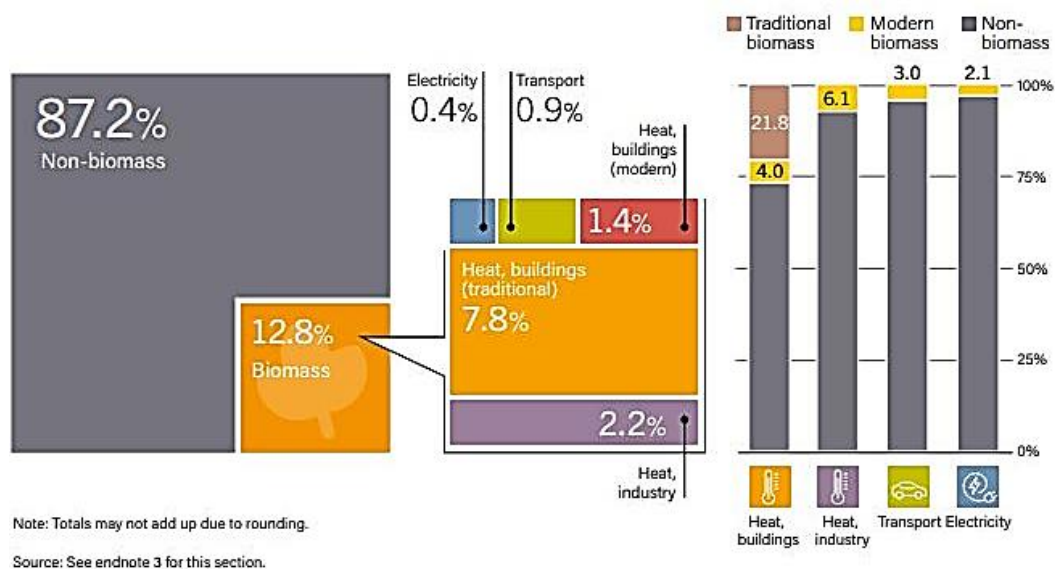
Figure 2: Shares of bioenergy in total final energy consumption, overall and by end-use sector, 2016 [6]

Regarding the sustainability of production and use, bioenergy remains a hot subject to be discussed. Nonetheless, when produced and used sustainably, there is a growing agreement that, bioenergy can contribute to reductions in greenhouse gas emissions and give a scope of other natural, social and economic benefits [8].

In 2017, various activities were progressed to grow the economic bioenergy state, including the recent buildup of 20 nation to promote the growth of a functional bio-economy, and the sustainable biofuels development test, which is a part of the extensive mission development program and has 22 participating countries [9].

Biomass integrates carbon dioxide and energy into chemical energy through photosynthesis. Biomass contains agricultural and forestry residues, wood, byproducts from the processing of biological materials, and the organic parts of municipal and sludge wastes. The utilization of biomass as a fuel is a natural carbon process since the carbon dioxide caught through photosynthesis is discharged during its combustion [10]. Photosynthesis by plants catches around 4000 EJ/year as energy in biomass. The

appraisals of the potential worldwide biomass energy have changed widely. The changeability emerges from the diverse styles of biomass and the unique strategies for deciding assessments for those biomasses. Parikka assessed the aggregate overall energy potential from biomass on an economic scale to be 104 EJ/year, of which woody biomass, energy products, and straw constituted 40.1%, 36%, and 16.6%, respectively [11]. Just around 40% of potential biomass energy used currently. In Asia, the present biomass used slightly exceeds the reasonable biomass potential. Right now, the aggregate worldwide energy request is about 470 EJ/year. Fischer and Schrattenholzer assessed the global biomass potential to be 91 to 675 EJ/year for the years 1990 to 2060 [12]. Their biomass contains crop and forestry residues, energy crops, and animal and municipal wastes. Hoogwijk evaluated these to be 33 to 1135 EJ/year [13]. Perlack assessed that, in the USA, 1.3 billion tons of biomass could be collected every year for biofuel generation [14]. 1.3 billion tons of biomass equates to almost 3.8 billion barrels of oil in energy content. The US's energy consumption is around 7 billion barrels every year [15]. Nonetheless, harvesting, gathering, and the capacity of biomass include another measurement of specific difficulties for the utilization of biomass for the production of bio power, chemicals, and fuels [14].

Biomass created reasonably the modern biomass avoids traditional employments of biomass as fuelwood as it incorporates electricity and heat generation in addition to transportation energizes, from forest residues, solid and agricultural waste. On the other hand, "traditional biomass" is created in an unsustainable way and it is utilized as a non-business source— usually with low efficiencies for cooking in numerous nations [16].

1.4 Biomass Pyrolysis: Principles and Technologies

1.4.1 Methods of Converting Biomass to Biofuel and Bioenergy

The two primary methods used to change biomass energy into biofuels and biopower are biochemical conversion and thermochemical conversion process. Biochemical conversion changes the biomass into a fluid or a gas by fermentation or anaerobic digestion. Anaerobic digestion prompts the generation of gas fuels fundamentally containing methane. Fermentation of the biomass (starch and cellulose) creates ethanol. Thermochemical conversion technology contains combustion, gasification, and pyrolysis.

Thermochemical conversion technology has certain advantages and of course, disadvantages. The primary advantages are that the feedstock for thermochemical transformation can be any biomass such as agricultural residues, forestry residues, byproducts of any bioprocessing facility and even organic municipal wastes. Additionally, the gases can be changed to different types of fuels (H_2, Fischer-Tropsch (FT) diesel, manufactured gas) and chemicals (methanol, urea) as alternatives for oil based chemicals. The main disadvantages are the high costs related with cleaning the produced gas from tar and unwanted contaminants like alkali compounds, inefficiency because of the high temperatures required, and the doubtful utilization of products (syngas and bio-oil) as transportation fuels [17].

The combustion of biomass is the most straight forward and uncomplicated process. The general efficiency of creating heat from biomass energy is low. The biomass gasification process consists of the transformation of a solid/fluid natural compound in a gas/ vapor phase and a solid phase. The gas phase namely called "syngas", has a high heating power and can be utilized in biofuel generation. The solid

phase, called "char", contains the unconverted natural division and the inactive material present in the processed biomass [18].

1.4.2 Pyrolysis Process

Pyrolysis, a promising method, can be considered as one of the big revolutions in producing energy. As one of the thermochemical conversion process, pyrolysis occurs at a range of temperature starting from 400°C – 500°C in the absence of oxygen as shown in Figure 3. It produces fuel gas, bio-oil in liquid form and charcoal in solid form. Fuel gas and bio-oil have many common applications such as the turbines and the boilers. However, the difference in the applications is that fuel gas is used in engines and synthesis, while the bio-oil is used in the upgrading and extraction applications. On the other hand, boilers can also use charcoal as a source of energy [19]. Large particles in biomass disintegrate or depolymerize at high temperature to gas phase abandoning some solid charcoal [20].
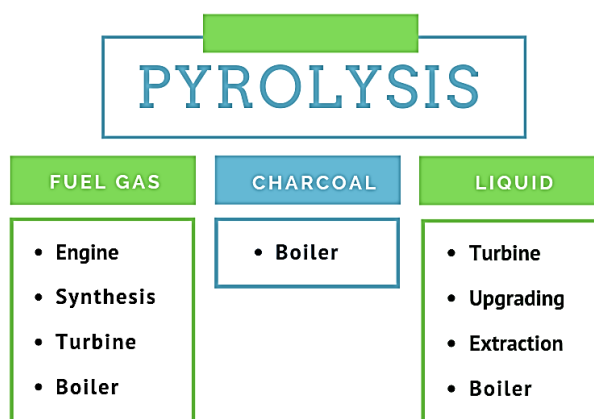
Figure 3: Pyrolysis process's products and its applications [19]

The gaseous phase contains condensable and incondensable compounds. The condensable compounds can be cooled to produce chemicals and bio-oils [15, 21]. Pyrolysis can occur through different methods such as conventional pyrolysis, where

a high amount of hydrogen-rich gas is produced that can work at high temperatures and for a long time [19, 22, 23]. Heat converted to the material by convection, conduction and radiation were it was noticeable that the heating manner of the material started from the surface to the inner parts [24, 25]. Conventional pyrolysis would be done by different methods in different systems such as fluidized bed, fixed bed, rotating cone, and transported bed [26]. Another conceivable pyrolysis alternative, called flash or fast pyrolysis, has been used to increase the yield of gas. In this case, a high heating rate, and temperatures of around 500°C are utilized [21].

Fast pyrolysis is a high-temperature process in which biomass is quickly heated without oxygen. Accordingly, it decomposes to produce vapors and vaporizers and some charcoal [27].

The primary highlights of a fast pyrolysis process are summarized by [21]: fast cooling of the pyrolysis vapors to give the bio-oil item. Cautiously controlled temperature. Moreover, by high heating and heat transfer rates that require a finely ground biomass feed [25].

The Kinetics of biomass pyrolysis is a hard topic as many of the researchers agree, they investigate the mechanism of biomass pyrolysis through the study of the decomposition mechanisms of its constituents; cellulose, hemicellulose, and lignin [28-31]. They examined the disintegration temperature of the three constituents utilizing Thermogravimetric Analysis (TGA). The researchers discovered that hemicellulose decomposition happens first at around 220– 315°C while cellulose deteriorates in the range 315– 400°C. Lignin was found to break down gradually over a wide temperature extend beginning from 150°C and proceeds up to 900°C [29]. The

pyrolysis of biomass constituents is a superposition of three primary mechanisms concerning product quality [30].

The primary mechanisms are shown in Figure 4 and described below:

- Char formation: This mechanism takes place at low reaction temperatures, beneath 500°C, and low heating rates. It is described as adjustment reactions prompting the development of a thermally steady solid product called char, which has a polycyclic aromatic structure. Water and incondensable gases are produced as a result of these reactions [30].

- Depolymerization: This pathway includes the breakage of the bonds between the monomer units prompting the arrangement of shorter chains. Depolymerization proceeds until the point when the delivered molecules wind up volatile at the working conditions. As a primary product with concentration to about 60%, "Cellulose Depolymerization" prompts the development of levoglucosan [32, 33]. Hemicellulose depolarization products rely upon the type of 27 monosaccharides included. Hexoses-rich hemicellulose depolymerizes into products wealthy in six-carbon compounds, for example, Hydroxymethylfurfural, while Xylose-rich hemicellulose depolymerizes into basically five-carbon compounds, for example, furfural [34]. The development of phenolic compounds, which could be monophenols or oligomers, leads by lignin depolymerization [35].

- Fragmentation: This includes the breakage of covalent bonds, including those inside the monomer units, prompting the development of atoms and incondensable gases. This mechanism is favored at the high temperatures of 600°C and more [30].
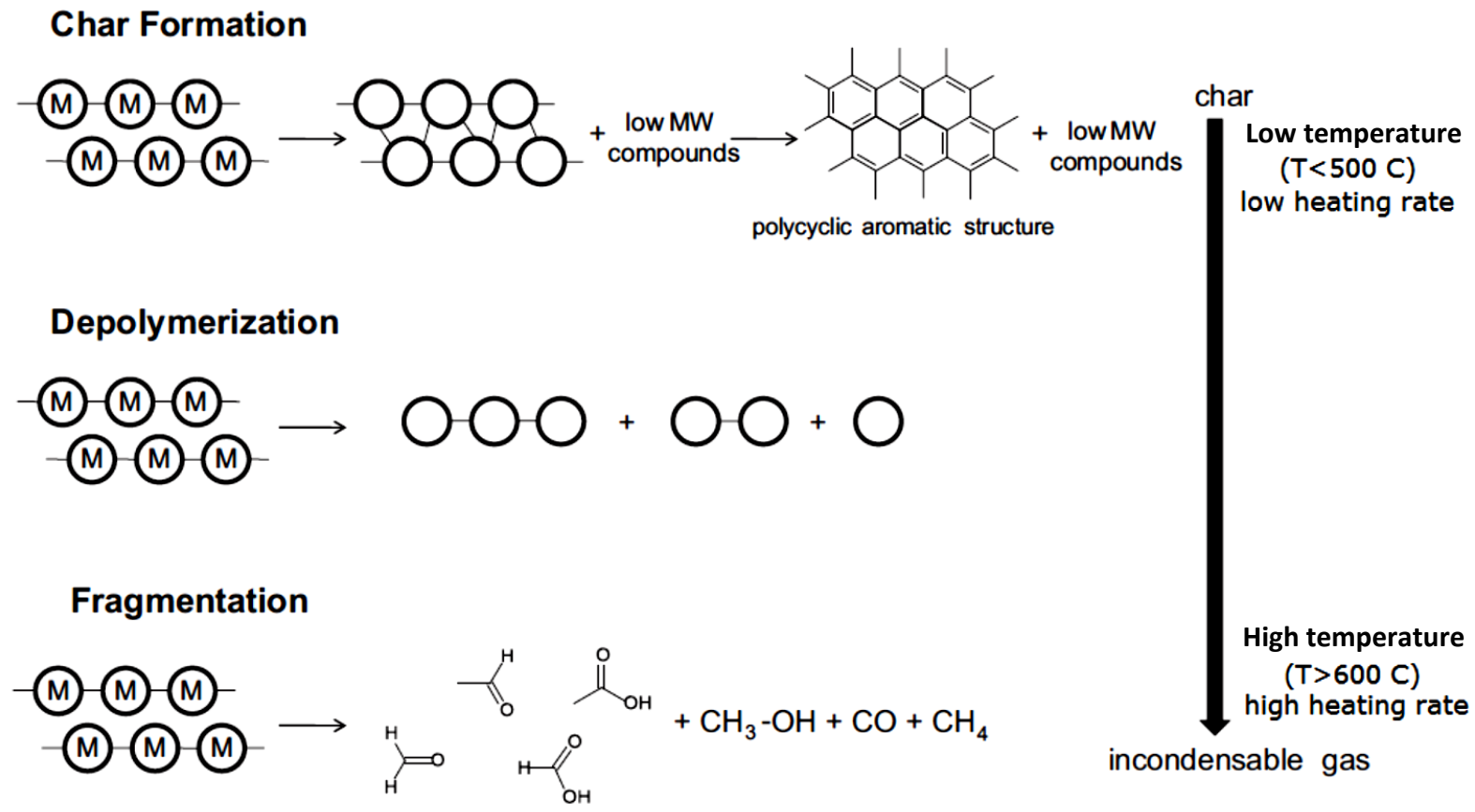
Figure 4: Primary mechanisms of biomass pyrolysis [1]

1.5 Microwave Heating

Microwave pyrolysis which is the main issue to be discussed in this thesis mainly depends on the microwave radiation as a source of heat to reach a suiTable temperature. Microwave heating is an alluring technique as it gives a volumetric heating process at improved heating efficiencies as contrasted with a conventional one. Uniform heating inside the material can be observed if the conditions controlled accurately. Therefore, materials vary in their reaction to microwave heating. Materials have distinctive ideal frequencies that can be estimated while not all materials absorb microwaves. Few materials reflect or seem transparent to microwaves and are consequently less receptive to heating. Materials that absorb microwaves are known as dielectrics and have two main properties [36]: they do not have that much of free charge carriers, a small amount of charge carried through the material matrix when an external electric field applied, and the atoms or molecules including the dielectric display a dipole development.

The microwave frequency is between 300 MHz and 300 GHz, and most microwave applications are made in the range of 3 and 30 GHz.

In industry, microwave heating is performed at either a frequency near 900 MHz or 2450 MHz [37]. The material's ability to absorb microwave energy is measured by its loss factor. Reflecting materials do not store microwave energy as heat since the waves go through the material.

Metal, as an example of the reflecting material, has a property in which waves reflect off the material surface. Materials with microwave absorbing properties can be adequately heated at room temperature. Nonetheless, due to the heating mechanism in microwave, insulators that are materials with low microwave conductivities, for

example, start to absorb microwave radiation effectively at the point when heating exceeds a critical temperature [38]. At the point when a dielectric is in an electric field (i.e., a microwave cavity), the dipoles inside the material start to organize themselves as indicated by the connected field. The dipoles in the material, exposed to an electromagnetic field, reorganize themselves around 2.5 billion times each second (for a microwave frequency of 2.45 GHz). This produces internal friction, causing the microwave responsive material to heat up [39].

1.6 Dielectric Material

Dielectric properties characterize the collaboration of materials with the electromagnetic field. Biomass materials are viewed as nonmagnetic materials and, in this manner, their connection is restricted to the electric field [40]. From the polarization loss, the numerical portrayal of the dielectric properties is generally clarified. A slight amount of energy is stored because of charges polarization, at the point when an electric field is applied to a dielectric material. The utilized value to quantitatively depict the stored energy is called the dielectric permittivity (ε). If the electric field is exchanging, as on account of microwave field where part of the energy is lost into heat, the dielectric permittivity is, at that point, shown as an aggregate amount [41, 42]:

$$\varepsilon = \varepsilon' - j\varepsilon''$$

The real part of the complex permittivity, the dielectric constant is (ε'), decides measures of the stored energy, meanwhile, the dielectric loss factor is called the imaginary part (ε''), and it shows the measure of power loss into heat.

The real part has generally been called the dielectric constant. The loss tangent or the dissipation factor (tan δ) is the ratio between the dielectric constant to the loss factor. The dissipation factor tan δ is ordinarily used to estimate the general capacity of a material to heat in an electric field [43]. When two materials have a similar loss factor, at that point, the material with the lower dielectric constant would heat better, because it has higher loss tangent.

As recorded in Table 3, the moisture content influenced the dielectric properties of biomass materials, fundamentally, at room temperature. Robinson et al. examined the loss factor of dried and undried (6.3% water content) pine pellets at 2.45 GHz [35].

For the dried and undried samples, they discovered that the loss factor is 0.05 and 0.81 respectively at room temperature. This study demonstrated the massive commitment of the water content in the dielectric properties of biomass materials, as just 6.3% of the moisture raises the loss factor with an order of magnitude. Other factors influence the dielectric properties of biomass materials including the packing density temperature and the frequency.

These varieties in the values from the Table are related to numerous reasons; the most important of which are the measurement conditions and the type of the biomass materials utilized, i.e., the frequency utilized, the material's moisture content, and density. It is, hence, critical to display the dielectric properties of biomass with their frequency, temperature, density, and the moisture content since these components fundamentally influence the dielectric properties.

Table 3: Dielectric properties of different biomass materials together with water at room temperature (25°C) [44]

Material	Moisture (%, d.b)	Density (g.cm³)	Frequency (MHz)	ε'	ε''	tan δ	Reference
Pine pellets	6.3 ±0	-	2450	-	0.81	-	[45]
	dry	-	2450	-	0.05	-	
Palm kernl Shell	8.5	-	2450	2.76	0.35	0.13	[46]
Palm Fibre	10	-	2450	1.99	0.16	0.08	
Switchgrass Pelletes	2.23	0.94	915	2.63	0.17	0.06	[47]
	2.23	0.94	2450	2.55	0.16	0.06	
Municipal solid waste	2.9	0.166	2450	2	<0.05	<0.03	[48]
Distilled Water	-	1	2450	77	13	0.17	[49]

The power dissipation (*P*) at the point when an electromagnetic field is applied on a dielectric nonmagnetic material, could be evaluated from [49]:

$$p = 2\pi f \varepsilon_0\ \varepsilon''\ E_i{}^2$$

Where p is the power dissipation density ($p = P/V$); f is the frequency of the applied field (Hz); Ei is the voltage stretch or the internal electric field intensity (V m⁻³); ε_0 is the free space permittivity ($\varepsilon_0 = 8.854 \times 10^{-12}\ F.m^{-1}$); ε'' is the dielectric material loss factor substituting the constant qualities, the equation could be composed as:

$$p = 55.63 \times 10^{-12}\ f\ Ei\ ^2\ \varepsilon''\ (W \cdot m^{-3})$$

The previous equation demonstrates that the frequency, the material's loss factor, and the field intensity are the variables of the power dissipation. Also, that the loss factor changes with the frequency which makes the relationship between the density, frequency, and the power dissipation not linear.

Even though the dielectric constant does not show up in the previous equation, through the electric field power, it influences the power dissipation [50]. The electric field intensity spread through the material could be shown graphically as in Figure 5.
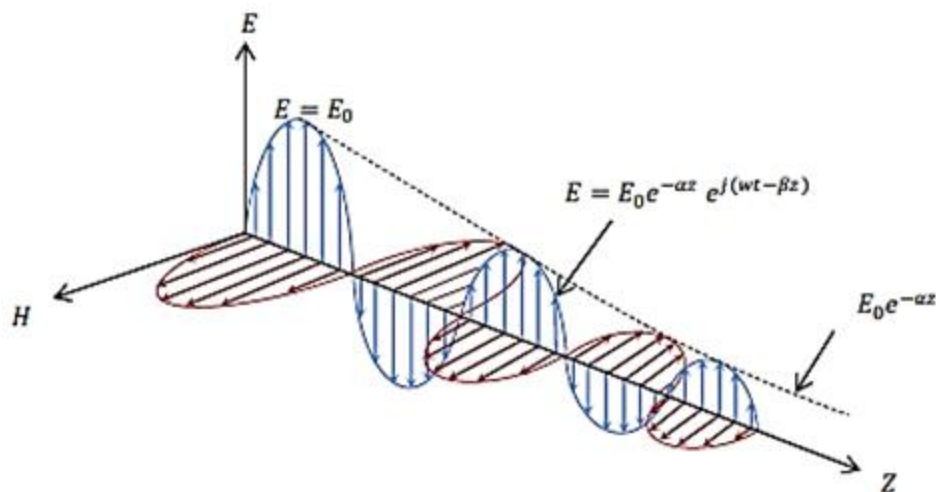
Figure 5: Electromagnetic field propagation in a dielectric medium [44]

Also, scientifically as pursues [50, 51]:

$$(z) = E_0 e^{-\gamma z} \, e^{-(\omega t - \beta z)}$$

Where α is known as the attenuation factor and β is the phase factor, both of them are elements of the loss factor and dielectric constant of the medium [50, 51].

The most extreme electric-field stress ought to be less than the critical value at which voltage breakdown (or electric breakdown) happens. This high electric field stress can ionize gases forming a conducting method at which large power dissipation happens (arcing).

This high nearby power dissipation density can harm a few sections of the microwave heating system and the workload also. The electric breakdown voltage of gas is relative to its density which can be reduced with raising in the temperature at

constant pressure [48]. The electric breakdown voltage of air at the standard conditions is around 30 kV·cm^{-1} [48]. Working at "the biomass pyrolysis reaction temperature of around 500°C" expands the chances of electric breakdown by decreasing the breakdown voltage to around 11 kV·cm^{-1}.

The penetration depth, which is a proportion of how deep the electric field can enter into a material, is another critical parameter in electromagnetic energy with the material interaction. The separation from the surface at which the power flux drops to 1/e (≈ 0.368) of its surface value is known as the infiltration profundity [49].

From the fact that as the wave advances inside a dielectric material, the power intensity and its related electric field intensity decrease exponentially with the distance from the surface as clarified from the previous figure this definition originates. The penetration depth can be assessed from the accompanying equation [51]:

$$D_p = \frac{\lambda_0}{2\pi\sqrt{2\varepsilon}} + \frac{2\pi\sqrt{2\varepsilon'}}{\sqrt{\left[\left(1 + \frac{\varepsilon''}{\varepsilon'}\right)^2\right)^{0.5} - 1\right]}}$$

It was noticeable that the previous definition does not propose that there will be no heating at a distance surpassing D_p as around 37% of the power is dissipated in the material at depth more noteworthy than D_p. From the previous equation, obviously the, penetration depth is a function of the free-space wavelength, λ_0, the dielectric constant and the loss factor.

Water, for instance, (as loose materials that have a short penetration depth) has a penetration depth of 1.3 cm at room temperature and 2.45 GHz. Materials with a complex permittivity of 2 - 0.1 j, or in other words, a value for a biomass material at room temperature, would have a penetration depth of 27.5 cm. In any case, the

dielectric properties of biomass materials change with temperature, and it progresses towards becoming loose when char begins to shape at high temperature prompting a decrease in the penetration depth.

1.7 Microwave Pyrolysis

Using the microwave as a source of energy for the pyrolysis was a sign offer a new trend generation in energy production, the most important factors in microwave pyrolysis reaction are recorded underneath [52]:

- Reaction time (residence time)

- Microwave output power

- Type and size of input biomass/materials

- Reactor design/type

- Moisture and water content of input biomass/materials

- Microwave type (multimode or single-mode)

- Microwave receptor type, size, and amount/concentration

- Catalyst type and concentration

- Reaction temperature

- Type and flow rate of carrier gas

Contrasted with conventional pyrolysis, which is carried out by an electric heater, microwave pyrolysis creates more H_2 and CO content [53, 54], which is the syngas. Huang examines the productivity of H_2 rich fuel gas from rice straw utilizing the microwave-induced pyrolysis [55].

The arrangement constituents of gas production and the instrument of its generation were likewise discussed. The essential segments of the gas product were

H_2, CO_2, CO, and CH_4, with average rates of 50.67, 22.56, 16.09, and 7.42 vol.%, respectively.

As indicated by the TA-MS investigation, it was proposed that focused heating, by microwaves, made the microwave-incited pyrolysis unique. A substance condition could almost be adjusted to outline the gas structure created from rice straw. From the perspective of energy consumption, near 60% of the input energy could be determined and used as bioenergy [55].

1.7.1 Microwave pyrolysis Advantages and Disadvantages

Like any new technology, microwave pyrolysis has several advantages and some disadvantages [54, 56-60]. The advantages can be summarized by the following:

- It is an active uniform rapid heating method to convert the biomass into solid, liquid and gaseous products

- Beats a few specific disadvantages of conventional pyrolysis techniques such as slow warming and need of feedstock ripping

- Expanded product production

- Low process time

- Saving energy

- Low necessities for space

- Creates microplasmas and hot spots which advance, the heterogeneous reaction that creates more concentrations of bio-syngas and hydrogen in the gas products

- Creates less polycyclic aromatic hydrocarbons (PAHs), and is resulting in the less risky compound

The fundamental disadvantage of microwave power is the innate issues of temperature estimation. The most customarily utilized sensors for high-temperature estimation amid pyrolysis forms are infrared pyrometers and thermocouples. Temperature estimation with infrared optical pyrometers requires a window in the response framework that permits, just the infrared, but not microwaves to go through; which, as a rule, prompts heat loss and accordingly the underestimation of the reaction temperature [61].

Conversely, thermocouples frequently overestimate the temperature concerning the fact that the thermocouple tip can act as an antenna, which makes a concentrated electric field, and creates a hot spot of a higher temperature. Thermocouple probes with a mix of infrared optical pyrometers may enhance the reliability of temperature estimation [62].

1.8 Relevant Literature

This section includes relevant literature reviews to the work in this thesis; covering the main areas of relevance to the topic. A sub-section of the background will note the basic knowledge about microwave pyrolysis covered and the list of the objectives, scope of the work, hypothesis and a summary of the thesis structure.

1.8.1 Microwave Pyrolysis

Zhoe [63] found that the main gas products from microwave pyrolysis of wheat and straw bale were CO, CO_2, H_2, CH_2, C_2H_6 with 35 vol.% of pure H_2, while Huang [55] examined that it is 50.67vol.% of the rice straw. A few pyrolysis studies have been led utilizing microwaves as a heating source, with a feedstock that included coal [64], espresso structures [65], rice straw [66], squander tea [67], and corn Stover [58].

From these researches, different products were created by microwave pyrolysis including gas, fluid, and solids. The essential elements influencing the productivities included reaction time, microwave power, reaction temperature, and molecule size.

Hong et al. studied three distinctive marine biomasses: microalgae-spirulina, chlorella, and macroalgaeporphyra, that were pyrolyzed in a research center scale multimode-microwave cavity at 400, 550 and 700°C. Ovalbumin and cellulose were, likewise, picked as model mixes to simulate algae. The impact of the heating rate on pyrolysis and the bi curves of various samples under various temperatures were examined. The Porphyra was observed to be the most responsive and delivered the most significant gaseous fraction (87.1 wt.%) over the three algae, which contained 73.3 vol.% of syngas. It was discovered that carbohydrate prompted the development of PAHs while nitrogenized mixes in bio-oil were obtained from protein in algae. For the generation of bio-oil, protein-rich microalgae are good contrasted with Porphyra because of their lower measure of PAHs, while Porphyra is more appropriate for the generation of $H_2 + CO$-rich gas, which is practically identical with that of conventional gasification processes.

Huang et al. [68] discussed the impacts of catalysis of aluminum oxide (Al_2O_3), molecule size, and pretreatment (acid pretreatment and steam explosion), on gaseous product composition. Additionally, heating efficiency and product distribution of corn stover pyrolysis utilizing microwave heating were examined. Both most extreme temperature and heating rate expanded with the decreasing molecule size of corn Stover. The heating efficiency was, additionally, improved over Al_2O_3 and by applying both pretreatment techniques. Including 10 mesh, Al_2O_3 enlarged the gaseous yield, however decreased the fluid yield. This might be inferable from that little catalysts

particles that are embodied by another catalyst and biomass particles to decrease their catalytic activity. Applying acid pretreatment considerably reduced the gas yield yet expanded the fluid yield, while the impact of the steam explosion was not significant. Around half of the CO was delivered at the first five minutes of the test, yet the yields of H_2, CH_4, and CO_2, created from microwave pyrolysis of corn Stover pretreated by acid, were generally small. The first-and-second-order reaction models is utilized to analyze the reaction kinetics for microwave pyrolysis of corn stover.

Li et al. [69] studied the impacts of moisture content, pyrolysis temperature, added substance, and the microwave power on H_2 yield. The feedstock is rice straw, which is the most common crop straw. What is more, a four-factor four-level symmetrical test is intended to reveal the position of these factors and the ideal pyrolysis conditions. The outcome demonstrates that: H_2 yield (vol.%) first expanded and afterward decreased when pyrolysis temperature and microwave power expanded, H_2 yield reduced; without added substance when moisture content expanded, H_2 yield was 36.14% which is the maximum value recorded. The rank of the four studied factors is moisture content, additives, pyrolysis temperature, and finally microwave power. At the point when the microwave power was 2.5 kW, the pyrolysis temperature was 700°C, $ZnCl_2$ was utilized as the added substance in the microwave-helped pyrolysis of the rice straw, and the moisture content was 61.84%, a high H_2 yield of 44.94% was accomplished.

Jimenez et al. [70] studied the pyrolysis of pecan nutshells and considered utilizing microwave at various input power and presentation time. The carbonaceous items were characterized utilizing potentiometric titration, elemental analysis, N_2 adsorption isotherms at −196°C, FT-IR spectroscopy, and thermogravimetric analysis.

The qualities of microwave carbonaceous items were contrasted by carbons arranged by conventional heating and commercial carbons. The outcomes show that it is conceivable to acquire carbonaceous materials with similar textural parameters in conventional and microwave systems, yet for microwave heating, the handling times are shorter, which reaches 3 min. Likewise, the exposure time of 2 min of the microwave is insufficient for the total depolymerization of the lignocellulosic matrix of the pecan nutshell, and a massive measure of cellulose and hemicelluloses stay in char after the microwave treatment.

Hossain [71] studied pyrolysis of oil palm fiber (OPF) for the generation of hydrogen-rich gas using various response parameters. Five distinctive OPF test sizes were tried: microwave power running from 400 W to 900 W, lengths less than 1 mm, 1–3 mm, 4–6 mm, 7–9 mm and 10–12 mm, N_2 flow rates running 200– 1200 cm^3/min, and reaction temperatures extending from 450°C to 700°C. The microwave pyrolysis was completed by utilizing a microwave reactor which has an ability of giving 2450 ± 25 MHz microwave frequency. It has been discovered that the use of small OPF molecule sizes, a higher microwave power, a higher reaction temperature, and a higher N_2 flow rate fundamentally yields more H_2 rich gas.

Al-Rubaye et al. [72] manages syngas creation from date palm seeds by utilizing microwave plasma technology. Three forms of date palm seeds were utilized: crushed, powdered and full with a variable flow rate of argon to expand the centralization of plasma. The outcomes demonstrate that there is no compelling reason to pre-treat (process) the date palm seeds to enhance biogas generation.

1.9 Study Objectives

The main objectives of this study can be summarized in the following:

- To explore microwave heating as an efficient method for the pyrolysis process.

- To examine the potential of using biomass waste material (Allig's date seed) as a source of renewable energy.

- To perform a parametric study to investigate the effect of the particle size, microwave power, and moisture content on the performance of the pyrolysis process, and to explore the limitations behind this process.

- To develop a theoretical model using Minitab, which can predict the main components of the bio-syngas yields such as CH_4 and CO as a function of the particle size, microwave power, and moisture content.

1.10 Scope of the Work

The scope of this work can be outlined as follows:

- To focus on studying the non-conventional technique of pyrolysis utilizing the microwave effect.

- To determine the benefit from the direct heating of the sample using microwave power compared to the conventional heating method, which requires heating the environment in order to heat the sample.

- The application of the pyrolysis process, using a microwave oven with various particle sizes, microwave powers, and moisture contents, to study their effects on the yield bio-syngas produced through the process.

- To develop a theoretical model to describe the gas yield percentages as a function of the three parameters for future industrial utilization.

- To explore the limitations of the parameters and their impact on the overall performance of the process.

1.11 Hypothesis

An altered microwave is to be utilized in an experimental study as a source of heat. The microwave will be modified to accommodate a specially designed double wall quartz reactor that will be integrated at the center of the microwave space. A biomass waste material (Allig Date seeds) is to be utilized in a pyrolysis process to produce bio-syngas. A syngas analyzer is to be implanted to measure the produced bio-syngas, and a thermocouple is also introduced into the samples to measure the temperature throughout the experiments. The data collected will be processed, through the reduction analysis, to calculate the output yield bio-syngas average concentration volume percentages, the gas produced energy, and the gas efficiency.

1.12 Summary of Thesis Structure

The structure of this thesis is divided into seven chapters. The first chapter is an introduction which is divided to: An Overview, a Statement of the problem, a Thesis Objectives, a Scope of the work and limitations, a Hypothesis, a Summary of the Thesis structure, a background about the Biomass, and a Biomass Pyrolysis: Principles and Technologies that contains two subsections: Methods of converting biomass to biofuel and bioenergy, and Pyrolysis. It also focused on Microwave Heating, Dielectric Material, Microwave Pyrolysis, Microwave pyrolysis Advantages and disadvantages, and Relevant Literature which contains Microwave Pyrolysis.

Chapter two "Experimental Methodologies" concentrates on Biomass Material, Material Characterization that describes: Sample Preparation, Thermogravimetric Analysis of Allig Date Seed and Particle size distribution. It also

discusses the Experimental Setup in details through Microwave, Reactor, and Sensors that describe: Gas analyzer, and Thermocouple and Digital flow meter. After that, it shows the Testing procedures, Parameters study, and Data Reduction.

The subsequent third chapter is mainly about the Results and Discussion which will discuss Physical and Chemical properties of Date Seed (Allig), the Effects of Microwave Power on bio-syngas yield, the Effect of Date Seed Size effect on bio-syngas production, the Effects of Moisture content on bio-syngas production, and the Statistical Analysis for CH_4 and CO cases. Moreover, in chapter four, it focused on the Conclusion that discussed briefly: Research Conclusions and Implications, the Effects of Microwave Power on bio-syngas production, the Effects of Date seeds size on bio-syngas production, the Effects of Moisture content on bio-syngas production, the General Remarks, and the Recommendations. Furthermore, chapter five shows the References used through the thesis in IEEE style. Chapter six shows the Appendices that contains Tables and figures. Finally, chapter seven includes List of Publications.

Chapter 2: Experimental Methodologies

In this chapter, the Characterization of Allig Date seed, a Thermogravimetric Analysis, proximate analysis for DSP and the experimental setup for the microwave pyrolysis process is to be described. Also, a detailed size measurement is explained with all of the equations regarding "Rosine Rammler Bennett distribution". The experimental procedures are discussed starting with the preparation of date seeds biomass to the last step which is analyzing the output bio-syngas yield data and temperature measurements throughout all the tests, using the gas analyzer and OMEGA thermocouple and controller.

2.1 Biomass Material (Allig Date Seed)

Date seeds are utilized as a feedstock for energy production. It stands out amongst the most widely recognized organic products in the Middle East and UAE specifically. The UAE is among the ten world leading date makers. Moreover, the number of date trees in the UAE is approximately 40 million, 8.5 of which is located in Al-Ain [73]. UAE has from 50,000 to 80,000 metric tons developed in overabundance in 2011. Allig is one of the main date types that is frequently produced in UAE for it is large benefits and for it is importance as a traditional food. Liwa dates factory is the leader in producing all types of dates, and were the source of the Allig date seeds used for this thesis [74].

2.2 Material Characterization

2.2.1 Sample Preparation

Allig date seeds -the biomass material- used in the experiment are washed by water, dried under the sun for two days, and then crushed into powders of different sizes using "GSMachine Crusher".

The second step was to measure the average sizes of the different particles produced from the crushing process based on the sieves accumulated weights. The statistical average sizing is explained in details in section 2.2.3.

"*MATEST an Auto Sieve Shaker*" in Figure 6 is used with several sieves with the following sizes: (2360 μm, 1180 μm, 1000 μm, 500 μm, 200 μm, 100 μm, 50 μm) as shown in Figure 10. After examining the three sizes of biomass that will be used in the tests (1790 μm, 783 μm, 467 μm), as shown in Figure 7, the last step before performing the pyrolysis test is drying the sample and getting rid of the moisture content. The drying process is carried out by placing the DSP sample in the Furnace's Chamber "Controlab" under 100°C for about 48 hours [75]. The sample is confirmed to be dry by monitoring the weight of the sample frequently until the weight of the sample is constant. The specific moisture content is controlled in different samples by adding a calculated mass of water to the dry sample based on the equation below. The sample is stirred to guarantee uniform distribution of moisture to the whole sample. In the end, each sample for each case is stored in a separate sealed plastic container to keep it isolated from the environmental effects. It is worth mentioning, that the total weight of each test sample is kept constant to 8 gm. Table 4 shows the mass of added water and the mass of dry date seeds used to prepare all the cases with the different moisture contents.

$$MC = \frac{m_{water}}{m_{Biomass}} 100\%$$

Table 4: The amount of water and dry biomass for different moisture content%

MC (%)	water weight (gm)	Dry DS weight (gm)	Total Sample weight (gm)
0	0	8	8
20	1.6	6.4	8
40	3.2	4.8	8

Figure 6: Auto Sieve Shaker by MATEST

467 μm   783 μm   1790 μm

Figure 7: Picture of the three different DSP sample sizes

Table 5: The weight loss for the three samples before and after the drying process

Sample Average size	Before Drying	After Drying	Weight loss
1790 μm	100 g	93.707 g	6.293 g
783 μm	100 g	92.928 g	7.072 g
467 μm	100 g	89.98 g	10.02 g

From Table 5, it's clear that whenever the size of the particles increase, the weight loss decreases; this can be explained from the fact that the small particles have the ability to get rid of more amounts of moisture, since it appears less solid and more powder-like than the large size samples. The smaller size will help the heat reach all of the sample particles resulting in a greater reduction in weight as evaporated moisture.

2.2.2 Thermogravimetric Analysis of Allig Date Seed

The thermogravimetric analysis (TGA) is accomplished using type TGA Q600 Thermal analyzer to determine the proximate analysis of the date seed powder. The reason behind this test is to figure out the percentages of: protein, carbohydrate, dehydration moisture, solid decomposition present and devolatilization lipid in the sample, by the degradation of the sample mass by combustion under inert conditions. The thermal behavior of any sample can be demonstrated by TGA, which is a critical parameter for the pyrolysis of date seeds in any designed reactor. The TGA test process can be described by the following. Initially, the temperature of the test chamber is stabilized at 25°C for 5 min; it is then heated at a steady heating rate of 20°C/min until it reaches 110°C. Then the sample is kept at 110°C for 5 min. Finally, the sample temperature is raised to 900°C under a similar heating rate, which is held steady for 15 min. A constant purging of nitrogen gas is connected with a flow rate of 100 ml/min during the whole process.

The percentage of weight reduction and its related thermogravimetric derivative analysis (DTG) as a function of temperature for "Allig DPS" is demonstrated in Figure 8. The pyrolysis stage of the Allig DSP, it is partitioned into three phases: Lack of hydration, Devolatilization, and Solid decomposition. Figure 8 demonstrates that the weight of the date seed sample suddenly decreases sharply after 220°C. Also where weight reduction stage the release of the volatile matter has begun. Besides, there are two different peaks relating to the decay of hemicellulose and cellulose, and it is observed that the thermal decomposition for date seeds is pyrolyzed at 450°C. There is a moderate drop in the weight reduction rate, after this temperature. This outcome could be explained by the decomposition procedure of the char or solid residues, which expands until 900°C. The unburned char is 20 wt.% of DP material Table 6 summarizes the proximate analysis results obtained from the TGA test.

Table 6 shows the proximate analysis results for the Allig date seeds. While Table 7 shows the Ultimate Analysis of DSP where it demonstrates the presence of approximately 6.84% (by weight) of hydrogen, and about 49.74 (% of weight). [56].

Table 6: Allig Date Seed Powder Proximate Analysis Results

Allig DSP	Mass Fraction
Dehydration stage (Moisture)	4.0%
Devolatilization Stage	75.0%
Protein and Carbohydrate	60.0%
Lipid	10.0%
Solid Decomposition Stage	21.0%
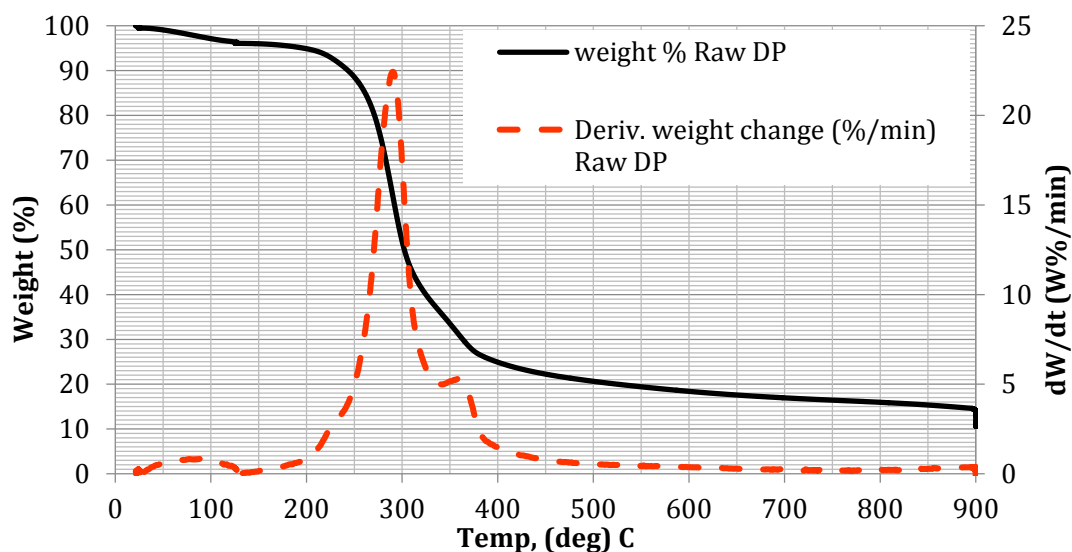
Figure 8: TGA and DTG curves for Allig DSP

Table 7: Elemental analysis of DSP [56]

Element Analysis	
Element	*% of weight*
Carbon (C)	49.74
Hydrogen (H)	6.84
Nitrogen (N)	1.37
Sulfur (S)	0.89
Oxygen (O)	41.16

2.2.3 Particle Size Distribution

Sieve analysis is an analytical procedure used to decide the particle size distribution of granular material with plainly visible granular sizes. The technique includes the layering of sieves with various values of sieves opening sizes. The best-measured sieve occurred at the base of the stack with each layered sieve stacked above one another arranged by expanding sieve size. At the point when a granular material is added to the top and winnowed, the particles of the material are separated at the last layer which the molecule couldn't pass. Sieve analysis (*MATEST an Auto Sieve Shaker*), determined the solid particles size distribution utilizing distinctive sifters

mesh sizes ranging from 50 – 3000 μm, with samples of 50-100 gram for 120 min sieving time.

Rosine Rammler Bennett distribution was considered for the evaluation of sieve analysis. The analysis is shown below, in which the biomass held on the sieves Retained percentage (R%) were utilized to decide the distribution after normalization concerning the total biomass weight. Data collection is accepted to pursue a Rosin-Rammler distribution. The Rosin Rammler parameters are decided by regression as the data index given from a sifter investigation. Table 4 demonstrates the screen sizes data and attained cumulative residue [73].

The general form of the Rosin-Rammler equation is given by:

$$R = e^{-\left(\frac{d}{do}\right)^n}$$

The Linearized equation is given as the following:

$$\ln(R) = -\left(\frac{d}{do}\right)^n$$

$$\ln\left(\ln\left(\frac{1}{R}\right)\right) = n\ \ln\left(\frac{d}{do}\right)$$

$$\ln\left(\ln\left(\frac{1}{R}\right)\right) = n\ \ln(d) - n\ln(do)$$

$$Y = n\,X - c$$

Where: Y= $\ln\left(\ln\left(\frac{1}{R}\right)\right)$, X=ln(do), n=slope of X vs Y, c= Intercept of X vs. Y. Further details are given in Appendix A: Particle size distribution.

2.3 Experimental Setup

2.3.1 Microwave Oven

Figure 11 shows the experimental setup used to carry out the tests for the different cases studied. A conventional off the shelf microwave type *"DAEWOO KOR-1N3A"* which support up to 1000 W at 2.4 GHz and another microwave type *"SAMSUNG MS23K3513AW"* that supports up to 800 W at 2.4 GHz are used in this study. Both of the used microwave ovens are modified to accommodate the designed reactor. The microwave casing is drilled from the top at the center of the top with a 3.6 cm diameter hole.

2.3.2 Reactor

A custom made annular reactor is used (see Figure 9). The reactor has a double-walled quartz tube with 1.5 cm inner diameter, a 3.5 cm outer diameter, and a height of 45 cm. The inner tube has a perforated plate from the bottom which serves as an inlet for the inert gases. Aquartz wool (which can handle up to 900$^{\text{o}}$C without burning) is placed above the perforated plate and under the biomass sample. Figure 9 which represents in details: the reactor design, dimensions, and the thermocouple inserted in it. More details about the reactor design are given in section 2.3.3.2.

2.3.3 Instruments

The tests were measured by different types of sensors as shown in Table 8. Various quantities have been measured during the experiments, such as N_2 flow rates, biomass temperatures, and gaseous species concentrations. A list of the instrumentations used to carry out these measurements with their percentage errors is given in Table 8.
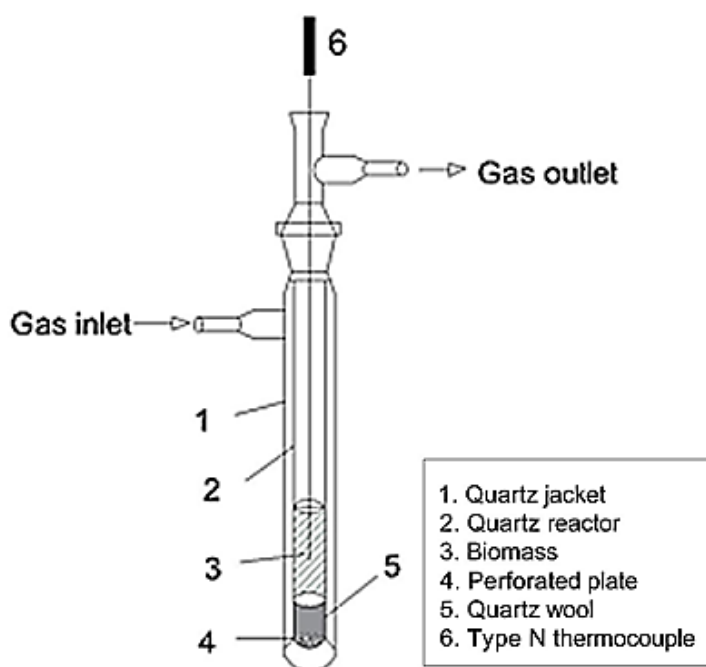
Figure 9: Schematic of the custom made double-walled quartz reactor

2.3.3.1 Gas Analyzer

The gas analyzer is shown in Figure 10, is used to measure the bio-syngas volume percentage concentrations of the gases produced through the pyrolysis process. These gases include CH_4, CO_2, CO, O_2, and H_2.

The produced gases from the pyrolysis process, pass through a multi filtration process in the sampling unit before they enter the gas analyzer unit. The new ETG Versatile syngas pre-treatment unit is used for residue/tar/moisture expulsion from the sample gas, with one fine filter with replaceable 0.3 μm filter component for tar expulsion, three refillable water scrubbers, and one refillable charcoal filter [74]. Tar vaporizers and stores lead to increased maintenance and fix of particularly gas cleaning parts and resultantly bring down plant limit factors. In gas analysis it is required to have a clean gas to bolster the analyzer, therefore, the system flow firstly removes most of the tar and residue through a washing gadget; then by a two-degree filter, the

gas chiller gives to evacuate the moisture and dust, as to acquire a sort of clean and dry air. In the end, the sample gas, through the assurance filter, goes into the analytical instruments.

This system is appropriate for the estimation of the bio-syngas in a point, and performs continuous measurement of the volume percentage concentrations of bio-syngas CO_2, CO, O_2, CH_4, and H_2. The analyzer is placed in safety case, outfitted with contact screen 5.7 inches, capable of recording up to 1000 data analysis, the system can work efficiently for 8 hours [74].

The system contains the following sensors and filters that are listed below, details on sensor types and uncertainties are given in Table 8:

- Sensor principle thermally conductive (TCD) for the estimation of H_2 real-time investigation.
- NDIR board for the estimation of CH_4, CO_2, CO.
- Electrochemical sensor (ECD) for the estimation of O_2.
- Display the most recent 30 minutes of the acquired data (plot).
- Heated line 3 m + with 30 cm process tube (up to 250°C process).
- Probe filter sintered steel.
- Analyzer filter.

Figure 10: The gas analyzer sampling unit (left) and the gas analyzer unit (right) [74]

1. Flow meter
2. Valve
3. Nitrogen Cylinder
4. Grounded
5. Conventional modified microwave oven
6. Type N thermocouple
7. OM-DAQPRO-5300
8. Gas filter
9. Gas Analyzer
10. Water filter
11. Gas outlet
12. Quartz jacket
13. Quartz reactor
14. Biomass
15. Perforated plate
16. Quartz wool
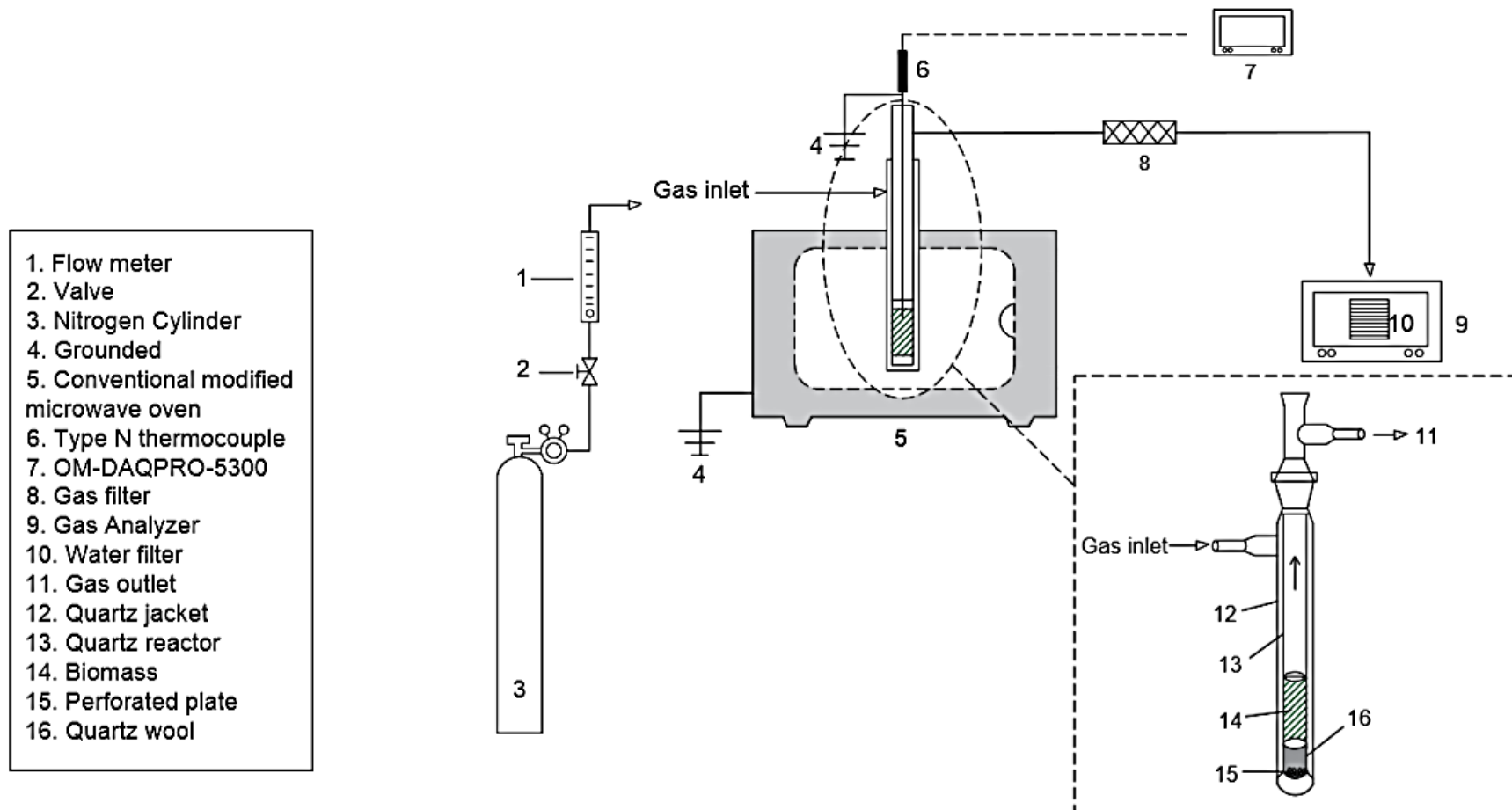
Figure 11: Schematic diagram of entire microwave pyrolysis experimental apparatus

Table 8: Instrumentation and measurement uncertainty

Measurement type	Sensor	Uncertainty
N_2 volumetric flow rate	LOW-PRESSURE DROP GAS MASS Flow Meters FMA-LP1600A	± 1.5%
Biomass Temperature	N-Type thermocouples	± 2.5°C
H_2 percentage in the sample	TCD H_2 measurement	± 2%
N_2 percentage in the sample	TCD N_2 measurement	± 2%
CO_2 percentage in the sample	NDIR board CO_2 measurement	± 2%
O_2 percentage in the sample	Electrochemical sensor (ECD) O_2 measurement	± 2%
CH_4 percentage in the sample	NDIR board CH_4 measurement	± 2%
CO percentage in the sample	NDIR board CO measurement	± 2%
The gas volumetric flow rate	flowmeter with a needle valve	± 2%

2.3.3.2 Thermocouple

An Omega N type thermocouple with sheet length of 60 cm and sheet diameter of 0.5 mm type "OMEGA NQXL-116U-12" in Figure 12 is used to measure the temperature throughout the experiment. The thermocouple can measure maximum temperatures measurement temperature up to 1335°C with a very low drift. Additionally Omega data acquisition type "OM-DAQPRO-5300" is connected to the thermocouple, this data acquisition can take the measurements for eight thermocouples in the same time, and it saves the data in the built-in memory at a sampling rate of 1 Hz. In order to overcome the microwave effect on the thermocouple, the body of the thermocouple is grounded by connecting it's the body to the ground of the microwave. The thermocouple is inserted through the top of the reactor to be located at the center of the biomass sample.

Figure 12: "OMEGA NQXL-116U-12" (left) and "OM-DAQPRO-5300" (right) [75]

2.3.3.3 Digital Flow Meter

The digital flowmeter is used to measure the N_2 flow rate that is used to purge and create an inert environment of the type "LOW-PRESSURE DROP GAS MASS Flow Meters FMA-LP1600A" and is given in Figure 13. The digital flowmeter's full measuring scale is up to 1500 ml/min with response times of less than ten milliseconds.

Figure 13: Digital Flow meter [76]

2.3.4 Testing Procedures

Before starting any test while the microwave is turned off, a steady flow rate of a N_2 gas is supplied from N_2 gas cylinder at a volume flow rate of 950 ml/min - measured by using a digital flowmeter- for 10 minutes, to ensure inert environment. A thermocouple of the type *"OMEGA NQXL-116U-12"* grounded to the body of the microwave is used to measure the temperature of the sample throughout the test operating time. The thermocouple data is collected at a sampling rate of 1 Hz by using Omega data acquisition type *"OM-DAQPRO-5300". A "DaqLab-Omega Engineering Inc. software"* is used to download the temperature measurements data to an Excel file for further processing. Before turning the microwave ON, the N_2 volume flow rate is reduced to 100 ml/min, and the power is adjusted to the required power, and the test is carried out for each sample for roughly 15 min. Each reported result is resolved by the average of at least two repetitions, performed at different times.

To ensure accurate measurements, the gas analyzer is cleaned before each test, filtering water is replaced if needed, and a micro sampling filter is cleaned. The gas analyzer starts collecting measurements from the moment the N_2 purging flow is started until the end of the experiment, which roughly lasts around 25 min. The gas analyzer type *"Syngas Analyzer PORTABLE MCA100 SYN P"* is used to measure and record the volume percentage concentrations of "CH_4, CO_2, CO, O_2, H_2" at a sample rate of 1 Hz. The gas analyzer sampler draws the yield gases at a flow rate of 60 liters/ hour. The gas analyzer has a special feature which is the pretreatment of the sample. All the data is stored on the gas analyzer internal memory, which will later on be used for data processing.

2.4 Parametric Study

    A full factorial analysis which is employed in designing the experimental work in this study namely, a combination: of three microwave powers (MWP) (1000 W, 700 W, 300 W), three particle sizes (DSP) (1790 μm, 783 μm, 467 μm), and three moisture content in the samples (MC) (0%, 20%, 40%). All the parameters studied in this experiment are summarized in Table 9.

Table 9: Summary list of the experimental test cases

Case Number	Size	MW power	MC%
Case 1	0.467 mm	1000	0
Case 2	0.783 mm	1000	0
Case 3	1.790 mm	1000	0
Case 4	0.467 mm	1000	20
Case 5	0.783 mm	1000	20
Case 6	1.790 mm	1000	20
Case 7	0.467 mm	1000	40
Case 8	0.783 mm	1000	40
Case 9	1.790 mm	1000	40
Case 10	0.467 mm	700	0
Case 11	0.783 mm	700	0
Case 12	1.790 mm	700	0
Case 13	0.467 mm	700	20
Case 14	0.783 mm	700	20
Case 15	1.790 mm	700	20
Case 16	0.467 mm	700	40
Case 17	0.783 mm	700	40
Case 18	1.790 mm	700	40
Case 19	0.467 mm	300	0
Case 20	0.783 mm	300	0
Case 21	1.790 mm	300	0
Case 22	0.467 mm	300	20
Case 23	0.783 mm	300	20
Case 24	1.790 mm	300	20
Case 25	0.467 mm	300	40
Case 26	0.783 mm	300	40
Case 27	1.790 mm	300	40

2.5 Results Processing and Data Reduction

In this section, a detailed results analysis and data reduction process is explained. The collected data from the gas analyzer is reported as a gas concentration volume percentage (x_i), at a sampling rate of 1 Hz. The gas analyzer is set fixed at a volume flow rate (V'_{sample}) of 60 liters/hr, and the temperature measurements are sampled at a rate of 1 Hz. The dry biomass mass used in the analysis is listed as a function of the moister content as shown in Table 4. The biomass chemical formula, per one mole of carbon used in the analysis, is calculated based on the biomass element analysis from reference [61], and it is reported in Table 10. The individual gas concentration volume percentage yield is indicated as: x_i, (i: 1= CH_4, 2= CO, 3= H_2, 4= CO_2, 5= O_2 and 6= N_2).

The data reduction analysis standard value from reference is used for the molecular weight, Calorific value, density and specific heat for all listed species. The data is listed in Table 10 [77].

Table 10: Gases properties used in data reduction

Item	ρ (gm/l)	MW (gm/mole)	CV (MJ/kmole)	C_p (kJ/kmole K)
CH_4	0.72	16.04	890.22	35.288
CO	1.25	28.01	282.901	29.4105
H_2	0.09	2.02	286.84	2.908
CO_2	1.326	44.01	-	47.96
O_2	0.9622	32	-	-
N_2	0.845	28.02	-	-
Ash	-	35.5	-	-

The reported results analysis is described in the following section:

The individual gas concentration volume percentage is given by (x_i):

$$x_i = \frac{V_i}{V_{total}} 100\% , \qquad (l_i/l_{total})$$

The volume rate of the sample species in liter/hr is given by (V_i):

$$V_i = \frac{x_i}{100} V_{Sample}, \qquad (l_i/hr)$$

The mass rate of the sample species in gm/hr is given by (m_i):

$$m_i = V_i\, \rho_i, \qquad (gm_i/hr)$$

The total mass rate of all sample species in gm/hr is given by (m_{total}):

$$m_{total} = \sum_{i=1}^{6} m_i, \qquad (gm_{total}/hr)$$

The mole rate of the sample species in mole/hr is given by (n_i):

$$n_i = \frac{m_i}{MW_i}, \qquad (mole_i/hr)$$

The total mole rate of all sample species in mole/hr is given by (n_{total}):

$$n_{total} = \sum_{i=1}^{6} n_i, \qquad (mole_{total}/hr)$$

The heating value of the Biomass-based on Channiwala formula is given by (HV_{BM}) [78]:

$$HV_{BM} = 0.3491 * C + 1.1783 * H + 0.1005 * S - 0.1034 * O - 0.051 * N - 0.0211 * ASH \ , (MJ/kg)$$

The empirical formula for biomass per one mole of Carbon based on the ultimate analysis is given by:

$$M = C\%/MW_C$$

$$y = (H\%/MW_C)/M$$

$$z = (O\%/MW_C)/M$$

$$p = (N\%/MW_C)/M$$

Biomass Chemical empirical formula: $CH_{1.6291}O_{0.7631}N_{0.015}$.

The Biomass molecular weight is given by (MW_{BM}):

$$MW_{BM} = MW_C + MW_C + z\, MW_C + p\, MW_C \ , (kg/kmole)$$

Biomass Energy Input is calculated as (Q_{BM-in}):

$$Q_{BM-in} = m_{BM}\ HV_{BM}\ , (MJ)$$

The Cold Energy Output is determined by the following equation based on room temperature analysis ($Q_{Cold-Out}$):

$$Q_{Cold-Out} = n_{CH4}\ CV_{CH4} + n_{CO}\ CV_{CO} + n_{H2}\ CV_{H2}\ , (MJ)$$

The Hot Energy Output is determined by the following equation based on high-temperature analysis ($Q_{Hot-Out}$):

$$Q_{Hot-Out} = n_{CH4}\ (CV_{CH4} + Cp_{CH4}(T - T_o)) + n_{CO}\ (CV_{CO} + Cp_{CO}(T - T_o)) + n_{H2}\ (CV_{H2} + Cp_{H2}(T - T_o))\ , (MJ)$$

Cold Gas Efficiency is determined by (η_{Cold}):

$$\eta_{Cold} = \frac{Q_{Cold-out}}{Q_{BM-in}}$$

Hot Gas Efficiency is determined by (η_{Hot}):

$$\eta_{Hot} = \frac{Q_{Hot-out}}{Q_{BM-in}}$$

Chapter 3: Results and Discussion

3.1 Introduction

In this chapter, the results obtained from the gas analyzer and temperature measurements throughout all tests, are reported and discussed. Section 3.2 covers the instant measurement of the gases yield of CH_4, CO, CO_2, H_2, N_2, and the sample temperature for three representative cases: case 2, case 10 and case 22 respectively (see Table 9). The repeatability tests are demonstrated by comparing two results for each case for the same test, which is performed at different times. Additionally, the calculated biomass input energy, the "cold gas produced energy", the "hot gas produced energy", and the cold and hot gas efficiency for the corresponding cases are displayed and discussed. In section 3.3, a parametric study effect, of all parameters investigated on the "average gas concentration volume percentage" of the bio-syngas yield, is stated and discussed. Finally, the statistical analysis, using Minitab to model the "average gas concentration volume percentage yield" as function of all dependent parameters, is determined for the main yield gases (CH_4 and CO).

3.2. Instantaneous Gas Yield Concentration Cases

3.2.1 Case 2: Microwave Power=1000 W, MC=0, DSP= 783 μm

In what follows, the results of case 2 (listed in Table 9) are presented and discussed. Figure 14 represents the instant gas concentration volume percentages for CH_4, CO, CO_2, H_2, N_2, and the temperature measurements respectively. It is noticeable, that the onset of the pyrolysis process takes place after about 60 seconds from the start of the heating process by the microwave action, where all bio-syngas components start showing a clear increase in their concentrations. This precisely

matches the time needed to start visually seeing the smoke released from the reactor, as well as the time for the tested biomass sample to reach a temperature of about 350°C. As time progresses, the sample temperature starts increasing further, resulting in a clearer increase in the concentrations of the bio-syngas produced. It can be observed that the peak yield concentration is achieved after about 160 seconds from the start of the heating process, which is concurrent with the maximum temperature of the sample. The figure displays clear concentration peaks with maximum gas concentration volume percentages (GCVP) of 48.46%, 26.01%, 11.04%, and 8.45% for CH_4, CO, CO_2, and H_2 respectively. Meanwhile, N_2 concentration reaches the lowest reading of 7.89%. The attained peak temperature of the sample was measured to be about 680°C, which corresponds with the point where the peak concentrations of the produced syngas are attained. Subsequently, the produced gas concentration starts decreasing; at the same time the N_2 concentration starts increasing until it goes back to its original concentration values after 650 seconds from the start of the heating process, where the yield gas concentration gradually hits zero. Also, the temperature maintains a plateau at a peak value for 150 seconds; then it slowly decreases to maintain a constant value at 590°C until the end of the experiment, which could be explained by the fact that most of the biomass was burnt. Overall, the time needed to complete the whole process is about 500 seconds from the moment the heating starts until the release of all yield gases obtained.
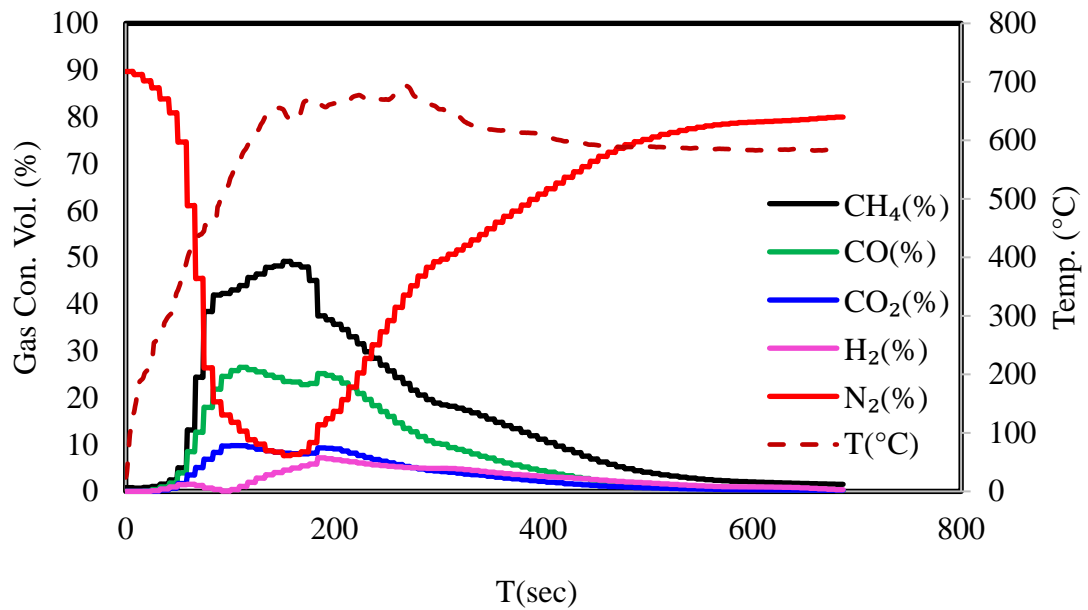
Figure 14: Instantaneous gas concentrations volume percentages and temperature measurements for case 2: MW power= 1000 W- DSP= 783 μm- MC= 0

Figure 15 displays the repeatability of the measurements of all gas concentration volume percentages for two separate tests of case 2. The results reveal an excellent repeatability for the two tests. As shown, the percentage difference in the two tests, at the peak value, is 3%, 5% for CH_4% and N_2% respectively. The repeatability graph exhibits how each experiment was performed so carefully with the exact steps under the same conditions correctly.
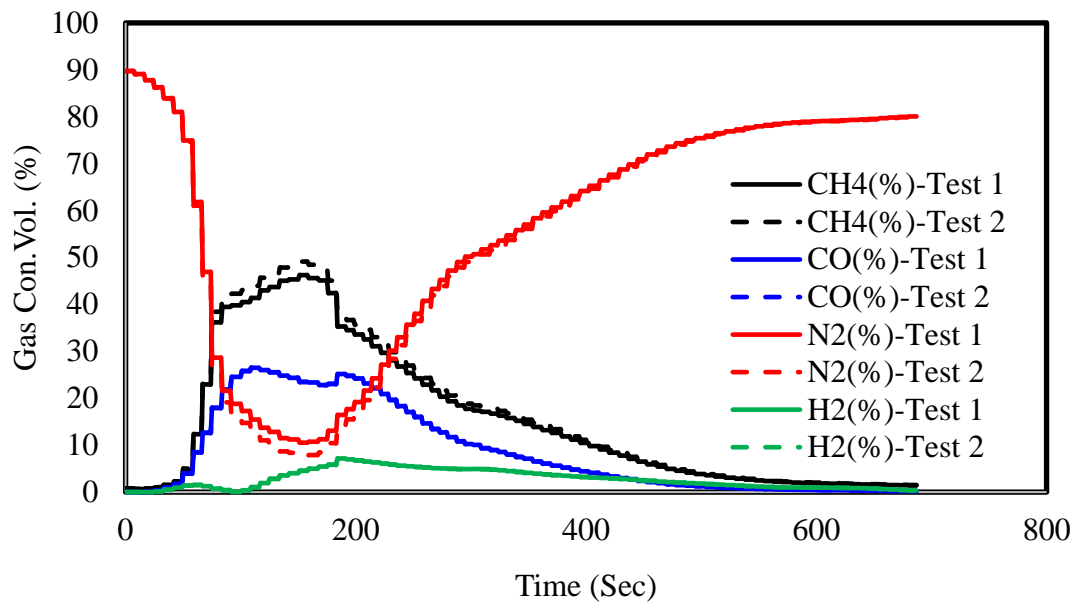
Figure 15: Repeatability check for the gas concentrations volume percentages of case 2: MW power= 1000 W- DSP= 783 μm- MC= 0

Figure 16 shows the biomass energy input (Qin) in (MJ), the accumulated hot gas produced energy (Q_out-Hot) in (MJ), the accumulated cold gas produced energy (Q_out-Cold) in (MJ), the accumulated hot gas efficiency (η_{Hot}%)and accumulated cold gas efficiency (η_{Cold}%) as functions of time. The gas efficiency represents the performance of the pyrolysis process, which is defined by the ratio between the yield gases produced energy and the energy contained within the biomass sample used in the test. From the figure, it can be noticed that the cold and hot gas produced energy, and the efficiency have the same trend, where from the onset of the yield gases the curve starts growing at the same rate as that of yield gas until it reaches the peak value. After that, stays almost constant with a minimal increase rate. The highest reported values for η_{Hot} (%) and η_{Cold} (%) are 63.21% and 61.82% respectively, corresponding to maximum values of Q_out-Hot and Q_out-Cold of 0.0971 MJ and 0.0952 MJ respectively.

Figure 16: Energy added, hot and cold gas produced energy in (MJ), hot and cold gas efficiency percentages for case 2: MW power= 1000 W- DSP= 783μm- MC= 0

3.2.2 Case 10: Power=700 W, MC=0, DSP= 467 μm

Figure 17 shows the instant gas concentration volume percentages for CH_4, CO, CO_2, H_2, N_2, and temperature measurements respectively for Case 10. It is clear, that the beginning of the pyrolysis process where all bio-syngas begin produced after roughly 60 seconds of the beginning of the heating process, which is accurately the time expected to begin seeing the smoke created from the reactor and the sample temperature achieved 291°C. As time progresses and the sample temperature begins increasing, in the same time, the GCVP of all yield gases begin increasing. It is noTable that the peak yield concentration is accomplished after 101 seconds from the beginning of the heating process, which stays constant with the highest temperature of the sample. The figure shows clear peaks with the highest GCVP of 61.36%, 17.4%, 9.5%, and 2.19% respectively for CH_4, CO, CO_2, and H_2.

On the other hand, N_2 achieves the minimum reading of 9.41%, and the peak temperature relating to the peak gas yield concentration is 675°C. It has been seen that as produced gas concentration begins decreasing the N_2 concentration increments until it retrains back to it is the original value. Likewise, the temperature stays at the maximum level for about 144 seconds, and afterwards, it starts to gradually decrease to stay constant at 630°C until the end of the experiment, which could be clarified by the fact that the majority of the biomass is consumed. It took around 310 seconds to release all the yield gases.

Figure 17: Instantaneous gas concentrations volume percentages and temperature measurements for case 10: MW power= 700 W- DSP= 467 μm- MC= 0

Figure 18 shows the repeatability of the results of case 10 for two tests conducted at different times under the same conditions. The results uncover very good repeatability everywhere throughout the two conducted tests. As demonstrated, the percentage difference in the peak concentrations of CH_4%, N_2% and H_2% in the two

conducted tests are 4%, 1%, and 0.5% respectively. The graph demonstrates good repeatability for the two reported cases.

Figure 18: Repeatability check for the gas concentrations volume percentages of Case 10: MW power= 700 W- DSP= 467 μm- MC= 0

Figure 19 displays the instant biomass energy input (Qin) in (MJ), the accumulated hot gas produced energy (Qout-Hot) in (MJ), the accumulated cold gas produced energy (Qout-Cold) in (MJ), the accumulated hot gas efficiency (η_{Hot}%) and accumulated cold gas efficiency (η_{Cold}%). From the figure it may be seen that the cold and hot yield energy and the efficiency have a similar pattern, the rate of increase in the reported quantities, with time, starts increasing clearly after reaching an effective pyrolysis temperature. After a while, the rate of pyrolysis becomes slow leading only to incremental changes in the reported values. The highest revealed values for η_{Hot} and η_{Cold} are 56.98% and 55.24% corresponding to Qout-Hot and Qout-Cold of 0.0844 MJ and 0.0819 MJ, respectively.
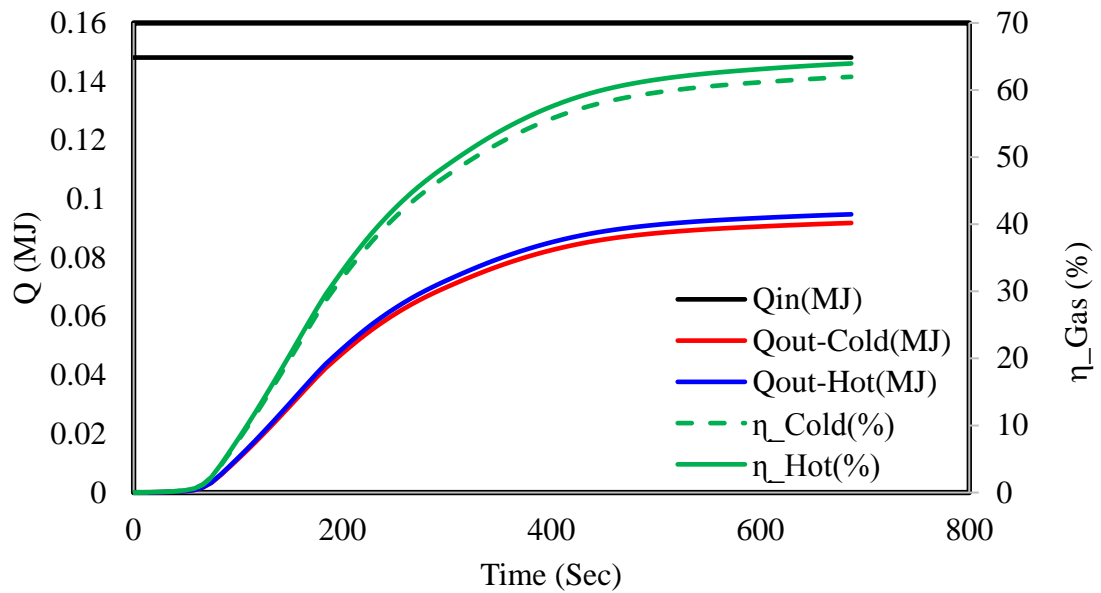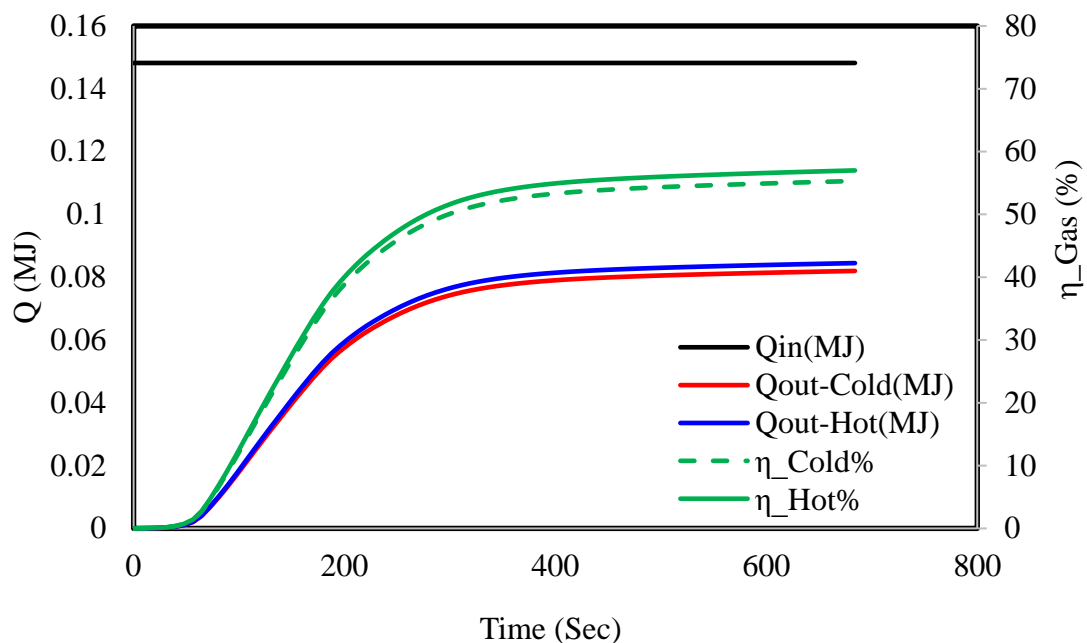
Figure 19: Energy added, hot and cold gas produced energy in (MJ), hot and cold gas efficiency percentages for case 10: MW power= 700 W- DSP= 467 μm- MC= 0

3.2.3 Case 22: Power=300 W, MC=0.2, DSP= 467 μm

Figure 20 presents the instant gas concentrations volume percentages for CH_4, CO, CO_2, H_2, N_2, and the temperature measurements for case 22. It might be seen, that the start of the pyrolysis process, where all bio-syngas start appearing, is after 69 seconds from the onset of the heating process. This is the time where the release of visible fumes, emerging from the exit port of the reactor, start to become noticeable. At that time, the temperature of the biomass sample measures to be about 212°C. As time progresses, and the sample temperature starts increasing, the GCVP of all yield gases start increasing. It will, in general, be seen that the peak yield concentration appeared after 192 seconds from the earliest starting point of the heating process, where the maximum temperature of the sample occurred. The figure indicates clear peaks with the most significant gas concentrations of 32.39%, 3.38%, 3.12%, and 3.08% for CH_4, CO, CO_2, and H_2 respectively. Where N_2 shows the most decreased

reading of 43.43%; the peak temperature occurred with the peak gas yield concentration is about 472°C. As the test progresses, the yield gases and N_2 behave similar to the previous cases. Similarly, the temperature stays at the peak for 67 seconds, subsequently, it gradually reduces to keep up steady at 370°C until the end of the experiment. It took around 610 seconds to discharge all the yield gases.
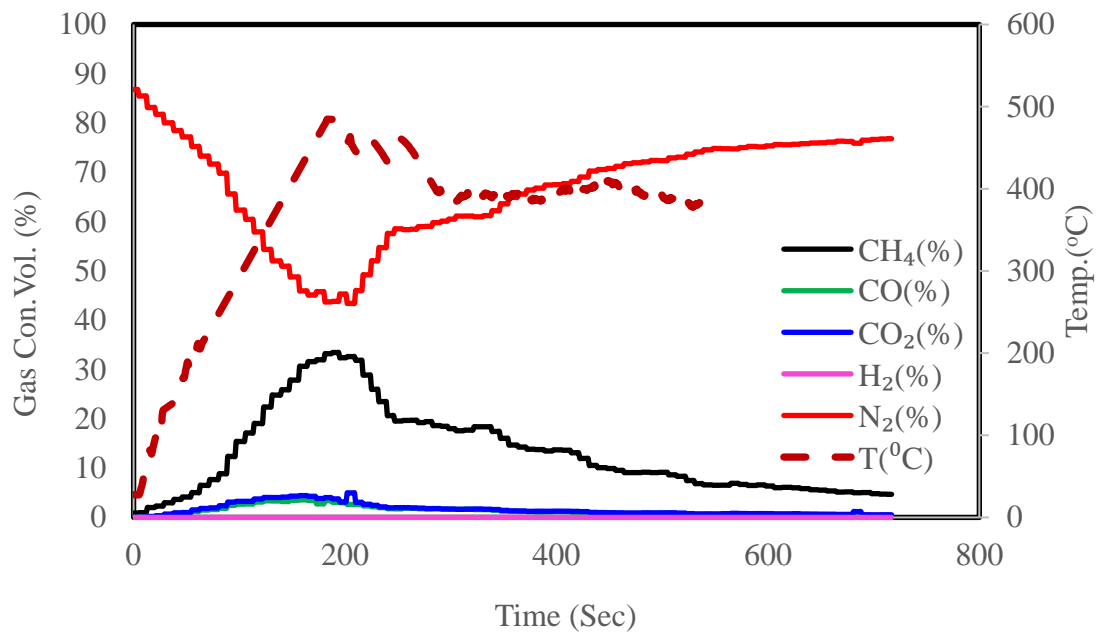
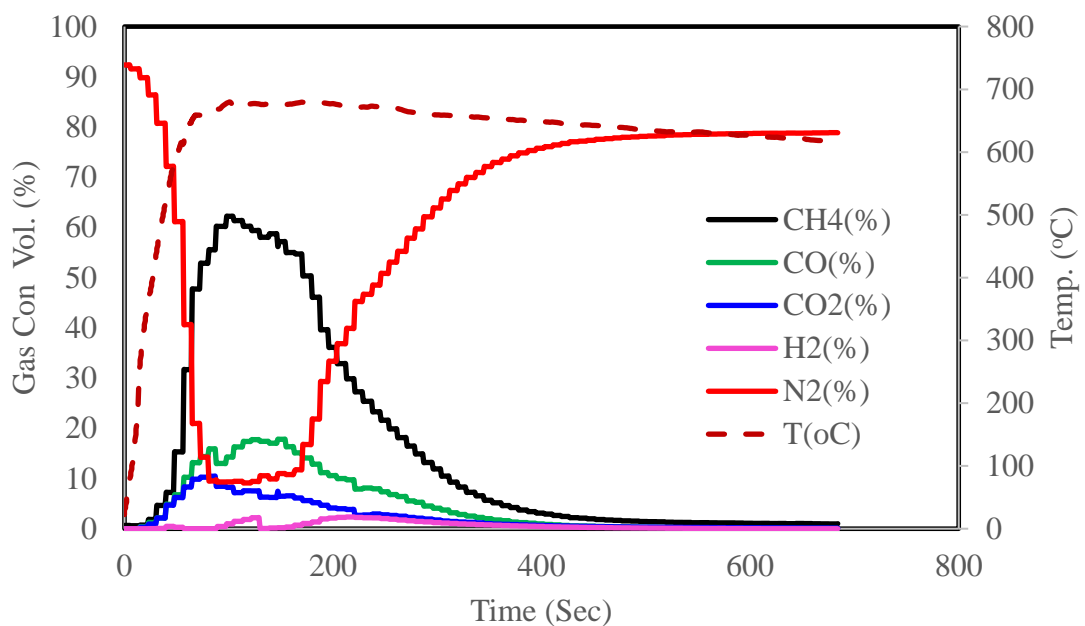Figure 20: Instantaneous gas concentrations volume percentages and temperature measurements for case 22: MW power= 300 W- DSP= 467 μm- MC= 0.2

Figure 21 demonstrates the repeatability of the measurements of all gas volume percentages concentrations for two separate tests of case 22. The results reveal significant repeatability. As can be seen, the difference in the peak concentrations in the two repeated tests are 0.2%, 0.5% exclusively for $CH_{4\%}$ and $N_2\%$.
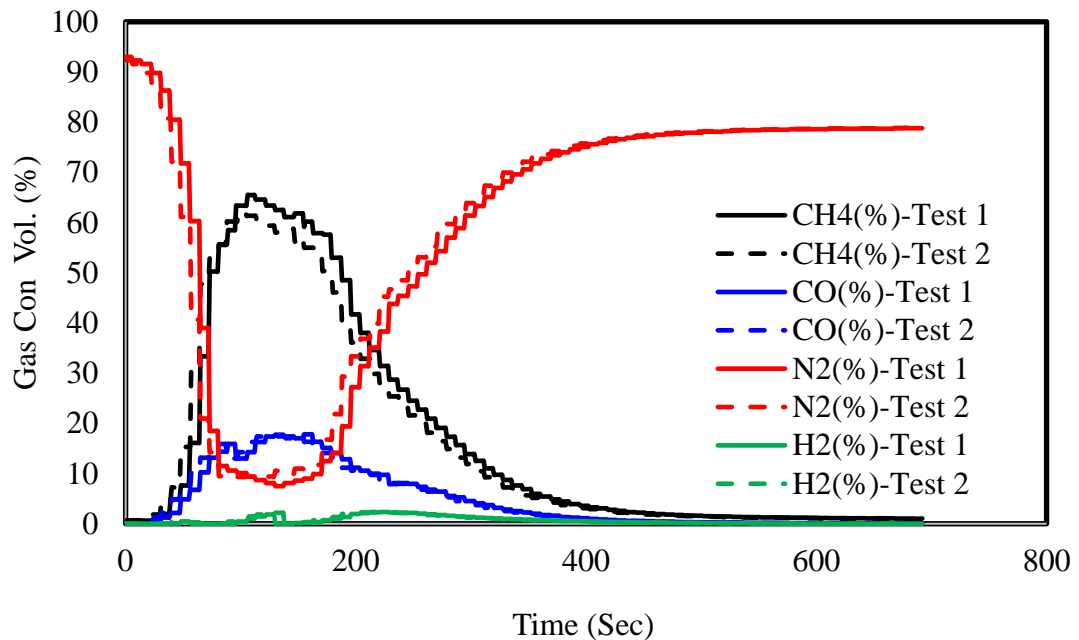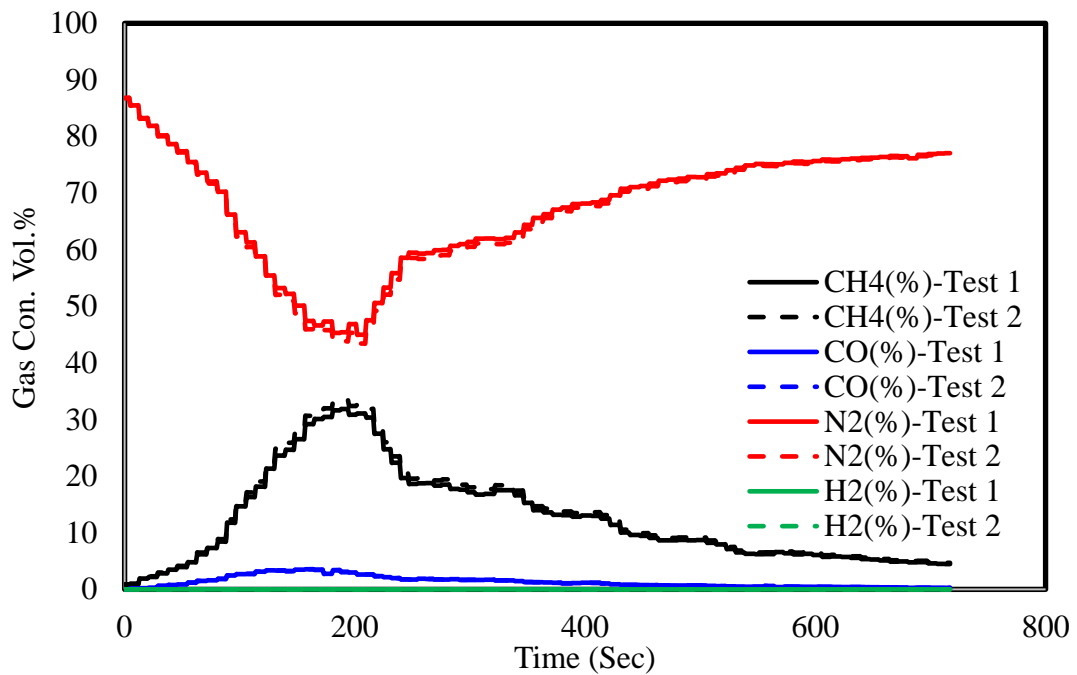
Figure 21: Repeatability check for the gas concentrations volume percentages of Case 22: MW power= 300 W- DSP= 467 μm- MC= 0.2

Figure 22 demonstrates the instant biomass heat input (Qin) in (MJ), the accumulated hot gas produced energy (Qout-Hot) in (MJ), the accumulated cold gas produced energy (Qout-Cold) in (MJ), the accumulated hot gas efficiency (η_{Hot}%) and accumulated cold gas efficiency (η_{Cold}%). The highest reported value for η_{Hot} (%) and η_{Cold} (%) are 56.55% and 54.99% respectively, identifying with most high estimations of Qout-Hot and Qout-Cold of 0.0668 MJ and 0.0641 MJ respectively. It can be noticed that some of the biomass material is not totally converted which leads to lower the yield gases and consequently, lower the gas produced energy compared to the previous cases.

It is observed from all studied cases that CH_4 concentration yield percentage is dominating the bio-syngas production. Meanwhile H_2 concentration yield percentage has the lowest value among all produce gases. This is may be due to the methanation process [79] that occurs during the heating process knowing that from previous

elementally study for the used DSP that it contains some metals such as P, Ca, Al, Mg, Cu, and Zn, which may act as a catalyst which promotes the process of methanation in temperature range of 250°C to 450°C [80].

It is worth mentioning in all previous cases that the pyrolysis process occurred under almost inert gas, and due to some leak of O_2 gas from the system a posible partial combustion process is taking place, which results in the generation of small quattity of CO_2 as shown in the results.
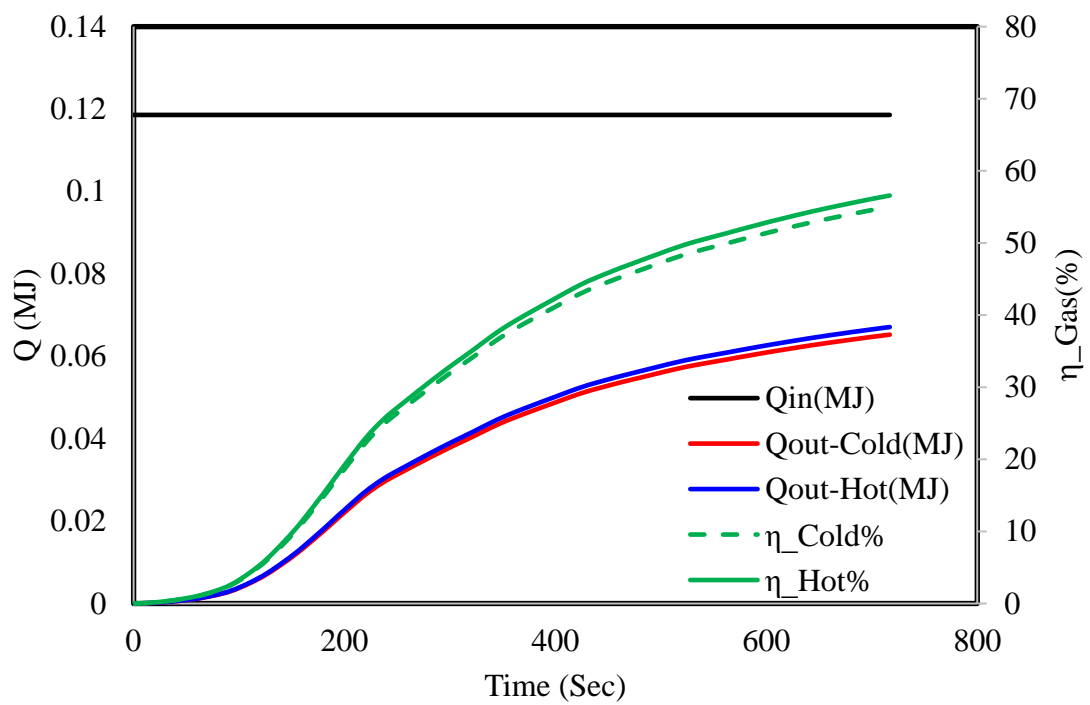
Figure 22: Energy added, hot and cold gas produced energy in (MJ), Hot and Cold Gas Efficiency percentages for Case 22: 300 W- DSP=467 μm- MC=0.2

3.2 Processed Data Analysis

3.2.1 Effects of Microwave Power on Bio-syngas Yield

Figure 23 shows the effect of microwave power on the average CH_4 concentration volume percentages yield for all particle sizes and moisture content percentages. The figure contains three groups with each group representing nine cases. In this section, it is worth mentioning that in all figures, the solid colored bars represent the dry solid mass cases where (MC=0); the diagonal pattern represents the case with a moisture content of (MC=0.2), and finally, the horizontal pattern refers to the case with a moisture content of (MC=0.4). The black color refers to the case of (DSP=467 mm), the red color represents the case of (DSP=783 mm) and the blue color is used to represent the case of (DSP=1790 mm).

A common observation for all three power cases, is that as the moisture content increases the average gas concentration volume percentage (Avg-GCVP) yield decreases at different rates. For the case of microwave powers of 1000 W and 300 W, it is noticed that the smaller the size of date particles in the sample, the higher the Avg-GCVP yield; except for the case of a microwave power of 700 W, where the large sample particle size reveals opposite results. It should be noted that this conclusion has been confirmed by repeating the test different times reaching the same outcomes.

In the case of a microwave power of 1000 W, the dry sample, and the smallest particle size, the maximum CH_4 average concentration volume percentage yield is about 17.91%. Meanwhile, the lowest is 8.8% for the same microwave power paired with the small particle size and a moisture content of 0.4. For the case of a microwave power of 700 W, the maximum CH_4 Avg-GCVP yield is 21% when coupled with the dry sample and the largest particle size; the lowest, on the other hand, is 9% for the

case of small particle size and moisture content of 0.4. Finally, when using a microwave power of 300 Wand a dry sample of the smallest size, the maximum CH_4 Avg-GCVP yield is 17.2%. However, the lowest is 8.4% for the case of small size and moisture content of 0.4 under the same microwave power of 300 W.

Figure 23: The effect of microwave power on CH_4 volume percentages for all of particle sizes and MC percentages cases

Figure 24 represents the effect of Microwave power on the average CO concentration volume percentages at all particle sizes and MC percentages. Qualitatively the behavior here is almost the same as the one observed in the case of the CH_4. However, quantitatively, the levels of CO concentrations are much lower than the CH_4 levels. The cases of 1000 W and 700 W led to more CO production than the case with 300 W, wherein the later case, the CO production level was almost platue for all tests conducted in this group.

For the case of a microwave power of 1000 W, the maximum CO average concentration yield is 8.67% when applied to a sample of dry and medium particle size; while the lowest is 2.32% if the power were to be applied on a sample of medium particle size and a moisture content of 0.2. When a microwave power of 700 W is used, the maximum CO Avg-GCVP yield is 6.83% for the case of dry and largest particle size, while the lowest is 2.3% for the case of small particle size and moisture content of 0.4. In the end, in the case of a microwave power of 300 W and a dry sample of the largest particle size the maximum CO Avg-GCVP yield is 2.44%. Meanwhile, the lowest is 1.3% for the case of smallest particle size and moisture content of 0.2 under the same microwave power.

Figure 24: The effect of microwave power on CO volume percentages for all of particle sizes and MC percentages cases

Figure 25 represents the effect of microwave power on the average CO_2 concentration volume percentages at all of the particle sizes and MC percentages.

The trend is not clear here because of the low concentrations of the CO_2 produced, in contrast to the cases of CH_4 and CO. The case of 700 W showed more CO_2 gas than the cases of 1000 W and 300 W. For the case of microwave power of 1000 W the maximum CO_2 Avg-GCVP yield is 3.41% when paired with a dry sample and medium particle size, while the lowest is 0.65% for the case of medium particle size and moisture content of 0.2. When using a microwave power of 700 W the maximum CO_2 Avg-GCVP yield is 3.38% for the case of dry and largest size, while the lowest is 1.58% for the case of medium size and a moisture content of 0.4. Finally, for the case of a microwave power of 300 W, the maximum CO_2 Avg-GCVP yield is 3.01% when used on a sample dry and medium sized particle; while the lowest is 1.43% for the case of medium size and moisture content of 0.4. As mentioned earlier the low Avg-GCVP of CO_2 is expected to be supplemented due to the partial combustion process in the system, because of some O_2 gas leak form the system.
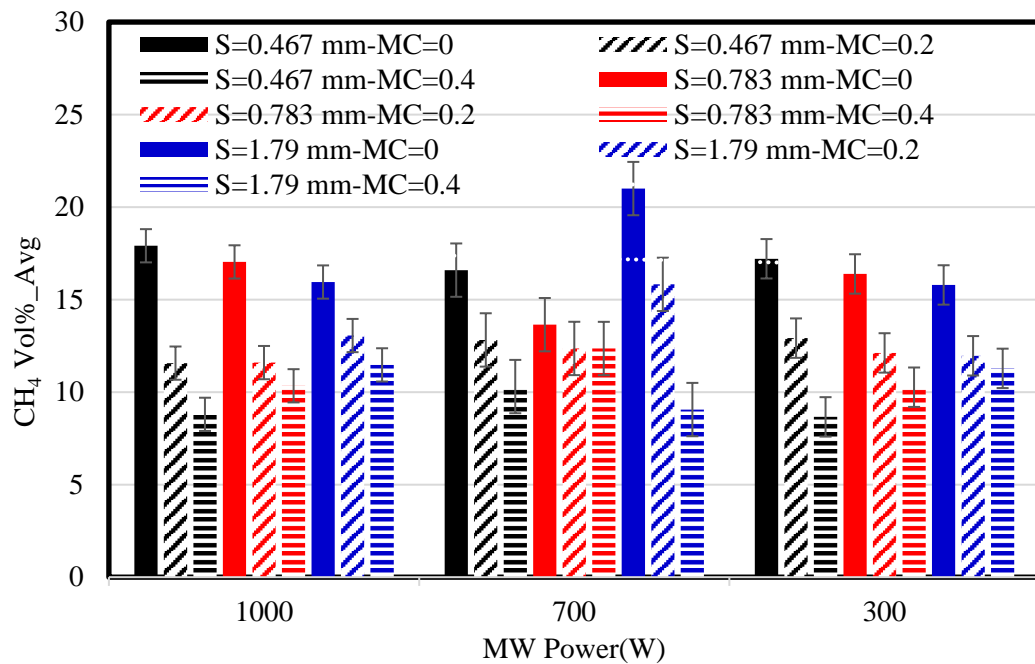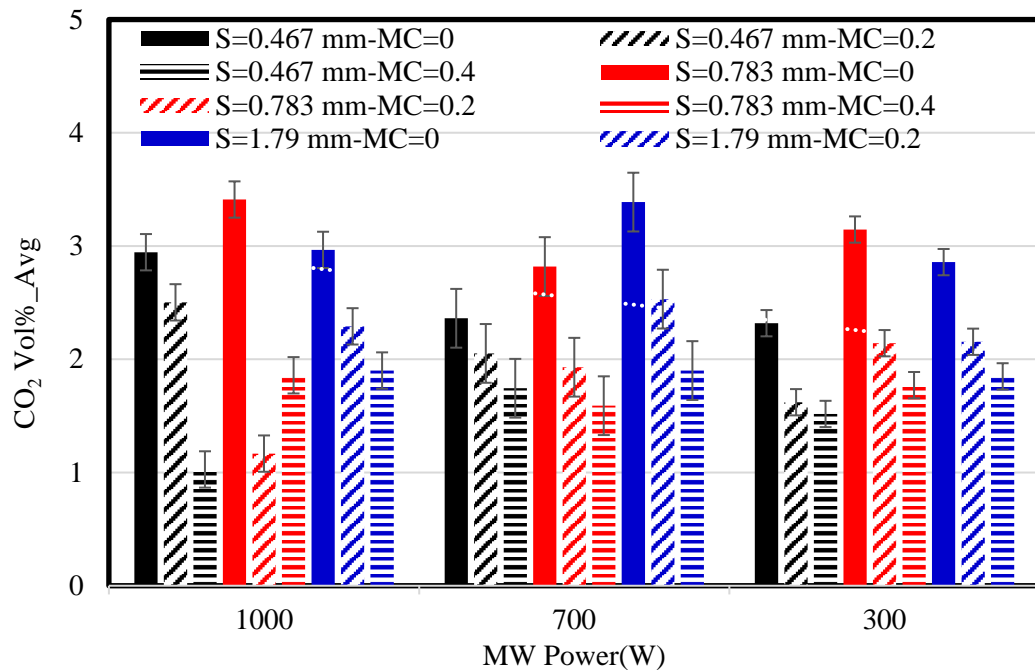

Figure 25: The effect of microwave power on CO_2 volume percentages for all of particle sizes and MC percentages cases

Figure 26 represents the effect of microwave power on the average H_2 concentration volume percentages at all of the particle sizes and MC percentages. It can be observed in all cases that the only measurable H_2 value is for 1000 W case. Meanwhile, the 300 W case has very low values, and it is hard to see any H_2 released from the pyrolysis process. For the case of 700 W, we can see that the percentages vary between 0.86% and 0.18%. For 1000 W microwave power case, the highest Avg-GCVP yield is 2.71% if applied on a sample of dry and medium particle size, while the lowest Avg-GCVP yield is 0.27% if it were to be applied on a sample of medium particle size and a moisture content of 0.4. We believe that the low concentrations of H_2 in the yield gas is possibly attribuTable to the depletion of H_2 due to methanation process, which is supported by the presence of catalytic metals and operating under the appropriate temperature range.
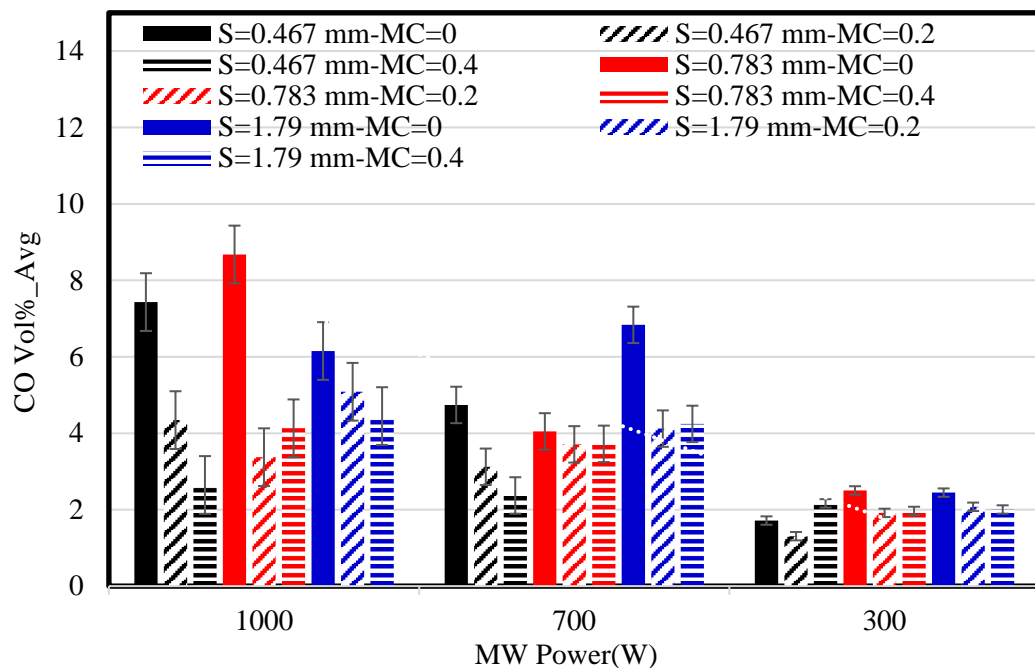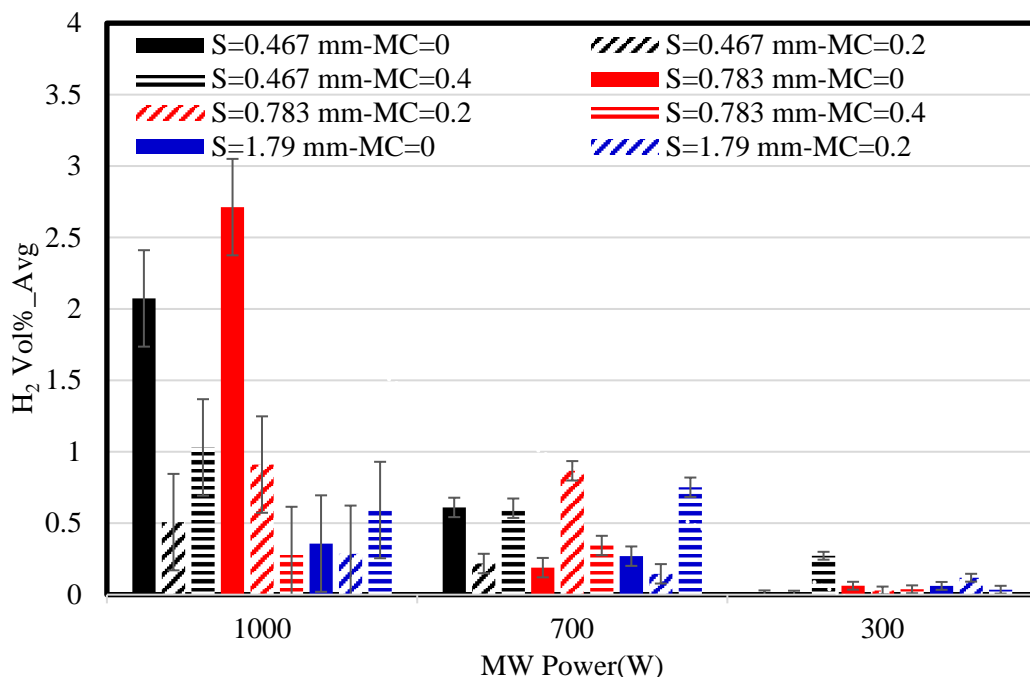

Figure 26: The effect of microwave power on H_2 volume percentages for all of particle sizes and MC percentages cases

Figure 27 gives the effect of Microwave power on the average Cold Gas Efficiency ($\eta_{Cold-Avg}$) at all of the particle sizes and MC percentages. Figure 28 presents the effect of Microwave power on the average Hot Gas Efficiency ($\eta_{Hot-Avg}$) at all of the particle sizes and MC percentages. The values of ($\eta_{Hot-Avg}$) and ($\eta_{Cold-Avg}$) have small differences, so both of them almost have almost the same values. The efficiency values for the different tests for the three microwave power groups tested do not show much variations nor a trend that may allow the drawinging of a conclusive conclusion. At 1000 W the highest values of ($\eta_{Cold-Avg}$) and ($\eta_{Hot-Avg}$) are 54.39% and 56.11% respectively for the case of largest particle size and the moisture content of 0.4. Meanwhile, the lowest ($\eta_{Cold-Avg}$) and ($\eta_{Hot-Avg}$) equal to 33.07% and 34.04% respectively for the case of smallest particle size and moisture content of 0.4.

For the 700 W group of samples, the highest reported values are 54.04% for ($\eta_{Cold-Avg}$) and 55.71% for ($\eta_{Hot-Avg}$) for the largest size and dry sample, while the lowest ($\eta_{Cold-Avg}$) and ($\eta_{Hot-Avg}$) are 29.88% and 30.79% respectively for the medium size and a moisture content of 0.2. The highest value of ($\eta_{Cold-Avg}$) and ($\eta_{Hot-Avg}$) for the 300 W group of samples occurred with 38.42% and 39.54% respectively for the case of the largest particle size and a moisture content of 0.2. On the other hand, the lowest values of ($\eta_{Cold-Avg}$) and ($\eta_{Hot-Avg}$) are 20.45% and 21.06%, respectively and are attained in the case of the smallest particle size and a moisture content of 0.4.

We conclude from this case that the higher the microwave power, the more the heat that will be applied on the biomass sample which will enhance the internal heating

process in the biomass sample, this will, in turn, will help to increase the amount of the yield produced gases.
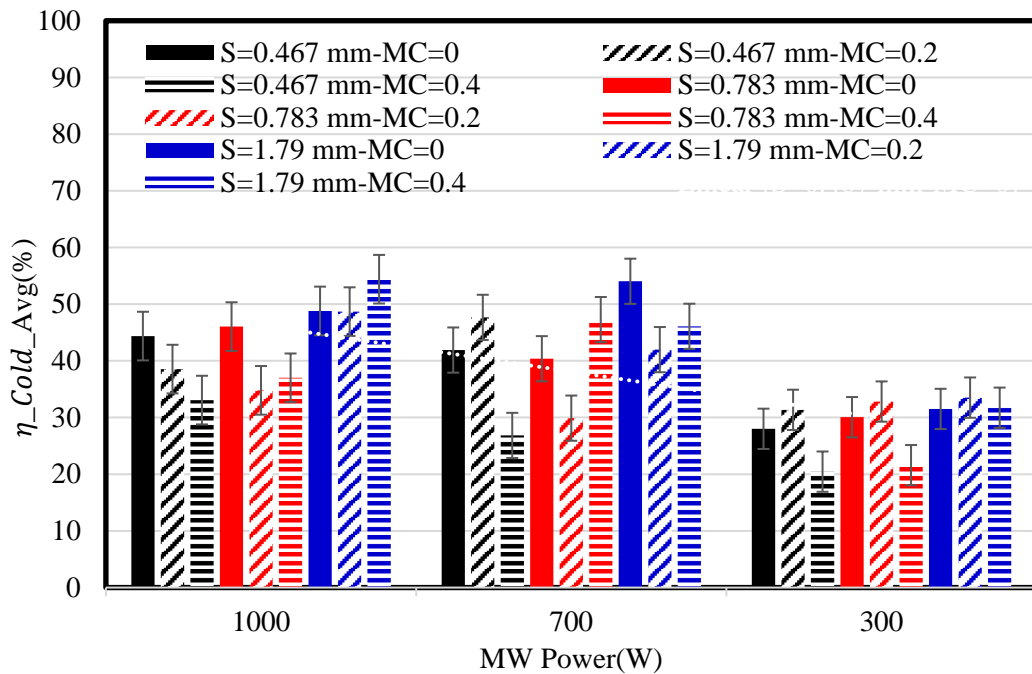
Figure 27: The effect of microwave power on the cold gas efficiency for all of particle sizes and MC percentages cases
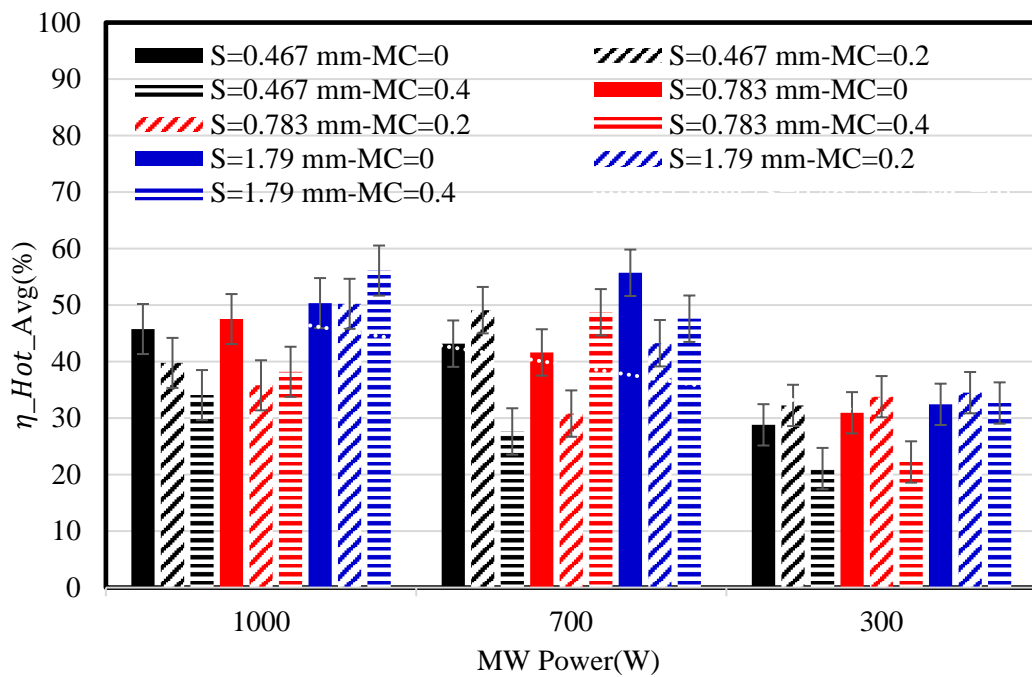
Figure 28: The effect of microwave power on the hot gas efficiency for all of particle sizes and MC percentages cases

3.2.2 Effect of Date Seed Particle Size Effect on Bio-syngas Production

Figure 29 represents the effect of the particle size on average CH_4 concentration volume percentages at all of the microwave powers and MC percentages. The cases were distributed into three groups; each group represents nine cases. In this section, in all figures: the solid colored bars represent the dry cases where (MC=0), the diagonal pattern represents the case with a moisture content of (MC=0.2), and finally, the horizontal pattern refers to the case with a moisture content of (MC=0.4). The black color refers to the case of 1000 W, the red color represents the case of 700 W, and the blue color used to represent the case of 300 W. It worth mentioning that all these cases have been discussed previously, but the primary purpose is to try to study the effect of the particle size sample on the Avg-GCVP yield.

For the case of 467 μm particle size: the maximum CH_4 Avg-GCVP yield is 17.91% when paired with the conditions of a dry sample and a microwave power 1000 W; the lowest is 8.66% with a microwave power 300 W and moisture content of 0.4. When using a dry sample size of 783 μm, with a microwave power of 1000 W the maximum CH_4 Avg-GCVP yield is 17.03%. Meanwhile, the lowest concentration is 8.37% for of a microwave power 300 W and moisture content of 0.4 in a sample of the same size. Finally, the maximum CH_4 Avg-GCVP yield is 21% is attainted with a dry sample with a particle size of 1790 μm under a microwave power of 700 W, on the other hand, the lowest concentration of 9.05% is achieved with a sample of the same size but with a moisture content of 0.4 and a microwave power of 700 W. We can conclude from the figure that the best performance is attained for the largest particle size.

Figure 29: The effect of the particle size on CH₄ volume percentages for all of microwave powers and MC percentages cases

Figure 30 shows the effect of the particle size on the average CO concentration volume percentages at all of the microwave powers and MC percentages. The trend here is not clear for all of the cases. For the case of 467 μm, it's noticed that the maximum CO Avg-GCVP yield is 7.43% when using a dry sample and a microwave power of 1000 W, and the minimum is 1.3% when using a microwave power of 1000 W and a sample of moisture content 0.2. As for a sample size of 783 μm, it's noticed that the maximum CO Avg-GCVP yield is 8.67% for the case of dry and Microwave power 1000 W, and the minimum is 1.6% in the case of microwave power 1000 W and moisture content 0.4. Lastly, In the case of 1790 μm, it is observed that the maximum CO Avg-GCVP yield is 6.83% and the minimum is 1.82% for the cases of dry and microwave power 700 W and the case of microwave power 300 W and moisture content 0.4 respectively. We can conclude that different sizes, in average, produce comparable results under different MW and MC.

Figure 30: The effect of the particle size on CO volume percentages for all of microwave powers and MC percentages cases

Figure 31 express the effect of the particle size on average CO_2 concentration volume percentages at all of the microwave powers and MC percentages. For all cases with moisture content above zero, the figure shows slightly more CO_2 production, the larger the particle size. For the cases with zero moisture content, the CO_2 production is, more or less, not affected by the particle size, especially for the intermediate to high particle size range studied in this research. For the cases with the same moisture content, the CO_2 production does not seem to be notably effected by the level of microwave power used.

For example, in the case of a dry sample with a particle size of 467 µm the maximum CO_2 Avg-GCVP yield was found to be about 2.94% when the microwave power is 1000 W. Meanwhile the lowest concentration is 1.02% when associated with the case when the moisture content, of a sample of the same particle size, is 0.4 and microwave power is 1000 W. In a sample particle size of 783 µm the maximum CO_2

Avg-GCVP yield is about 3.41% and this is attained when the sample is dry and the microwave power is 1000 whoever, the minimum CO_2 Avg-GCVP was found to be about 1.16% and this happens when the microwave power is 1000 W, and the moisture content is 0.2. Finally, for the test group with maximum particles size of 1790 μm the highest CO_2 Avg-GCVP yield is about 3.38% and this is associated with the case of a dry sample and a microwave power of 700 W. The lowest CO_2 Avg-GCVP for this same group is about is 1.85% and this corresponds to the case of microwave power of 300 W and moisture content of 0.4.

In general, the test group with the smallest particle sizes resulted in lowest CO_2 concentrations. This may mean that the particle sizes (although they have larger surface area than the bigger particles) are very compact and have low porosity in the inner body of the sample. In comparison with the bigger particles in the other two groups, containing more voids between them, which may allow for an easier access for the O_2 to pass within these bigger pores in the core of the sample. This will possibly give more chances for carbon oxidation within the sample, since, effectively, the surface area of the sample, that is exposed to the oxygen environment, becomes greater as the particles increase in size. Compare this with the case of the smaller particle size sample, where the inner core of this sample would effectively be hidden and not have easy access to the surrounding oxygen that came with the circulated gas in the reactor.
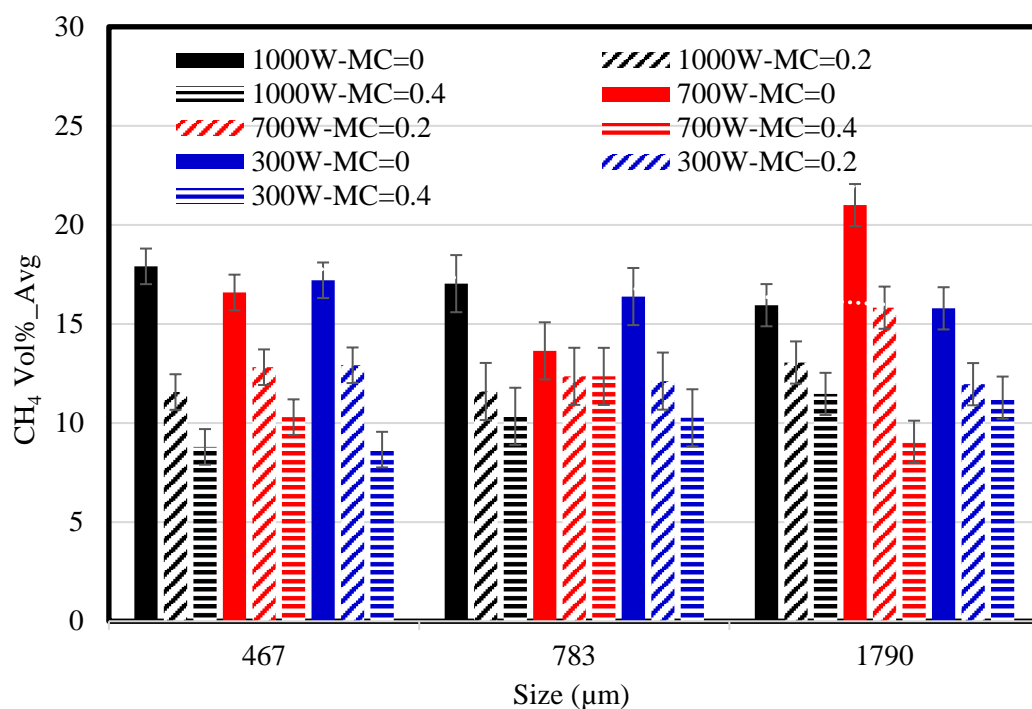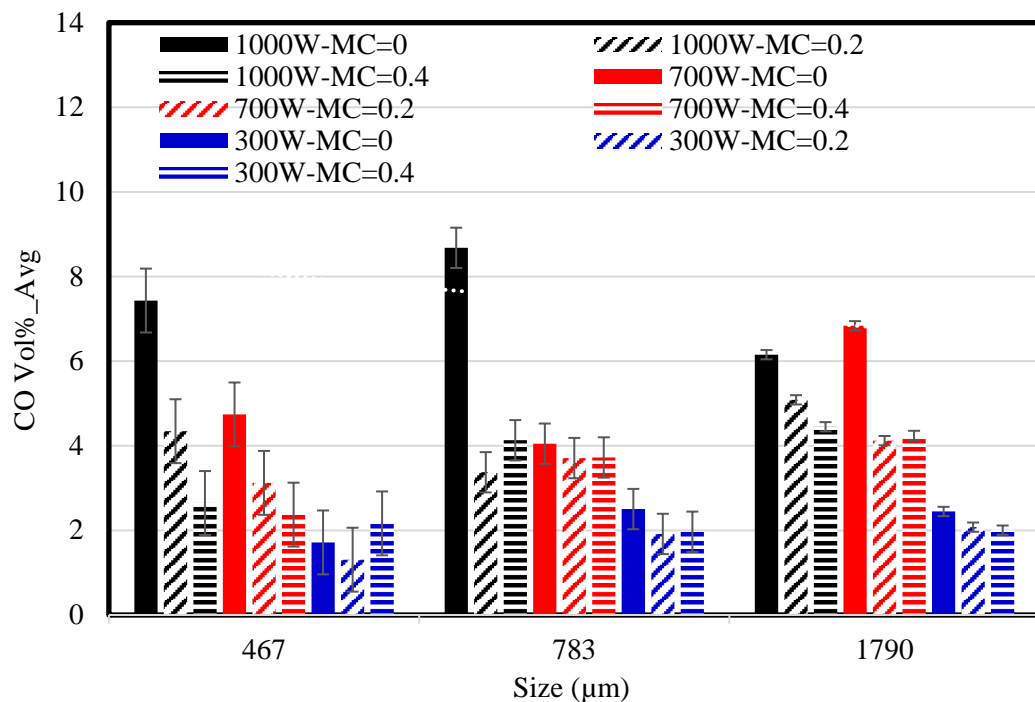
Figure 31: The effect of the particle size on CO_2 volume percentages for all of microwave powers and MC percentages cases

Figure 32 shows the effect of the particle size on average H_2 concentration volume percentages in the yield gas at all of the microwave powers and MC percentages. The results show that it is hard to see any significant amounts of H_2 released from the pyrolysis process, except in some certain cases in each sample size. For the case of particles with size of 467 μm, we can see that the maximum H_2 Avg-GCVP yield is 2.07% for the dry sample and microwave power of 1000 W.

As for the case of particles with size of 783 μm the highest H_2 Avg-GCVP yield is 2.71% when paired with a dry sample and microwave power of 1000 W. For the case of particles with a 1790 μm size in a sample with a moisture content of 0.4 the maximum H_2 Avg-GCVP yield is about 0.75% under a microwave power of 700 W.

Finally, to explain the trends seen in Figure 32, we might recall the methanation process described earlier. Through that process the produced hydrogen might have gone through methane production steps that may explain the higher methane production rates, as compared to low H_2 production. Hence, it might be reasonable to explore, in a future study, this point in further details. It is clear from Figure 32 that such a possible scenario is more pronounced when the test sample contains moisture and when the size of the particles in the sample is relatively large.
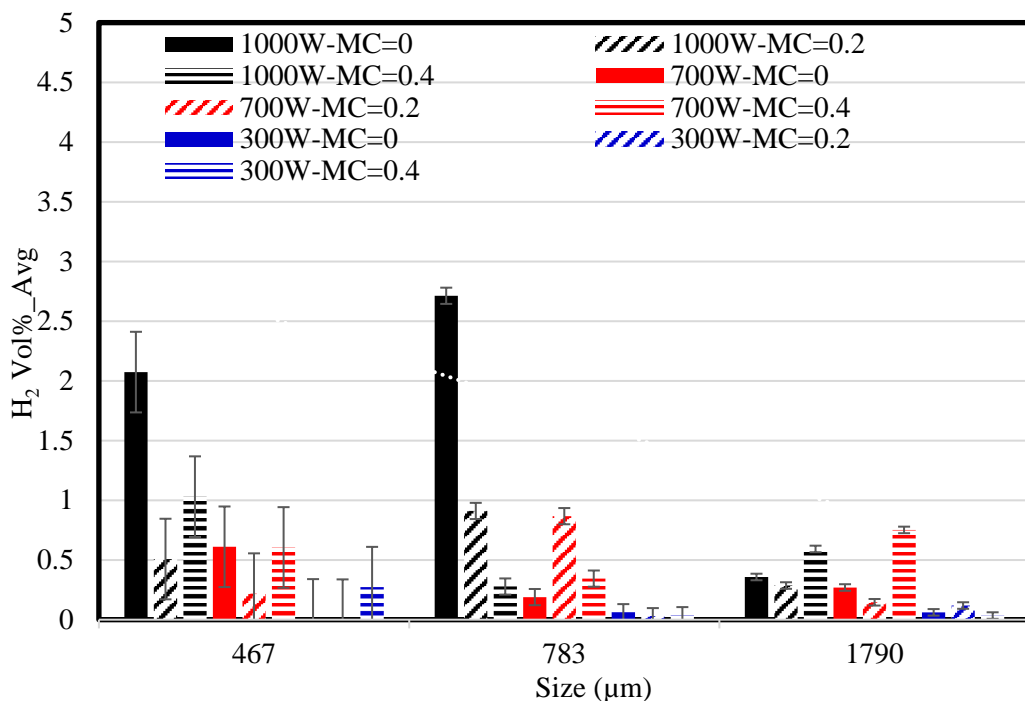
Figure 32: The effect of the particle size on H_2 volume percentages for all of microwave powers and MC percentages cases

Figures 33 and 34 express the effect of the particle size on the cold and hot gas efficiency for all of the microwave powers and MC percentages. The difference in values of $\eta_{Hot-Avg}$ and $\eta_{Cold-Avg}$ is insignificant. For the case of 467 μm particles the highest values for $\eta_{Cold-Avg}$ and $\eta_{Hot-Avg}$ are 47.67% and 49.1% respectively and this happens when the microwave power is 700 W and the moisture content is 0.2. The lowest efficiency values for this small particle sized test group is 20.45% and 21.06%

respectively and this corresponds to the case of microwave power 300 W and moisture content of 0.4. In the situation of 783 μm particle size, the maximum is 47.27% for $\eta_{Cold-Avg}$ and 48.72% for $\eta_{Hot-Avg}$ under a microwave power of 700 W and a moisture content of 0.2; while, on the other hand, the minimum $\eta_{Cold-Avg}$ and $\eta_{Hot-Avg}$ values are 26.25% and 27.03% respectively for a microwave power 300 W and a moisture content of 0.4 . The highest $\eta_{Cold-Avg}$ and $\eta_{Hot-Avg}$ values of 54.39% and 55.71% respectively, are attained in the case of 1790 μm particle size, a microwave power of 1000 W, and a moisture content of 0.4. The lowest values of 29.43% and 30.30% respectively, in contrast, are achieved when a dry particle sample of the same size and a microwave power of 300 W is used.
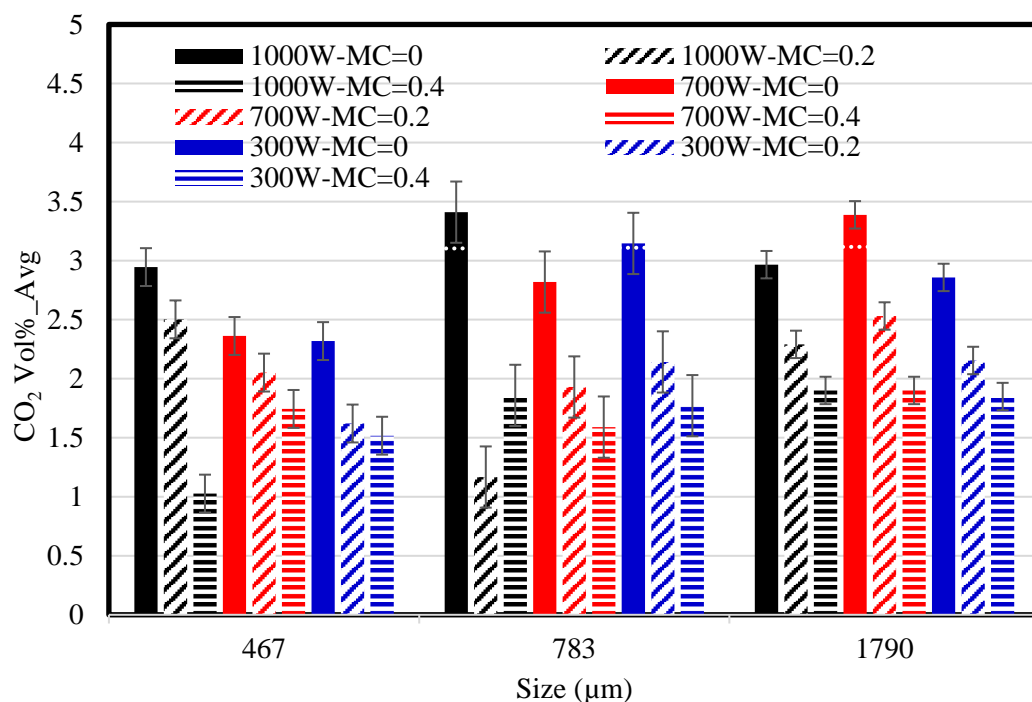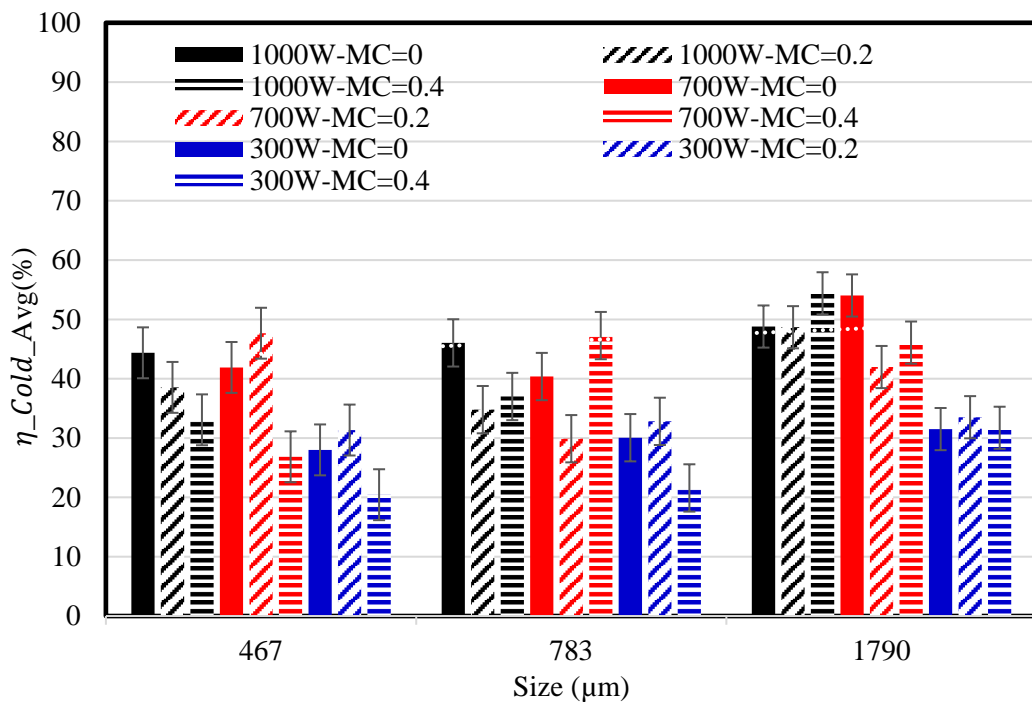

Figure 33: The effect of the particle size on the cold gas efficiency for all of microwave powers and MC percentages cases
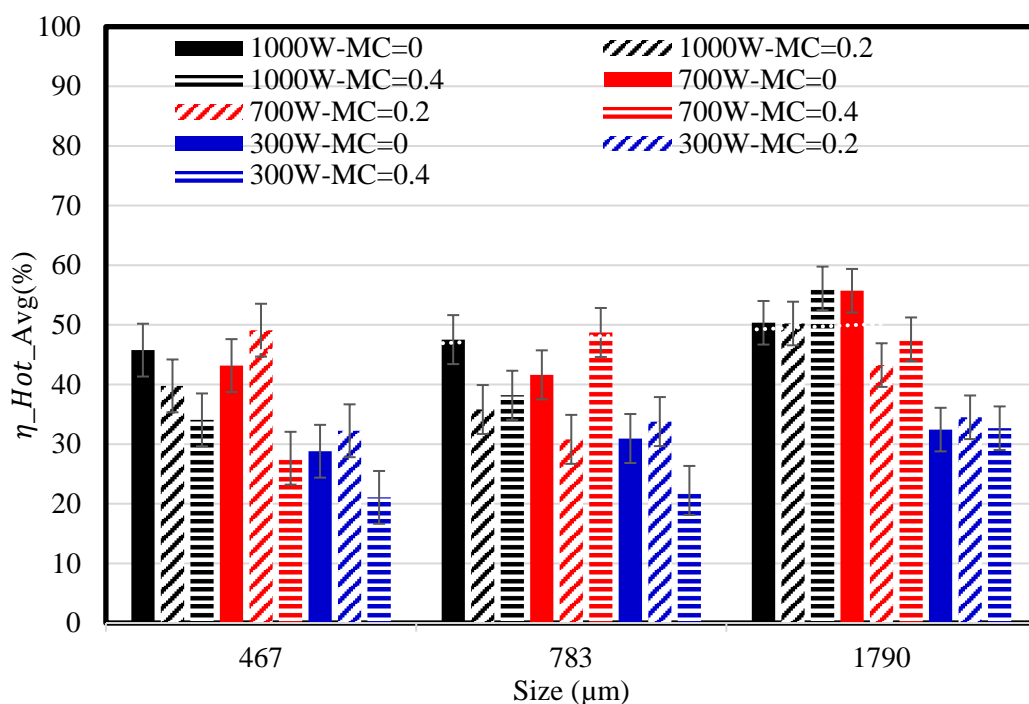
Figure 34: The effect of the particle size on the hot gas efficiency for all of microwave powers and MC percentages cases

3.2.3 Effects of Moisture Content on Bio-syngas Production

Figure 35 represents the effect of moisture content on the average CH_4 concentration volume percentages at all of the microwave powers and particle sizes. In this section, in all figures, the solid colored bars represent the case with smallest size 0.467 μm, the diagonal patterns represent the case with the medium size 0.783 μm, and finally, the horizontal patterns refer to the case with the largest size 1790 μm. The black color used refers to the case of 1000 W, the red color represents the case of 700 W and the blue color is used to represent the case of 300 W. All cases presented in this section were discussed previously, but in this section the main purpose is to try to focus on the overall effect of the moisture content on the studied pyrolysis process. The values in the figure are similar, with minor differences. For the case of a dry sample where MC is zero, the highest CH_4 Avg-GCVP yields 21% when the microwave power is 700 W and the particle size is 1790 μm, while the lowest is Avg-

GCVP 13.64% when the microwave power is 700 W and the particle size is 783 μm. As for the instance with a MC of 0.2 the highest CH_4 Avg-GCVP yield of 15.82% is achieved with a microwave power of 700 W and a particle size of 1790 μm. The lowest Avg-GCVP of 11.56%, on the other hand, is obtain accompanied by a microwave power of 1000 W and a particle size of 1790 μm.

Under the condition of a MC of 0.3 the maximum CH_4 Avg-GCVP yield is 12.35%, when paired with a microwave power 700 W and a particle size of 783 μm. Meanwhile, the minimum Avg-GCVP is 8.37% under the same MC but with a microwave power 300 W and particle size of 783 μm. In general, we can conclude that the CH_4 Avg-GCVP yield is inversely proportional to the MC in the sample. Where the dry samples produce the highest yield average amongst all the other samples with higher MC.

Figure 35: The effect of moisture content on CH_4 average concentration volume percentages for all of microwave powers and particle sizes cases

Figure 36 shows the effect of moisture content on the average CO concentration volume percentages at all of the microwave powers and particle sizes. There is no clear trend for any of the MCs. For the cases that have zero MC, the maximum CO Avg-GCVP yield and the lowest are associated with the cases of a microwave power of 1000 W and a particle size of 783 µm, and a microwave power 300 W and a particle size of 467 µm with 8.67% and 1.71% respectively. For the MC of 0.2, case 8 is the highest CO Avg-GCVP, and the lowest Avg-GCVP are cases of microwave power 1000 W and particle size of 467 µm with 5.08%, and microwave power 300 W and particle size of 467 µm with 1.30% respectively. Finally, for the case of MC is 0.4 the maximum CO Avg-GCVP yield is for the situation of a microwave power of 1000 W and a particle size of 1790 µm with 4.44%. While the minimum CO Avg-GCVP yield for this case is achieve with a microwave power 300 W and a particle size of 783 µm with 1.6%. Consequently, we can conclude that the CO Avg-GCVP yield is inversely relative to the MC in the sample. Where the dry samples produce the most astounding yield normal among every single other sample with higher MC.
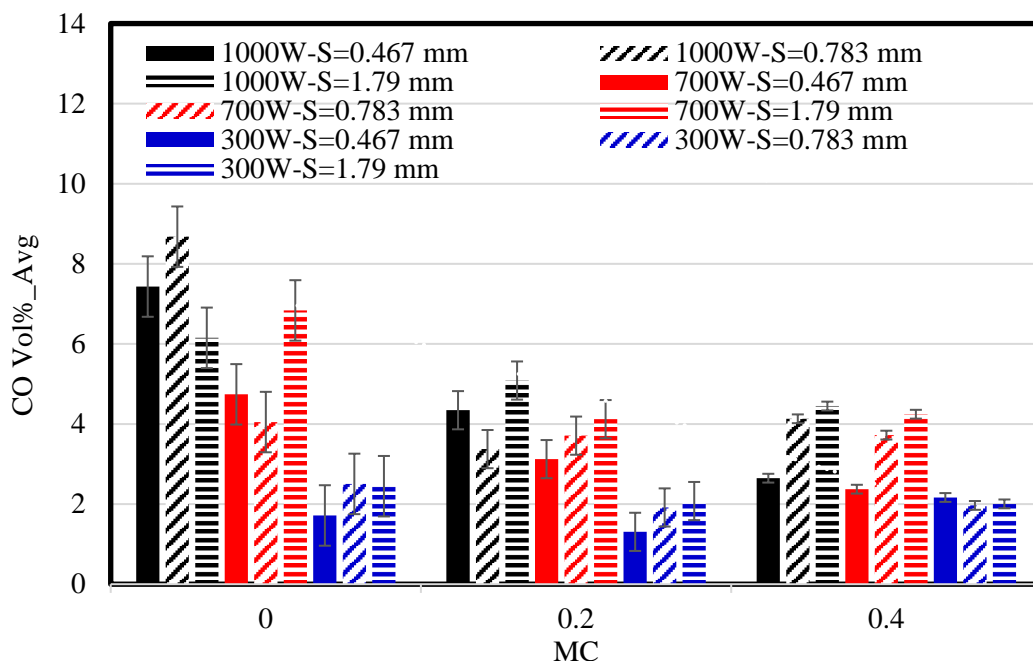
Figure 36: The effect of moisture content on CO average concentration volume percentages for all of microwave powers and particle sizes cases

Figure 37 expresses the effect of moisture content on the average CO_2 concentration volume percentages at all of the microwave powers and particle sizes. For the dry cases where MC is zero, the highest CO_2 Avg-GCVP yields 3.4% when the microwave power is 1000 W and the particle size is 783 μm, and the lowest Avg-GCVP is 2.31% for the case of a microwave power of 300 W and a particle size of 467 μm. Samples with a MC of 0.2, on the other hand, have a maximum CO_2 Avg-GCVP yield of 2.53% when accompanied by a microwave power of 700 W and a particle size of 1790 μm; and a minimum of 0.65% when accompanied with a microwave power of 1000 W and a particle size of 783 μm.

For the circumstances of a MC of 0.4 the maximum CO_2 Avg-GCVP yield is 1.9%, when the microwave power is 1000 W and the particle size is 1790 μm, and the minimum Avg-GCVP is 1.02% for the case of a microwave power of 1000 W and a particle size of 467 μm.

In the instances of zero moisture, the sample contains more carbon that will eventually convert to CO_2 in the presence of the oxygen. Therefore, the higher CO_2 levels seen in the figure when the samples are dry. Generally, in the cases with intermediate to high particle sizes, more CO_2 is generated. This may be related to the higher porosity in the samples where the particles are larger, and so the chance for the oxygen to get inside the core of the sample is easier than when the particles are small and very compact, hindering, thereby, effective O_2 penetration into the inner core of the sample.
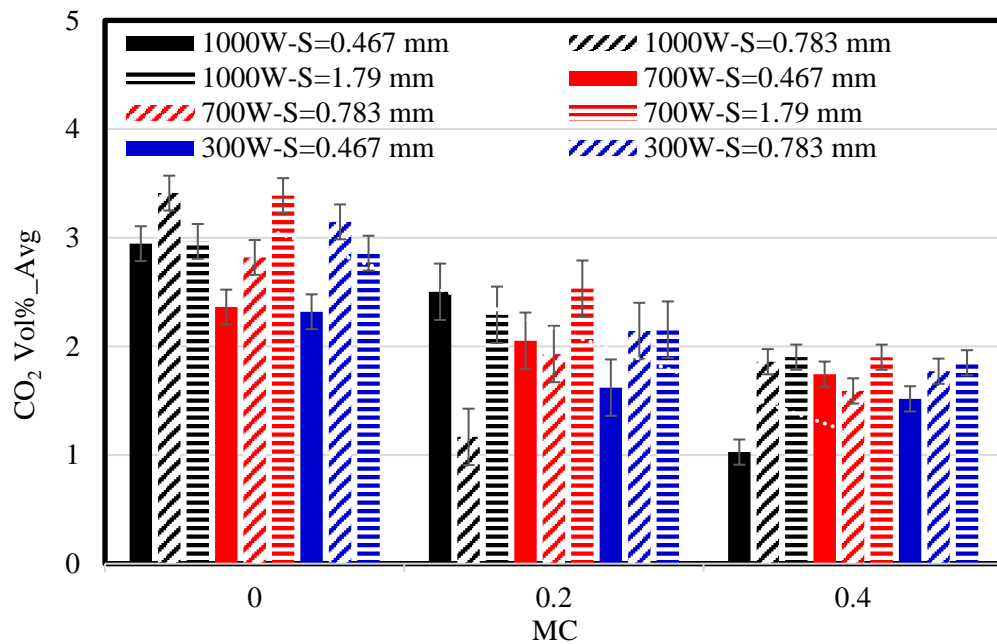
Figure 37: The effect of moisture content on CO_2 average concentration volume percentages for all of microwave powers and particle sizes cases

Figure 38 shows the effect of moisture content on the average H_2 concentration volume percentages at all of the microwave powers and particle sizes. By observing the dry cases, we can conclude that the maximum H_2 Avg-GCVP yield is 2.71% when the microwave power is 1000 W and a particle size is 783 μm. In the occurances where the MC is 0.2, the highest H_2 Avg-GCVP yield is 0.91% if coupled with the microwave power of 1000 W and a particle size of 783 μm. Finally, if the MC is 0.4, the maximum

H$_2$ Avg-GCVP yield is 1.03% for the case of a microwave power of 1000 W and a particle size of 467 μm. The level of H$_2$ is generally very low, especially when the sample contains moisture and, concurrently, when the microwave power is low.
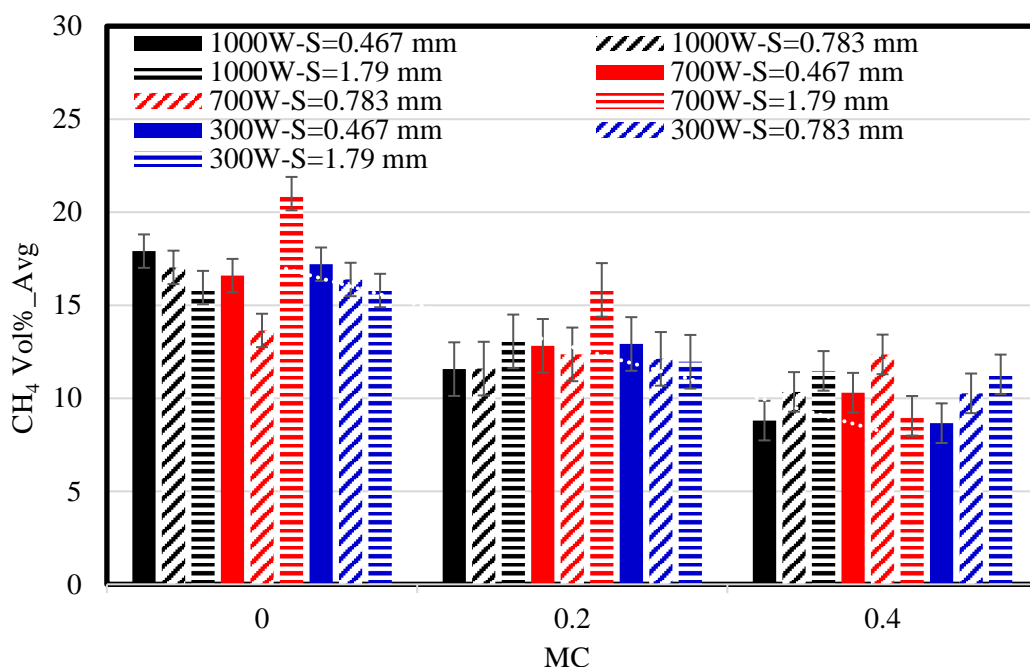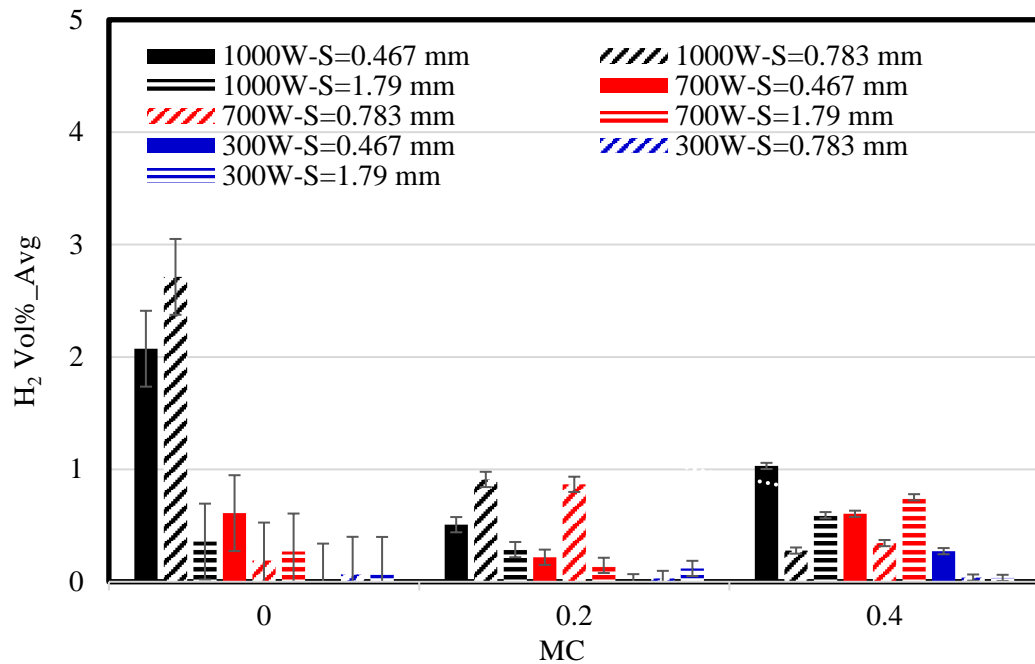

Figure 38: The effect of moisture content on H$_2$ average concentration volume percentages for all of microwave powers and particle sizes cases

Figure 39 express the effect of moisture content on the cold gas production efficiency at all of the microwave powers and particle sizes. Fig. 40 presents the effect of moisture content on the hot gas production efficiency at all of the microwave powers and particle sizes. The values of $\eta_{Hot-Avg}$ and $\eta_{Cold-Avg}$ have small differences.

When the MC is zero the highest $\eta_{Cold-Avg}$ and $\eta_{Hot-Avg}$ values are 54.03% and 55.71% respectively for a microwave power of 700 W and a particle size of 1790 μm, while the lowest values are 28% and 28.8% respectively for a microwave power of 300 W and a particle size of 467 μm. As for the tests with a MC of 0.2, the maximum $\eta_{Cold-Avg}$ is 48.68% and maximum $\eta_{Hot-Avg}$ 50.22% in the case of a microwave power of 1000 W and a particle size of 1790 μm; meanwhile, the minimum $\eta_{Cold-Avg}$

and $\eta_{Hot-Avg}$ values are 31.35% and 32.24% respectively when matched with a microwave power of 300 W and the particle size is 783 μm . Lastly, the maximum values of $\eta_{Cold-Avg}$ and $\eta_{Hot-Avg}$ in a sample of MC is 0.4, are 54.39% and 56.11% respectively under a microwave power 1000 W and a particle size of 1790 μm, on the other hand, the lowest values are 20.45% and 21.06% respectively in the case of a microwave power of 300 W and a particle size of 467 μm.

It is noticeable that samples with a lower moisture content produces higher CH_4 and CO Avg-GCVP yield. This behavior, may be, due to the fact that whenever the moisture content increases in the sample, it requires more energy to evaporate the water content, leaving less amounts of heat dedicated for the pyrolysis process compared to the one used for the dry sample, resulting in less amount of Avg-GCVP yield.
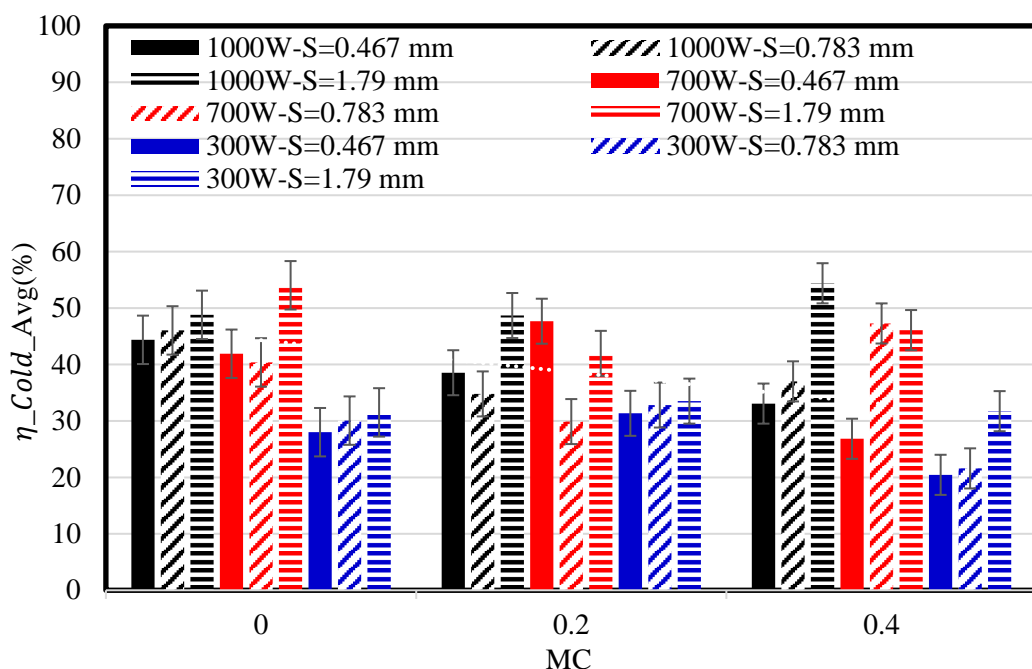
Figure 39: The effect of moisture content on the cold gas efficiency for all of microwave powers and particle sizes cases
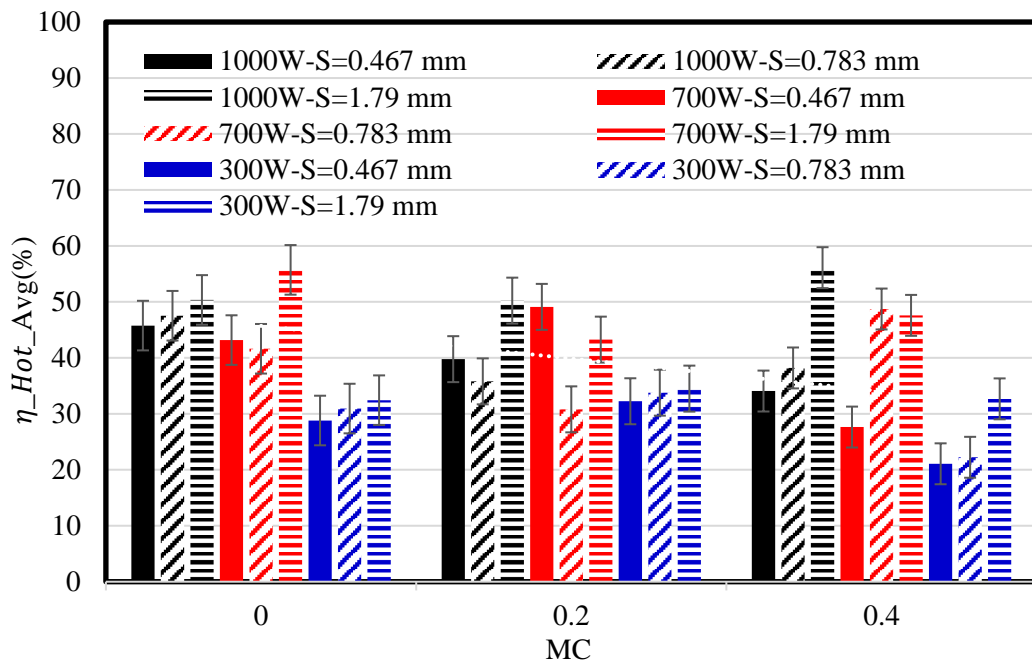
Figure 40: The effect of moisture content on the hot gas efficiency for all of microwave powers and particle sizes cases

3.3 Statistical Analysis

The statistical analysis using Minitab-18 is implemented, in this section, in order to determine the nonlinear correlation modeling the CH_4 and CO gas yield average concentration volume percentage, as a function of all studied parameters. Also, to determine the level of dependance of each parameter. Where, in the model, CH_4 and CO (Avg-GCVP) – the main produced gases- are used as the dependent values, while the sample size, the MWP, and the MC are used as the independent parameters. The process is performed through several steps. Firstly, all the experimental data with the corresponding Avg-GCVP values are used in the program; then the DOE option is selected. Lastly, the analyze response surface design option is applied to generate a nonlinear model. In this process, a null hypothesis and an alternate hypothesis is used for the statistical tests. The P-value revealed, from a statistical test, is the probability of the outcome, given that the theory was right. This is the reason that small P-values are exceedingly attractive. The lower they are, the

more uncertain the result would be, if the null-theory is true. If the P-value is small enough (for example < 0.05) the null hypothesis is accepted. Likewise, the P-value of lack of fit must be > 0.05 to be measurably unimportant to assume that the model represents the data. Table 11 represents CO & CH4 experimental data, the model prediction results, and the corresponding error difference.

Table 11: CO & CH4 experimental and statistical analysis

Case	MC	Power	Size	CH_4%(AVG) Exp.	CH_4%(AVG) Prediction	%Error Diff.	CO%(AVG)- Exp.	CO%(AVG) Prediction	%Error Diff.
1	0.0	1000	467	17.910	16.572	7.473	7.432	6.287	15.415
2	0.0	1000	783	17.037	16.644	2.304	8.678	6.612	23.804
3	0.0	1000	1790	15.950	18.208	-14.155	6.152	6.317	-2.679
4	0.2	1000	467	11.568	12.336	-6.645	4.344	3.623	16.615
5	0.2	1000	783	11.596	12.413	-7.050	3.373	4.016	-19.039
6	0.2	1000	1790	13.059	13.991	-7.143	5.086	3.936	22.601
7	0.4	1000	467	8.800	9.837	-11.783	2.647	2.531	4.413
8	0.4	1000	783	10.343	9.918	4.104	4.130	2.991	27.577
9	0.4	1000	1790	11.472	11.510	-0.336	4.449	3.127	29.708
10	0.0	700	467	16.593	17.200	-3.655	4.741	4.769	-0.587
11	0.0	700	783	13.646	17.178	-25.880	4.049	5.094	-25.823
12	0.0	700	1790	21.000	18.439	12.195	6.836	4.799	29.798
13	0.2	700	467	12.820	13.042	-1.725	3.123	2.847	8.847
14	0.2	700	783	12.361	13.024	-5.365	3.709	3.240	12.649
15	0.2	700	1790	15.825	14.300	9.636	4.122	3.160	23.328
16	0.4	700	467	10.301	10.620	-3.092	2.373	2.497	-5.244
17	0.4	700	783	12.358	10.606	14.175	3.723	2.958	20.560
18	0.4	700	1790	9.058	11.896	-31.339	4.244	3.094	27.111
19	0.0	300	467	17.207	16.357	4.939	1.716	1.905	-10.990
20	0.0	300	783	16.386	16.208	1.087	2.504	2.230	10.935
21	0.0	300	1790	15.792	17.067	-8.073	2.447	1.935	20.920
22	0.2	300	467	12.919	12.302	4.775	1.307	0.972	25.621
23	0.2	300	783	12.119	12.158	-0.321	1.916	1.366	28.737
24	0.2	300	1790	11.964	13.031	-8.916	2.076	1.286	38.067
25	0.4	300	467	8.663	9.983	-15.240	2.166	1.612	25.554
26	0.4	300	783	10.267	9.843	4.121	1.967	2.073	-5.365
27	0.4	300	1790	11.285	10.731	4.909	2.005	2.209	-10.139

3.3.1 Statistical Analysis CH$_4$ Case:

After finding multiple regressions for the CH$_4$ data, the following equation was found to represent the CH$_4$ Avg-GCVP yield prediction, as a function of the three used parameters and their interactions. Table 12 is a way to express the coefficients of the equation. Where constants represent the y-intercept from the equation. The most important values to be checked are the P-values and T-Values. Both of the values are used to check how significant the parameters or the terms, in the equation, are. The P-Value checking method, that is used, states: If the P-Value for the term is < α= 0.05, then the term is significant in the equation. Table 14 shows that MC is the only significant term in the corresponding equation. The Pareto chart, of the standardized effects (Fig. 41), is a bar chart to show which parameter is vital in our study case. Knowing that any bar that exceeds the red line with a value higher than 2.11 is the most significant parameter, which in this case is MC. It is clear that the Pareto chart of the standardized effect and the Table of the uncoded coefficient both conclude to the same result that MC is the most significant parameter.

CH$_4$ regression equation in uncoded units is given by:

$$CH4\ \%(AVG) = 15.19 - 24.26 * MC + 0.00764 * Power - 0.00202 * Size$$
$$+ 21.7 * MC^2 - 0.000006 * Power^2 + 0.000001 * Size^2$$
$$- 0.00129 * MC * Power + 0.00007 * MC * Size + 0.000001$$
$$* Power * Size$$

Table 12: Uncoded coefficients

Term	Coef	SE Coef	T-Value	P-Value	VIF
Constant	15.19	3.61	4.20	0.001	
MC	-24.26	9.15	-2.65	0.017	21.63
Power	0.00764	0.00779	0.98	0.341	48.36
Size	-0.00202	0.00546	-0.37	0.716	91.94
MC*MC	21.7	17.0	1.27	0.220	13.00
Power*Power	-0.000006	0.000006	-1.09	0.291	43.64
Size*Size	0.000001	0.000002	0.43	0.676	85.03
MC*Power	-0.00129	0.00686	-0.19	0.853	7.91
MC*Size	0.00007	0.00349	0.02	0.985	5.73
Power*Size	0.000001	0.000002	0.44	0.668	9.63
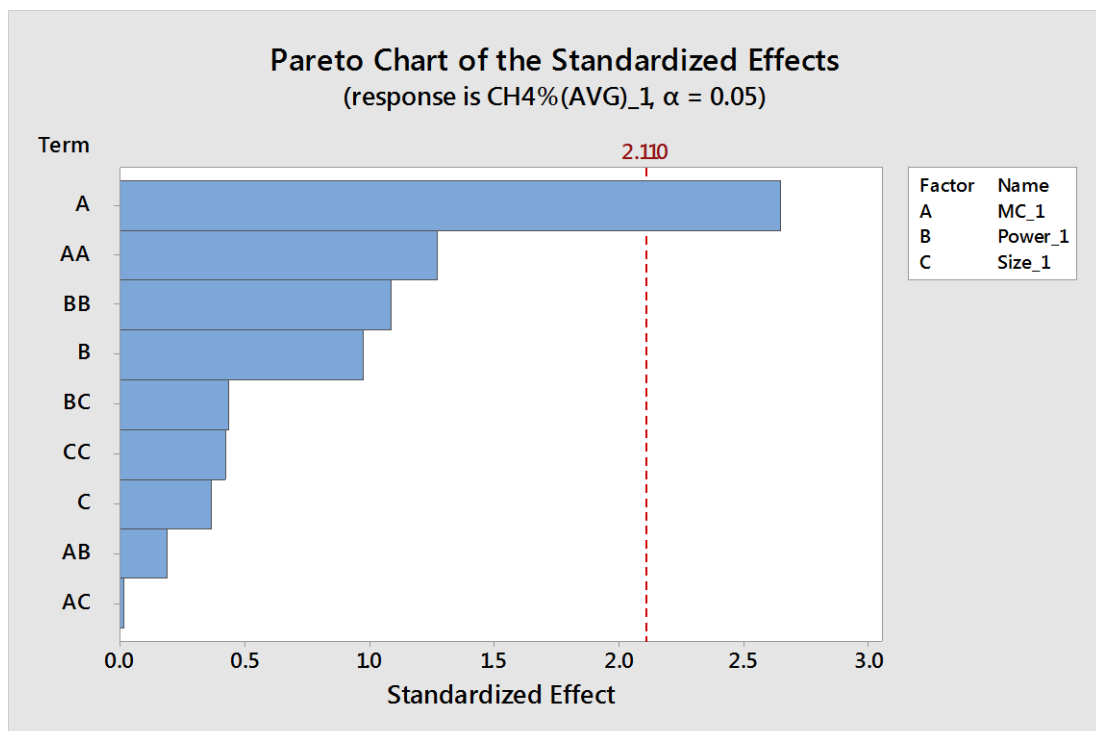
Figure 41: Pareto chart of the standardized effects CH_4 case

The model summary in Table 13 represents the R-sq value which expresses how much the independent variables explains or represents the dependent variable. We got, in our model for the CH_4 Avg-GCVP case, a R-sq value of about 81.43%, from this value we can get $r = \sqrt{R - sq} = \sqrt{0.8143} = 0.902 = 90.2\%$ which shows how the correlation is strong between the dependent variable " CH_4 Avg-GCVP " and the

independent variables: MC, microwave power and size of the particles. It is well known, in the statistics field, that if r = 90.2%, then we have very strong positive correlation between the dependent and the independent variables.

R-sq (adj) is a value that represents how much the independent variables explained the dependent variable, if the software removes the non-effected independent variables. We obtained the values of about 71.60% and r = 84.625% , which is in the region where we can suppose that there is a very strong positive strength between the dependent and the independent variables.

From Table 14 (Analysis of variance), we will focus on two columns, F-Value and P-Value. Using the same method explained above, we reach the same conclusion from the previous Tables and chart.

Figure 42 shows the scattered plot where R^2 is 0.8143, meanwhile the error is randomly distributed and the values are too close between the experiment and prediction values. Through this, we can notice the linear relation where the data is scattered around the line.

Figure 43 displays 3D surface graphs for each sample size showing the CH_4 yield as a function of the power and MC. The surface graph is used to give a better visual idea about the independence of the three parameters and demonstrate the results.

Table 13: Model summary

S	R-sq	R-sq(adj)	R-sq(pred)
1.66970	81.43%	71.60%	52.44%

Table 14: Analysis of variance

Source	DF	Adj SS	Adj MS	F-Value	P-Value
Model	9	207.845	23.094	8.28	0.000
Linear	3	188.393	62.798	22.53	0.000
MC	1	184.253	184.253	66.09	0.000
Power	1	0.166	0.166	0.06	0.810
Size	1	3.956	3.956	1.42	0.250
Square	3	8.333	2.778	1.00	0.418
MC*MC	1	4.512	4.512	1.62	0.220
Power*Power	1	3.316	3.316	1.19	0.291
Size*Size	1	0.505	0.505	0.18	0.676
2-Way Interaction	3	0.632	0.211	0.08	0.972
MC*Power	1	0.099	0.099	0.04	0.853
MC*Size	1	0.001	0.001	0.00	0.985
Power*Size	1	0.533	0.533	0.19	0.668
Error	17	47.394	2.788		
Total	26	255.239			
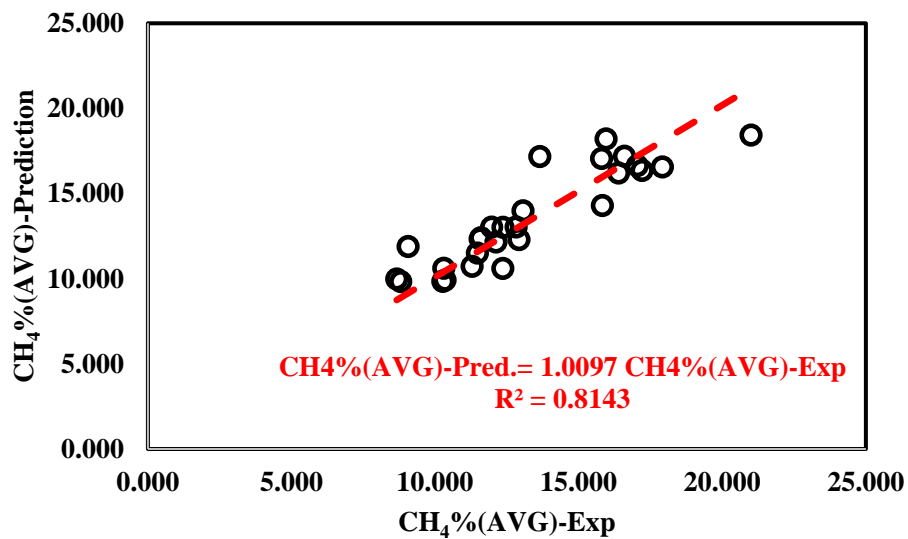
Figure 42: CH_4%(AVG)-Exp. vs CH_4%-(AVG)-Prediction

Table 15 shows the fits and diagnostics for unusual observations:

Table 15: Fits and diagnostics for unusual observations

Obs	CH_4%(AVG)_1	Fit	Resid	Std Resid	
4	13.646	16.541	-2.895	-3.28	R
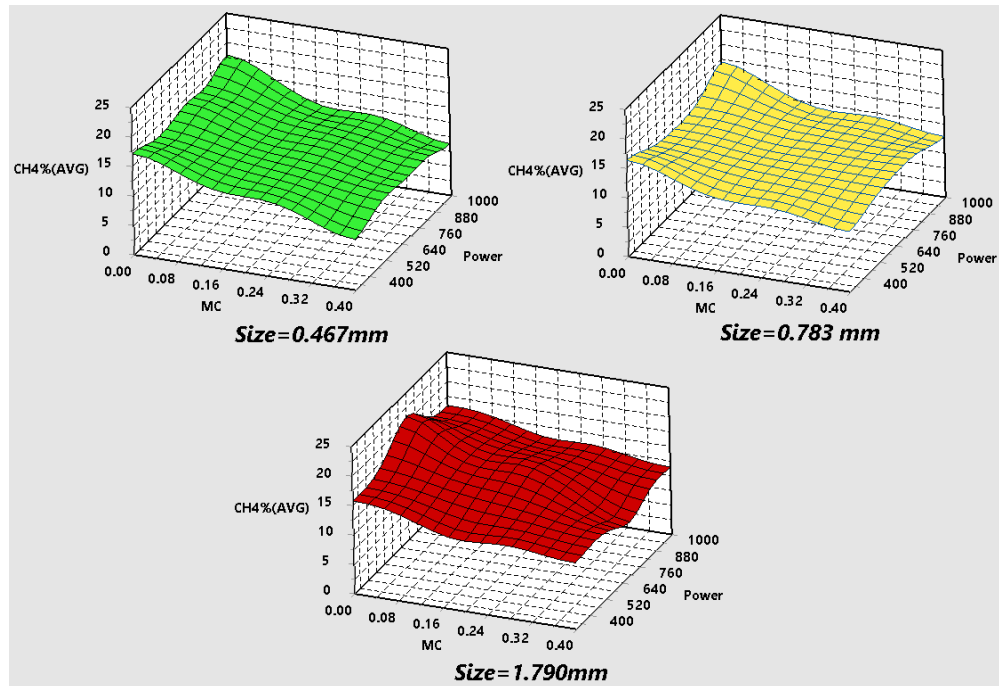
Figure 43: 3D Surface plot of CH$_4$ volume% as function of particle sizes, microwave power, and MC

3.3.2 Statistical Analysis CO Case:

As explained in the previous subsection, the equation below represents the CO% (Avg-GCVP) as a predicted value. From Table 16, after applying the P-Value method, it is noticeable that MC, Particle Size, MW Power, MC^2 and (MC * MW Power) are the most significant parameters that have p-Value less than 0.05. This is graphically exhibited in the Pareto chart of the standardized effects (Fig 44). The fact that the two ways to explore the significance of the parameters agrees on the same result also proves the previous finding.

CO regression equation in uncoded units is as follows.

$$CO \% (AVG) = -1.72 - 5.38 * MC + 0.01016 * Power + 0.00228 * Size$$

$$+ 19.65 * MC^2 - 0.000003 * Power^2 - 0.000001 * Size^2$$

$$- 0.01237 * MC * Power + 0.00107 * MC * Size + 0.000001$$

$$* Power * Size$$

Table 16: Uncoded coefficients

Term	Coef	SE Coef	T-Value	P-Value	VIF
Constant	-1.72	1.78	7.14	0.000	
MC	-5.38	4.50	-4.40	0.000	1.05
Power	0.01016	0.00383	7.93	0.000	1.05
Size	0.00228	0.00269	2.17	0.045	1.09
MC*MC	19.65	8.39	2.34	0.032	1.00
Power*Power	-0.000003	0.000003	-0.89	0.384	1.01
Size*Size	-0.000001	0.000001	-0.76	0.458	1.09
MC*Power	-0.01237	0.00338	-3.66	0.002	1.00
MC*Size	0.00107	0.00172	0.63	0.540	1.04
Power*Size	0.000000	0.000001	0.04	0.965	1.05

Pareto Chart of the Standardized Effects
(response is CO%(AVG)_1, α = 0.05)

Factor	Name
A	MC_1
B	Power_1
C	Size_1
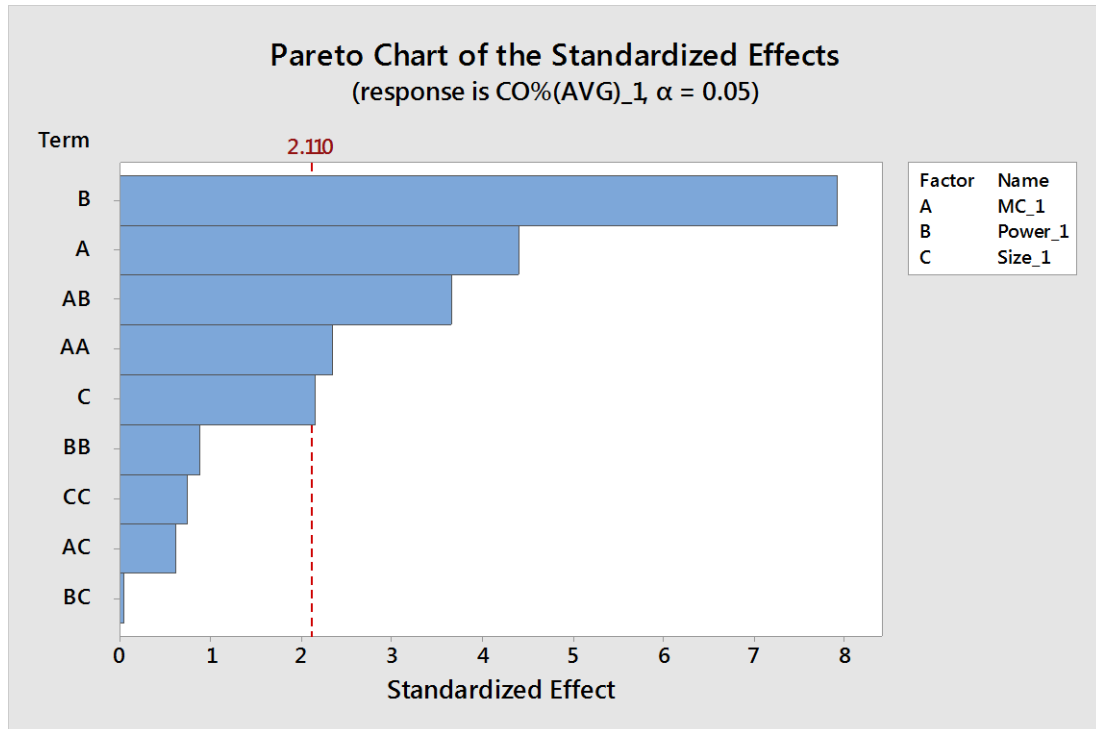
Figure 44: Pareto chart of the standardized effects CO case

The model summary in Table 17 lists the R-sq value, which represents how significantly the independent variables explains or represents the dependent variable. We got, in our model for CO Avg-GCVP Case, a R-sq value of 87.14%; from this value we can get $r = \sqrt{R-sq} = \sqrt{0.8714} = 0.9335 = 93.35\%$ which shows how strong the correlation is between the dependent variable CO Avg-GCVP and the independent variables MC, microwave power and size of the particles. It is well known, in the statistics field, that if r = 93.35% then we have very strong positive strength between the dependent and the independent variables.

R-sq (adj) is a value that represents how much the independent variables explain the dependent variable, if the software removes the non-effected independent variables. We found, in this instance, 80.34% and r = 89.63% which is also in the region where we can suppose that there is a very strong positive strength between the dependent and the independent variables.

From Table 18 (Analysis of variance), we will focus on two columns, the F-Values and P-Values. Using the P-Value method, we reach the same conclusion from the previous Tables and chart.

Figure 45 shows the scattered plot in which R^2 is 0.8714. Meanwhile, the error is randomly distributed, and the difference between the values are insignificant between the experiment and the prediction values. Using this, the linear relation where the data is scattered around the line can be observed.

Figure 46 shows the correlation between particle sizes, microwave powers and MCs of CO Avg-GCVP in a 3D representation for the three particle sizes: 1790 μm, 783 μm, and 467 μm respectively. Moreover, the results from the bar code are presented in the 3D visual image.

Table 17: Model summary

S	R-sq	R-sq(adj)	R-sq(pred)
0.821605	87.14%	80.34%	64.47%

Table 18: Analysis of variance

Source	DF	Adj SS	Adj MS	F-Value	P-Value
Model	9	77.7857	8.6429	12.80	0.000
Linear	3	58.9494	19.6498	29.11	0.000
MC	1	13.0422	13.0422	19.32	0.000
Power	1	42.4795	42.4795	62.93	0.000
Size	1	3.1651	3.1651	4.69	0.045
Square	3	4.6332	1.5444	2.29	0.115
MC*MC	1	3.7052	3.7052	5.49	0.032
Power*Power	1	0.5393	0.5393	0.80	0.384
Size*Size	1	0.3887	0.3887	0.58	0.458
2-Way Interaction	3	9.3211	3.1070	4.60	0.016
MC*Power	1	9.0558	9.0558	13.42	0.002
MC*Size	1	0.2640	0.2640	0.39	0.540
Power*Size	1	0.0013	0.0013	0.00	0.965
Error	17	11.4756	0.6750		
Lack-of-Fit	26	89.2613			
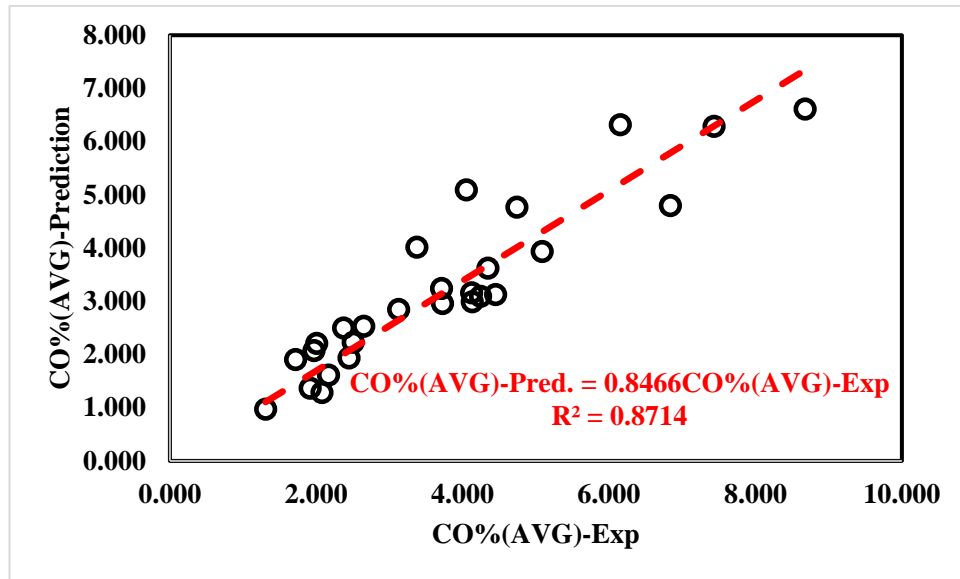
Figure 45: CO% -Exp. vs Prediction

CO%(AVG)-Pred. = 0.8466CO%(AVG)-Exp
R² = 0.8714
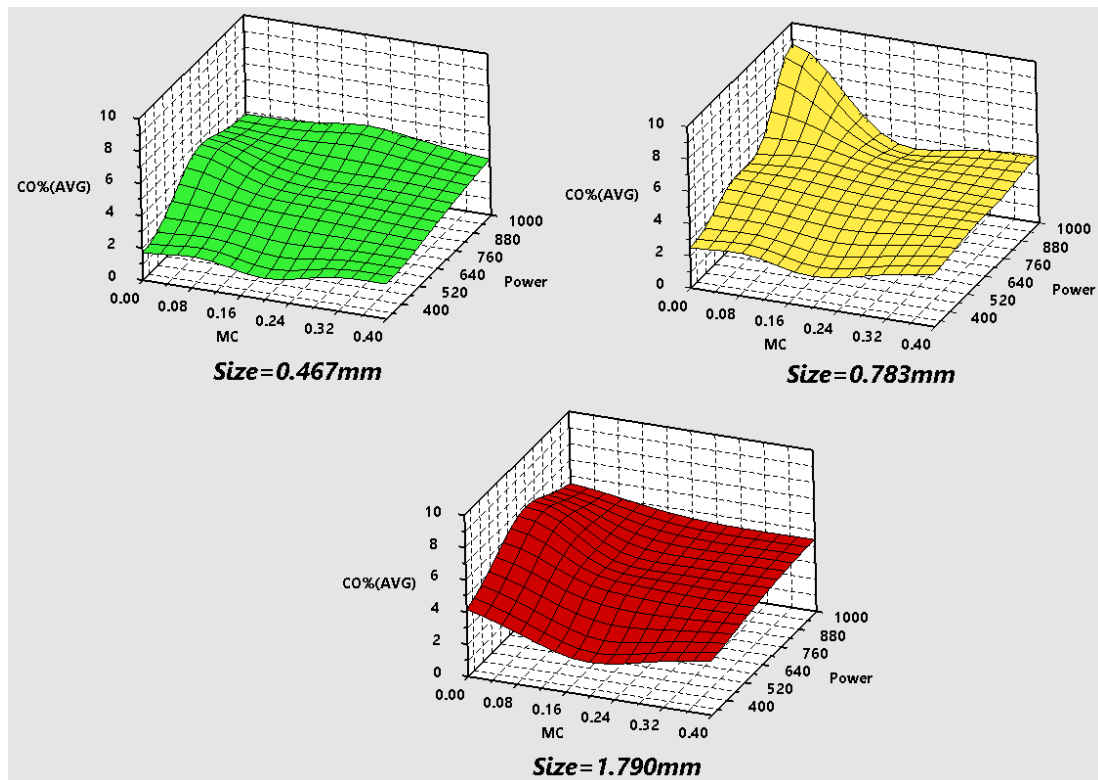
Figure 46: 3D Surface plot of CO volume% as function of particle sizes, microwave power and MC

Table 19: Fits and diagnostics for unusual observations

Obs	CO%(AVG)	Fit	Resid	Std Resid	
3	4.049	5.463	-1.414	-2.01	R
20	6.152	7.416	-1.263	-2.25	R
27	8.678	7.243	1.435	2.17	R

Chapter 4: Conclusion

4.1 Research Conclusions and Implications

Over the course of this chapter, the main observations of the conducted experiments, covering the studied cases and parameters, will be briefly specified. Overall, the findings are summarized in the following key points. Lastly, several recommendations are mentioned to help further develop and facilitate this idea, for future research and applications.

Through the analysis of the previous studies, the following can be concluded:

- From the previous chapter, it was recognizable that when the microwave power increases, the sample will be exposed to more heat, leading to the elevation in the internal heating process in the biomass sample. As a result, the production of the yield gases will increase.

- According to the verdicts of chapter 3, the smaller the size of the particles is, the higher the CH_4 average concentration volume percentage yield is. It assumed that this occurs due to samples of small-sized particles giving the heat a chance to reach all the portions in the sample.

- It is understandable that samples produce higher CH_4 and CO Avg-GCVP yield at lower moisture content values. This behavior ensues as a result of the fact that, at a high moisture content, the sample needs more energy to evaporate the water; thus leaving, in contrast to dry samples, fewer amounts of heat dedicated for the pyrolysis procedure.

4.2 Recommendations and Future Work

After carrying out numerous experiments and facing various challenges, many recommendations and suggestions can be extracted.

- The experimental setup can be improved to provide better control and measurement, by enhancing the design of the reactor and using advanced microwaves with more alternative microwave power options.

- The usage of different types of date seeds would help in the better evaluation of the effect of the biomass types on the pyrolysis process.

- Metal catalysts can be added to enrich further the understanding and reasoning, of having a high production of CH_4 gas and a low production of H_2 gas.

- Using other gas analyzers with a broader range of gas measurements will help in highlighting the expected produced gases from the pyrolysis process.

- Having a more robust sealed, heated piping system, from the reactor to the gas analyzer, will ensure the minimization of the air-gas leak to the system, consequently, a complete pyrolysis process.

References

[1]   F.-X. Collard and J. Blin, "A review on pyrolysis of biomass constituents: Mechanisms and composition of the products obtained from the conversion of cellulose, hemicelluloses and lignin," *Renewable and Sustainable Energy Reviews,* vol. 38, pp. 594-608, 2014/10/01/ 2014.

[2]   F. H. M. Inamullah Haneef, "Energy Crisis and it's Statistics," Department of Petroleum & Natural Gas Engineering, Mehran University of Engineering & Technology SZAB Campus Khairpur Mir's.

[3]   V. O. F. M. E. ELECTRICITY, "GCC Power Market Report 2017," Meddile East Electricity Enirgizing and Industry 2017.

[4]   N. T. U. of, "RENEWABLES 2018 Global status report," REN212018.

[5]   "Renewable Energy Prospects: United Arab Emirates", Masdar Institute and IRENAApril-2015.

[6]   N. T. University, "RENEWABLES 2018 Global status report," REN21 2018.

[7]   S. D. Y. El May, M. Jeguirim, G. Trouvé, and R. Said,, "Measurement of gaseous and particulate pollutants during combustion of date palm wastes for energy recovery," *Aerosol and Air Quality Research,* vol. 12, pp. 814-825, 2012.

[8]   "Bioenergy for Sustainable Development," IEA Bioenergy2017.

[9]   I. C. M. Innovation. Mission-innovation.net. Available: http://mission-innovation.net/our-work/innovation-challenges/

[10]   D. J. a. M. H. A. Kumar, "Thermochemical Biomass Gasification: A Review of the Current Status of the Technology," *Energies,* vol. 2, pp. 556-581, 2009.

[11]   M. Parikka, "Global biomass fuel resources," *Biomass and Bioenergy,* vol. 27, pp. 613-620, 2004.

[12]   G. Fischer, & Schrattenholzer, L., "Global bioenergy potentials through 2050," *Biomass and Bioenergy,* vol. 20, pp. 151-159, 2001.

[13]   A. F. M. Hoogwijk, R. van den Broek, G. Berndes, D. Gielen and W. Turkenburg, "Exploration of the ranges of the global potential of biomass for energy," *Biomass and Bioenergy,* vol. 25, pp. 119-133, 2003.

[14]   F. E. S. Thorsell, R. Huhnke and C. Taliaferro, "Economics of a coordinated biorefinery feedstock harvest system: lignocellulosic biomass harvest cost," *Biomass and Bioenergy,* vol. 27, pp. 327-337, 2004.

[15]   J. W. M. Chen, M. Zhang, M. Chen, X. Zhu, F. Min and Z. Tan, "Catalytic effects of eight inorganic additives on pyrolysis of pine wood sawdust by

microwave heating," *Journal of Analytical and Applied Pyrolysis,* vol. 82, pp. 145-150, 2008.

[16]   J. Goldemberg, & Coelho, S. T., "Renewable energy—traditional biomass vs. modern biomass," *Energy Policy,* vol. 32, pp. 711-714, 2004.

[17]   M. Wu, Wu, Y., & Wang, M., "Energy and Emission Benefits of Alternative Transportation Liquid Fuels Derived from Switchgrass: A Fuel Life Cycle Assessment," *Biotechnology Progress,* vol. 22, pp. 1012-124, 2006.

[18]   S. C. a. D. M. A. Molino, "Biomass gasification technology: The state of the art overview," *Journal of Energy Chemistry,* vol. 25, pp. 10-25, 2016.

[19]   Y. Li, He, D., Zhang, Q., Xu, B., & Zhu, Q., "Influence of reactor materials on i-C4 synthesis from CO hydrogenation over ZrO2 based catalysts," *Fuel Processing Technology,* vol. 85, pp. 401-411, 2004.

[20]   D. Christian, "Biomass for Renewable Energy, Fuels, and Chemicals," *Journal of Environment Quality,* vol. 29, p. 662-663, 2000.

[21]   D. H. Y. Li, Q. Zhang, B. Xu and Q. Zhu, "Influence of reactor materials on i-C4 synthesis from CO hydrogenation over ZrO2 based catalysts," *Fuel Processing Technology,* vol. 85, pp. 401-411, 2004.

[22]   W. Iwasaki, "Magnetic refrigeration technology for an international clean energy network using hydrogen energy (WE-NET)," *International Journal of Hydrogen Energy,* vol. 28, pp. 559-567, 2003/05/01/ 2003.

[23]   J. M. A. Domínguez, Y. Fernández, J. Pis, J. Nabais, P. Carrott and M. Carrott, "Conventional and microwave induced pyrolysis of coffee hulls for the production of a hydrogen rich fuel gas," *Journal of Analytical and Applied Pyrolysis,* vol. 79, pp. 128-135, 2007.

[24]   E. T. Thostenson and T. W. Chou, "Microwave processing: fundamentals and applications," *Composites Part A: Applied Science and Manufacturing,* vol. 30, pp. 1055-1071, 1999/09/01/ 1999.

[25]   Y. K. W. L. S. L. C. Huang, "Total recovery of resources andenergy from rice straw using microwave-induced pyrolysis " vol. 99, ed: Bioresource Technology, 2008   pp. 8252-8258

[26]   R. L. L. Zhang, R. Yin and Y. Mei, "Upgrading of bio-oil from biomass fast pyrolysis in China: A review," *Renewable and Sustainable Energy Review,* vol. 24, pp. 66-72, 2013.

[27]   D. M. A.V.Bridgwater, D.Radlein, "An overview of fast pyrolysis of biomass," *Organic Geochemistry,* vol. 30, pp. 1479-1493, 1999.

[28]   H. Yang, R. Yan, H. Chen, D. H. Lee, and C. Zheng, "Characteristics of hemicellulose, cellulose and lignin pyrolysis," *Fuel,* vol. 86, pp. 1781-1788, 2007/08/01/ 2007.

[29]   P. Giudicianni, G. Cardone, and R. Ragucci, "Cellulose, hemicellulose and lignin slow steam pyrolysis: Thermal decomposition of biomass components mixtures," *Journal of Analytical and Applied Pyrolysis,* vol. 100, pp. 213-222, 2013/03/01/ 2013.

[30]   M. Van de Velden, J. Baeyens, A. Brems, B. Janssens, and R. Dewil, "Fundamentals, kinetics and endothermicity of the biomass pyrolysis reaction," *Renewable Energy,* vol. 35, pp. 232-242, 2010/01/01/ 2010.

[31]   H. Yang, R. Yan, H. Chen, C. Zheng, D. H. Lee, and D. T. Liang, "In-Depth Investigation of Biomass Pyrolysis Based on Three Major Components: Hemicellulose, Cellulose and Lignin," *Energy & Fuels,* vol. 20, pp. 388-393, 2006/01/01 2006.

[32]   A. Demirbaş, "Mechanisms of liquefaction and pyrolysis reactions of biomass," *Energy Conversion and Management,* vol. 41, pp. 633-646, 2000/04/01/ 2000.

[33]   P. R. Patwardhan, D. L. Dalluge, B. H. Shanks, and R. C. Brown, "Distinguishing primary and secondary reactions of cellulose pyrolysis," *Bioresource Technology,* vol. 102, pp. 5265-5269, 2011/04/01/ 2011.

[34]   S. Wang, B. Ru, H. Lin, and W. Sun, "Pyrolysis behaviors of four O-acetyl-preserved hemicelluloses isolated from hardwoods and softwoods," *Fuel,* vol. 150, pp. 243-251, 2015/06/15/ 2015.

[35]   X. Bai, K. H. Kim, R. C. Brown, E. Dalluge, C. Hutchinson, Y. J. Lee*, et al.*, "Formation of phenolic oligomers during fast pyrolysis of lignin," *Fuel,* vol. 128, pp. 170-179, 2014/07/15/ 2014.

[36]   J. M. Osepchuk, "A History of Microwave Heating Applications," *IEEE Transactions on Microwave Theory and Techniques,* vol. 32, pp. 1200-1224, 1984.

[37]   R. MEREDITH, " Engineers' Handbook of Industerial Microwave Heating," vol. 99, ed. London: The Institution of Engineering and Technology, 1998, pp. 8252-8258

[38]   D. K. Xia and C. A. Picklesi, "Microwave caustic leaching of electric arc furnace dust," *Minerals Engineering,* vol. 13, pp. 79-94, 2000/01/01/ 2000.

[39]   W. Vorster, N. A. Rowson, and S. W. Kingman, "The effect of microwave radiation upon the processing of Neves Corvo copper ore," *International Journal of Mineral Processing,* vol. 63, pp. 29-44, 2001/06/01/ 2001.

[40]   S. O. Nelson, "Fundamentals of Dielectric Properties Measurements and Agricultural Applications," *Journal of Microwave Power and Electromagnetic Energy,* vol. 44, pp. 98-113, 2010/01/01 2010.

[41]   M. RJ., *Engineers_ handbook of industrial microwave-heating.* Stevenage: Institution of Electrical Engineers, 1998.

[42]   Y. V. Bykov, K. I. Rybakov, and V. E. Semenov, "High-temperature microwave processing of materials," *Journal of Physics D: Applied Physics,* vol. 34, pp. R55-R75, 2001/06/19 2001.

[43]   J. Robinson, S. Kingman, D. Irvine, P. Licence, A. Smith, G. Dimitrakis, *et al.*, "Understanding microwave heating effects in single mode type cavities— theory and experiment," *Physical Chemistry Chemical Physics,* vol. 12, pp. 4750-4758, 2010.

[44]   T. J. Appleton, R. I. Colder, S. W. Kingman, I. S. Lowndes, and A. G. Read, "Microwave technology for energy-efficient processing of waste," *Applied Energy,* vol. 81, pp. 85-113, 2005/05/01/ 2005.

[45]   J. P. Robinson, S. W. Kingman, R. Barranco, C. E. Snape, and H. Al-Sayegh, "Microwave Pyrolysis of Wood Pellets," *Industrial & Engineering Chemistry Research,* vol. 49, pp. 459-463, 2010/01/20 2010.

[46]   A. A. Salema, Y. K. Yeow, K. Ishaque, F. N. Ani, M. T. Afzal, and A. Hassan, "Dielectric properties and microwave heating of oil palm biomass and biochar," *Industrial Crops and Products,* vol. 50, pp. 366-374, 2013/10/01/ 2013.

[47]   F. Motasemi, M. T. Afzal, A. A. Salema, J. Mouris, and R. M. Hutcheon, "Microwave dielectric characterization of switchgrass for bioenergy and biofuel," *Fuel,* vol. 124, pp. 151-157, 2014/05/15/ 2014.

[48]   D. Beneroso, A. Albero-Ortiz, J. Monzó-Cabrera, A. Díaz-Morcillo, A. Arenillas, and J. A. Menéndez, "Dielectric characterization of biodegradable wastes during pyrolysis," *Fuel,* vol. 172, pp. 146-152, 2016/05/15/ 2016.

[49]   R. MEREDITH, *Engineers' Handbook of Industerial Microwave Heating.* London: The Institution of Engineering and Technology, 1998.

[50]   S. O. Nelson, "DIELECTRIC PROPERTIES MEASUREMENT TECHNIQUES AND APPLICATIONS," *Transactions of the ASAE,* vol. 42, pp. 523-529, 1999.

[51]   A. C. M. METAXAS, R. J., *Industrial microwave heating.* London: Peter Peregrinus Ltd., 1983.

[52]   A. C. R. Prashant M. Ingole, Satyajit M. Deshmukh,Dr Sameer K. Deshmukh, "MICROWAVE ASSISTED PYROLYSIS OF BIOMASS: A REVIEW,"

International Journal of Advanced Technology in Engineering and Science, vol. 4, pp. 78-84, 2016.

[53]   J. A. Menéndez, A. Domínguez, M. Inguanzo, and J. J. Pis, "Microwave pyrolysis of sewage sludge: analysis of the gas fraction," *Journal of Analytical and Applied Pyrolysis,* vol. 71, pp. 657-667, 2004/06/01/ 2004.

[54]   J. A. Menéndez, A. Domínguez, Y. Fernández, and J. J. Pis, "Evidence of Self-Gasification during the Microwave-Induced Pyrolysis of Coffee Hulls," *Energy & Fuels,* vol. 21, pp. 373-378, 2007/01/01 2007.

[55]   Y. F. Huang, W. H. Kuan, S. L. Lo, and C. F. Lin, "Hydrogen-rich fuel gas from rice straw via microwave-induced pyrolysis," *Bioresource Technology,* vol. 101, pp. 1968-1973, 2010/03/01/ 2010.

[56]   F. Yu, S. Deng, P. Chen, Y. Liu, Y. Wan, A. Olson*, et al.*, "Physical and Chemical Properties of Bio-Oils From Microwave Pyrolysis of Corn Stover," in *Applied Biochemistry and Biotecnology: The Twenty-Eighth Symposium Proceedings of the Twenty-Eight Symposium on Biotechnology for Fuels and Chemicals Held April 30–May 3, 2006, in Nashville, Tennessee*, J. R. Mielenz, K. T. Klasson, W. S. Adney, and J. D. McMillan, Eds., ed Totowa, NJ: Humana Press, 2007, pp. 957-970.

[57]   S. Zhang, Q. Dong, L. Zhang, and Y. Xiong, "High quality syngas production from microwave pyrolysis of rice husk with char-supported metallic catalysts," *Bioresource Technology,* vol. 191, pp. 17-23, 2015/09/01/ 2015.

[58]   H. Lei, S. Ren, and J. Julson, "The Effects of Reaction Temperature and Time and Particle Size of Corn Stover on Microwave Pyrolysis," *Energy & Fuels,* vol. 23, pp. 3254-3261, 2009/06/18 2009.

[59]   M. Miura, H. Kaga, A. Sakurai, T. Kakuchi, and K. Takahashi, "Rapid pyrolysis of wood block by microwave heating," *Journal of Analytical and Applied Pyrolysis,* vol. 71, pp. 187-199, 2004/03/01/ 2004.

[60]   S. Ren, H. Lei, L. Wang, Q. Bu, S. Chen, J. Wu*, et al.*, "Biofuel production and kinetics analysis for microwave pyrolysis of Douglas fir sawdust pellet," *Journal of Analytical and Applied Pyrolysis,* vol. 94, pp. 163-169, 2012/03/01/ 2012.

[61]   S. Grundas, *Advances in Induction and Microwave Heating of Mineral and Organic Materials*. 10.5772/562: Bohdan Dobrzanski Institute of Agrophysics, 2011.

[62]   N. ZHOU, " Characterization and Microwave Assisted Pyrolysis of Oklahoma Native Microalgae Strains for Bio-Oil Production," Xi'an Jiaotong University, Xi'an, China2013.

[63]   X. Zhao, J. Zhang, Z. Song, H. Liu, L. Li, and C. Ma, "Microwave pyrolysis of straw bale and energy balance analysis," *Journal of Analytical and Applied Pyrolysis,* vol. 92, pp. 43-49, 2011/09/01/ 2011.

[64]   P. Monsef-Mirzai, M. Ravindran, W. R. McWhinnie, and P. Burchill, "Rapid microwave pyrolysis of coal: Methodology and examination of the residual and volatile phases," *Fuel,* vol. 74, pp. 20-27, 1995/01/01/ 1995.

[65]   A. Domínguez, J. A. Menéndez, Y. Fernández, J. J. Pis, J. M. V. Nabais, P. J. M. Carrott*, et al.*, "Conventional and microwave induced pyrolysis of coffee hulls for the production of a hydrogen rich fuel gas," *Journal of Analytical and Applied Pyrolysis,* vol. 79, pp. 128-135, 2007/05/01/ 2007.

[66]   Y. F. Huang, W. H. Kuan, S. L. Lo, and C. F. Lin, "Total recovery of resources and energy from rice straw using microwave-induced pyrolysis," *Bioresource Technology,* vol. 99, pp. 8252-8258, 2008/11/01/ 2008.

[67]   E. Yagmur, M. Ozmak, and Z. Aktas, "A novel method for production of activated carbon from waste tea by chemical activation with microwave energy," *Fuel,* vol. 87, pp. 3278-3285, 2008/11/01/ 2008.

[68]   Y. Hong, W. Chen, X. Luo, C. Pang, E. Lester, and T. Wu, "Microwave-enhanced pyrolysis of macroalgae and microalgae for syngas production," *Bioresource Technology,* vol. 237, pp. 47-56, 2017/08/01/ 2017.

[69]   H. Li, X. Li, L. Liu, K. Li, X. Wang, and H. Li, "Experimental study of microwave-assisted pyrolysis of rice straw for hydrogen production," *International Journal of Hydrogen Energy,* vol. 41, pp. 2263-2267, 2016/01/30/ 2016.

[70]   G. D. Jiménez, V. Hernández-Montoya, M. A. Montes-Morán, S. W. Kingman, T. Monti, and E. R. Binner, "Microwave pyrolysis of pecan nut shell and thermogravimetric, textural and spectroscopic characterization of carbonaceous products," *Journal of Analytical and Applied Pyrolysis,* vol. 135, pp. 160-168, 2018/10/01/ 2018.

[71]   M. A. Hossain, J. Jewaratnam, P. Ganesan, J. N. Sahu, S. Ramesh, and S. C. Poh, "Microwave pyrolysis of oil palm fiber (OPF) for hydrogen production: Parametric investigation," *Energy Conversion and Management,* vol. 115, pp. 232-243, 2016/05/01/ 2016.

[72]   D. A.-K. N. Al-Rubaye, B. Kabalan, and A. Al-Shammaa., "Syngas Production from Date Palm Seeds by Using Advanced Microwave Technology," *British Journal of Science,* vol. 3, pp. 159-166, February 2012.

[73]   A. T. Particle, *Size Measurement.* 3rd ed. London: Chapman and Hall, 1981.

[74]   E. R. E. TECNOLOGIA, " TrasporTable Syngas Pre-Treatment Sample," Italy.

[75]   O. Company. (2019). *Low Pressure Drop Gas Mass FlowMeters*. Available: https://www.omega.com/pptst/FMA-LP1600A.html.

[76]   O. Company. (2019). *PorTable Handheld Data Logger*. Available: https://www.omega.com/pptst/OM-DAQPRO-5300.htm

[77]   D. W. Robert HP, *Perry's chemical engineers handbook. Sixth edition*. New York: McGraw Hill, 1984.

[78]   S. A. Channiwala and P. P. Parikh, "A unified correlation for estimating HHV of solid, liquid and gaseous fuels," *Fuel,* vol. 81, pp. 1051-1063, 2002/05/01/ 2002.

[79]   S. Rönsch, J. Schneider, S. Matthischke, M. Schlüter, M. Götz, J. Lefebvre*, et al.*, "Review on methanation – From fundamentals to current projects," *Fuel,* vol. 166, pp. 276-296, 2016/02/15/ 2016.

[80]   N. B. Rasmussen, "Technologies relevant for gasification and methanation in Denmark - Detailed analysis of bio-SNG technologies and other RE-gases ForskNG 10689," Danish Gas Technology Centre, Denmark September 2012.

Appendices

Appendix A: Practical Size Distribution

This appendix represent Rosin Rammier Regression Check for the three Date seeds powder sizes, (a) X vs. Y and (b) the Sieve Size vs. Cumulative% Retained. While Table 20 shows the size calculations that dependent on the equations in section 2.2.3.
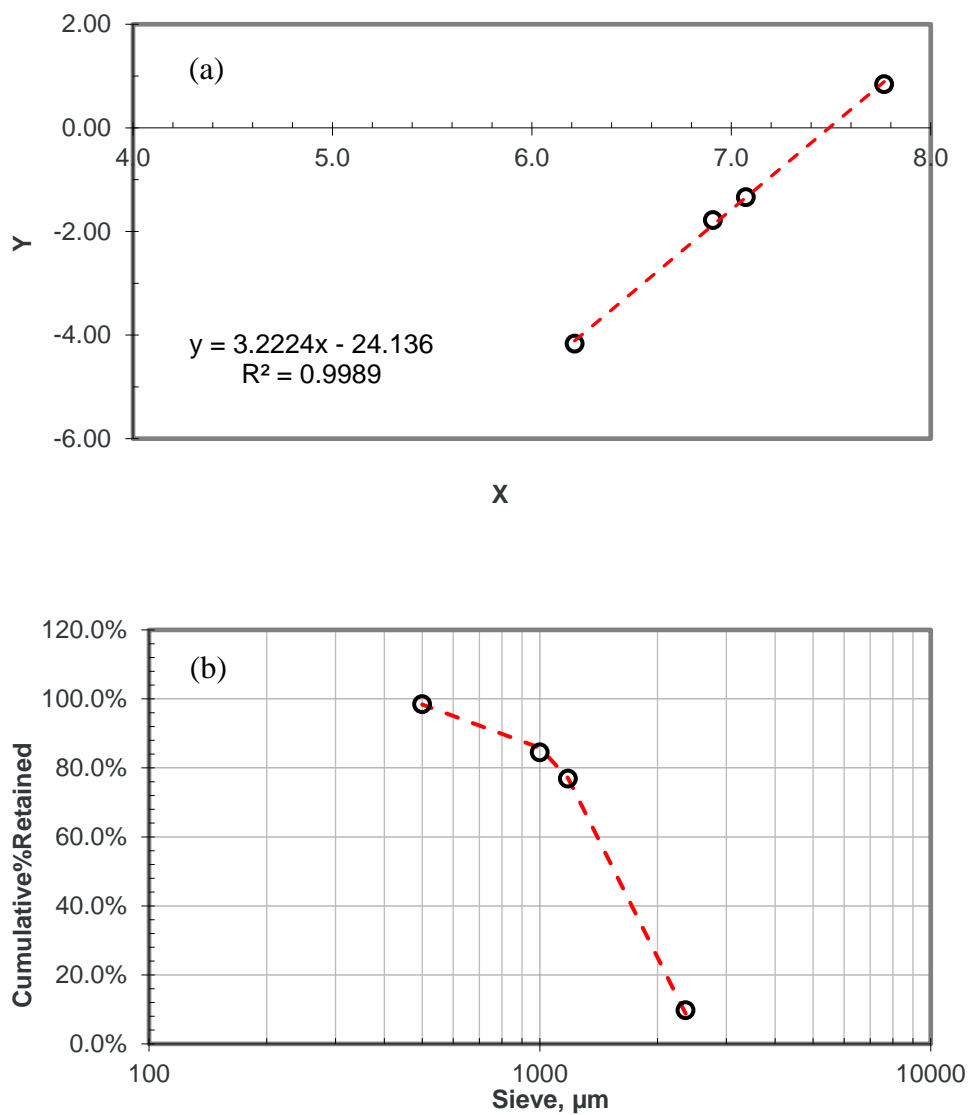

Figure 47: Rosin Rammier Regression Check for (400<DSP<3000 µm), (a) X vs. Y (b) the Sieve Size vs. Cumulative% Retained

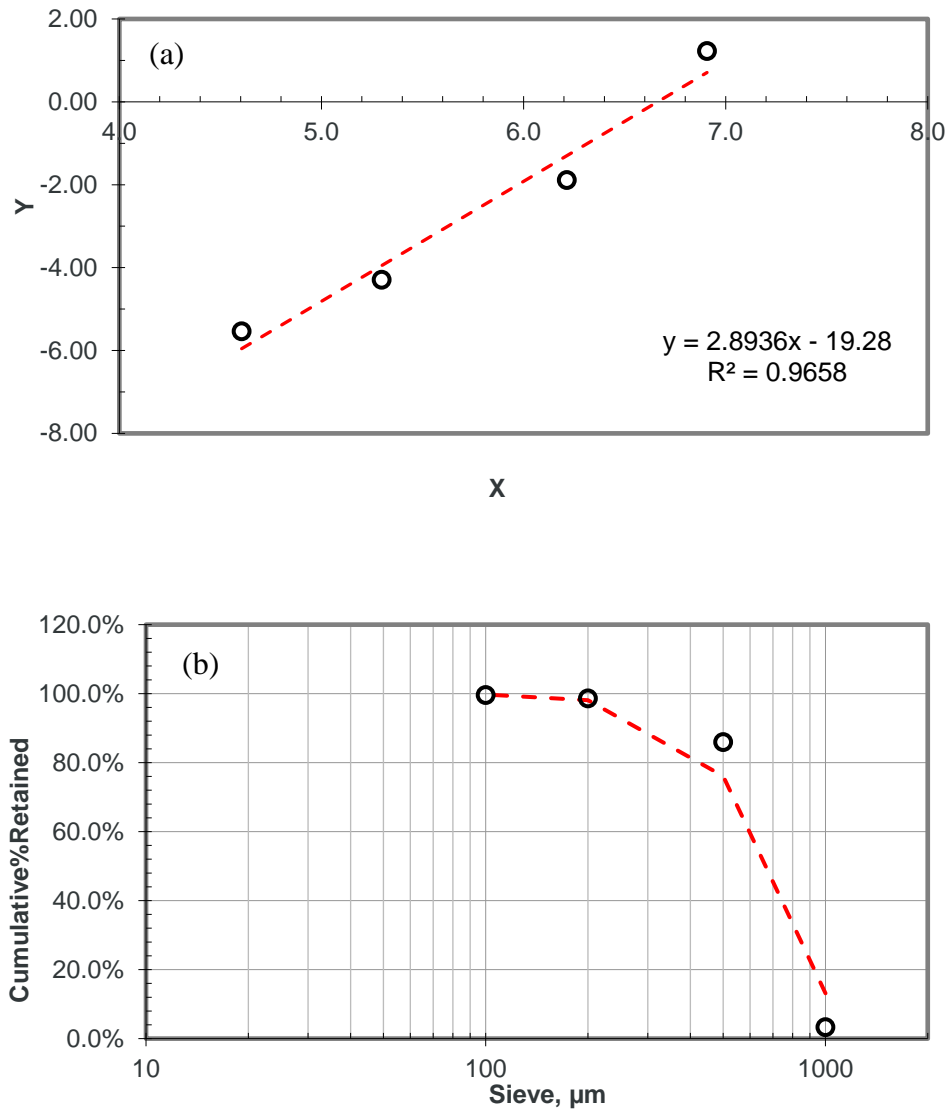Figure 48: Rosin Rammier Regression Check (50<DSP<2000 µm), (a) X vs. Y (b) the Sieve Size vs. Cumulative% Retained

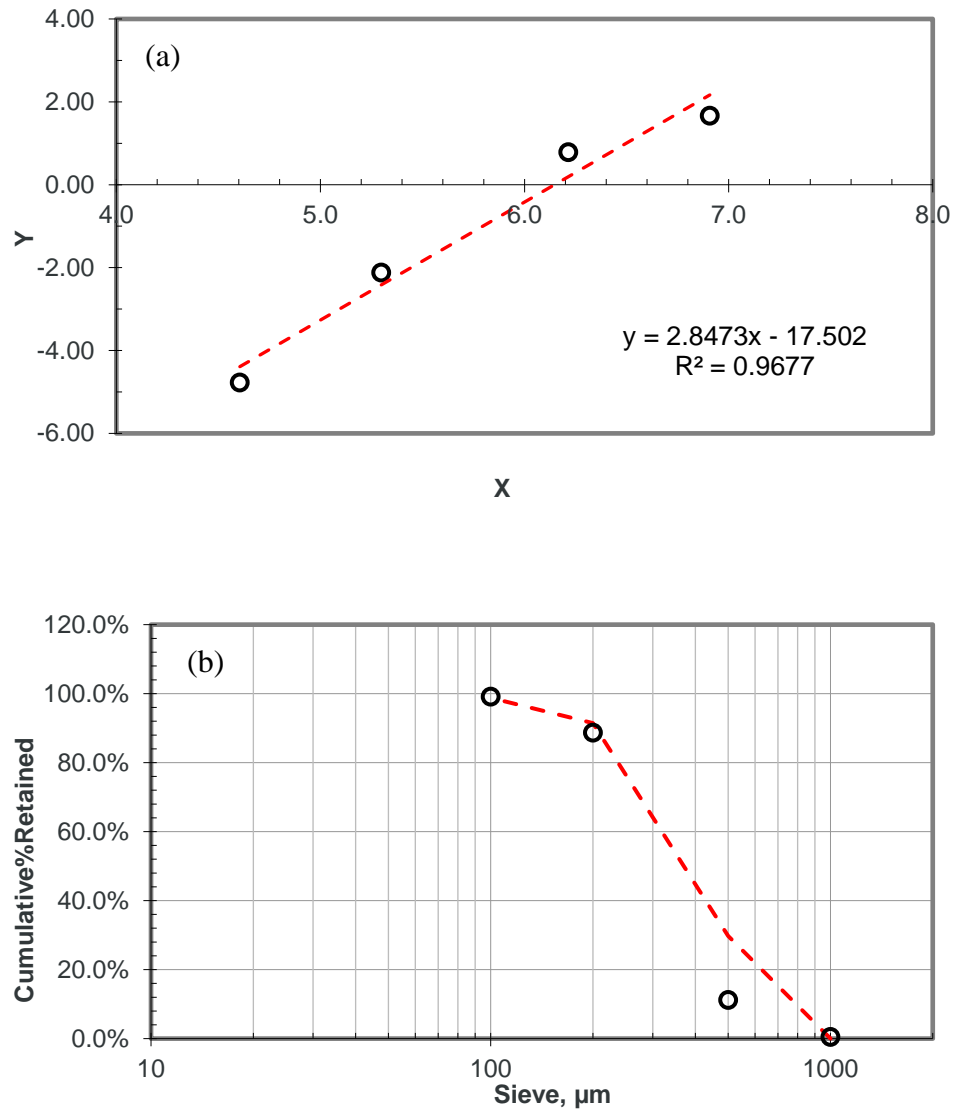Figure 49: Rosin Rammier Regression Check (50<DSP<1500 µm), (a) X vs. Y (b)
the Sieve Size vs. Cumulative% Retained

Table 20: Size calculations

Large Particles Size	400<DSP<3000 μ							
Sample size	92.137 gm							
Particle Average Size	1790 μm							
Weights		**Normalized**	**D**	**R**	**X**	**Y**		**Fitted %**
		Cumulative	**Sieve,**	**Cumulative**				**%**
gm	**Cumulative**	**%Retained**	**μm**	**%Retained**			**Fitted Y**	**retained**
0	0	0	3000	0.0%	x	Y		0
8.991	0.09758	9.8%	2360	9.8%	7.7664	0.8446	0.8907	8.7%
61.867	0.67147	76.9%	1180	76.9%	7.0733	-1.3371	-1.3428	77.0%
6.980	0.07576	84.5%	1000	84.5%	6.9078	-1.7799	-1.8762	85.8%
12.880	0.13979	98.5%	500	98.5%	6.2146	-4.1656	-4.1098	98.4%
1.419	0.01540	100.0%	0	100.0%				100.0%
Large Particles Size	50<DSP<2000 μ							
Sample size	50.08 gm							
Particle Average Size	783 μm							
Weights		**Normalized**	**D**	**R**	**X**	**Y**		**Fitted %**
		Cumulative	**Sieve,**	**Cumulative**				**%**
gm	**Cumulative**	**%Retained**	**μm**	**%Retained**			**Fitted Y**	**retained**
0	0	0	2000	0.0%	x	Y		0
1.667	0.0333	3.3%	1000	3.3%	6.9078	1.2245	0.7077	13.1%
41.384	0.8264	86.0%	500	86.0%	6.2146	-1.8889	-1.2979	76.1%
6.350	0.1268	98.6%	200	98.6%	5.2983	-4.2939	-3.9493	98.1%
0.482	0.0096	99.6%	100	99.6%	4.6052	-5.5362	-5.9550	99.7%
0.197	0.0039	100.0%	0	100.0%				100.0%
Small Particles Size	50<DSP<1500 μ							
Sample size	45.104 gm							
Particle Average Size	467 μm							
Weights		**Normalized**	**D**	**R**	**X**	**Y**		**Fitted %**
		Cumulative	**Sieve,**	**Cumulative**				**%**
gm	**Cumulative**	**%Retained**	**μm**	**%Retained**			**Fitted Y**	**retained**
0	0	0	2000	0.0%	x	Y		0
0.227	0.0050	0.5%	1000	0.5%	6.9078	1.6662	2.1668	0.0%
4.833	0.1072	11.2%	500	11.2%	6.2146	0.7828	0.1931	29.7%
34.952	0.7749	88.7%	200	88.7%	5.2983	-2.1220	-2.4158	91.5%
4.712	0.1045	99.2%	100	99.2%	4.6052	-4.7723	-4.3894	98.8%
0.380	0.0084	100.0%	0	100.0%				100.0%

Appendix B: Error and Uncertainties

The standard uncertainty, $ui\ (x)$, of a n estimation repeats of an amount, x, is the standard deviation of the outcomes, and it is determined by the accompanying equation:

$$\mathbf{u}_i(\mathbf{x}) = \sqrt{\frac{\sum_{j=1}^{n}\left(\mathbf{x}_j - \bar{\mathbf{x}}\right)^2}{n-1}}$$

Where $\bar{x}$ is the normal of estimation aftereffects of the amount, x. The uncertainty interims (blunder bars in charts) depended on the standard uncertainty. The repeated results estimations were, in this manner, shown as: $x \pm ui\ (x)$